

G3/20 0026149

1994 NASA/USRA/ADP Design Projects

FINAL REPORT

11-20-92
36149
135 p



Vanderbilt University
Department of Mechanical Engineering
Nashville, Tennessee
Dr. Thomas Cruse
Joseph Richardson, Teaching Assistant
Robert Tryon, Teaching Assistant

ORIGINAL CONTAINS
COLOR ILLUSTRATIONS

Student Teams:
Universal Test Facility
Mike Laughery (Team Leader),
Mary Connelly, Aaron Detling, Jim Lipsey,
Terry Madewell, Pete Miham, Aldo Pezzia
Automated Protein Crystal Growth Facility
Stacey Donald (Team Leader),
Samuel McGuire, Takayuki Nakajima, Brandon Owen,
Steve Puricelli, Andrew Sheridan, Rennie Williamson
Stiffening of the ACES Deployable Space Boom
Vince Sidwell (Team Leader),
Keith Avery, Bill Chisman, Scott Clements,
Luke Nelson, Jim Puckett, Al Wood
Launch System Design for Access to Space
Corbin Barnes (Team Leader),
Mike Lester, Mike Hale, Scott Trail,
Tim Sullivan, Marshall Brown, Jeff Wright
LH₂ Fuel Tank Design for SSTO
Geff Wright (Team Leader),
Richard Bratcher, Scott Crafton,
Steve Lynch, Wayne Owen, Greg Roberts
Feed System Design for a Reduced Pressure Tank
Hubert Lui (Team Leader),
Adam Corsi, Chris Fasano,
John Miller, Mark Taylor, David Wegrich

Table of Contents

1	Vanderbilt University Mechanical Engineering Design	
1.1	Program	
1.2	Summer Internship	
1.3	Fall Term (ME 202 Mechanical Engineering Design Synthesis)	
1.4	Spring Term (ME 203 Mechanical Engineering Design Projects)	
2	Universal Test Facility	
2.1	Summary	2.1
2.1.1	Design Objective	2.1
2.1.2	Abstract	2.1
2.2	Glossary	2.2
2.3	Background	2.2
2.3.1	Protein Crystal Growth	2.2
2.3.2	Hydroponics Food Growth	2.3
2.3.3	Gas Combustion	2.5
2.3.4	Gallium Arsenide	2.6
2.3.5	Cell Encapsulation	2.6
2.3.6	Microorganism Development	2.7
2.4	Design Concept	2.8
2.4.1	Overall Rack Design	2.8
2.4.2	Canister Design	2.9
2.4.3	Visual Monitoring System Design	2.11
2.4.4	Universal Interface Design	2.11
2.4.5	Telerobotics System Design	2.11
2.5	Conclusion	2.12
2.6	Recommendations	2.13
3	Automated Protein Crystal Growth Facility	3.1
3.1	Summary	3.1
3.1.1	Design Objective	3.1
3.1.2	Abstract	3.1
3.2	Glossary	3.2
3.3	Background	3.3
3.3.1	Importance of Protein Crystals	3.3
3.3.2	Vapor Diffusion Method	3.3
3.3.3	Sensing	3.3
3.3.4	Robot End Effector	3.4
3.4	The Design Concept	3.4
3.4.1	Protein Crystal Chamber	3.4
3.4.1.1	Previous Chamber Designs	3.4
3.4.1.2	New Chamber Designs	3.4
3.4.1.3	Syringes	3.6
3.4.2	Experimental Facility	3.6
3.4.2.1	Geometry	3.6
3.4.2.2	Active Sites, Storage Site, and Drawers	3.7
3.4.3	Sensing Device	3.8

	3.4.3.1 Light Diffraction Method	3.8
	3.4.3.2 Two Possible Sensing Methods	3.8
	3.4.3.3 Selected Sensing System	3.9
	3.4.3.4 Lighting Within the Chamber	3.10
3.4.4	Electronic Control System	3.11
3.4.5	Robot End Effector	3.13
	3.4.5.1 Zymate Robot	3.13
	3.4.5.2 Overall End Effector Design	3.13
	3.4.5.3 Gripper Arm Design	3.14
	3.4.5.4 Syringe Plunger Design	3.15
	3.4.5.5 Motors and Gearheads	3.15
	3.4.5.6 Fabrication	3.15
3.4.6	Robot Simulation	3.16
3.5	Conclusions	3.16
	3.5.1 Overall Progress	3.16
	3.5.2 Chamber and Experimental Facility	3.16
	3.5.3 Sensing System	3.16
	3.5.4 Control System	3.17
	3.5.5 End Effector	3.17
3.6	Recommendations	3.17
	3.6.1 Chamber and Experimental Facility	3.17
	3.6.2 Sensing	3.18
	3.6.3 Control System	3.18
	3.6.4 End Effector	3.18
3.7	References	3.18
 4	Stiffening of the ACES Deployable Space Boom	4.1
4.1	Summary	4.1
	4.1.1 General Background Information	4.1
	4.1.2 Design Objective	4.2
	4.1.3 Abstract	4.2
4.2	Glossary	4.2
4.3	Background Information	4.2
	4.3.1 Customer Requirements	4.2
	4.3.2 ACES Structure Background	4.3
4.4	Analysis	4.4
4.5	Design Concept	4.6
4.6	Active Tensioning Mechanism	4.6
4.7	Testing	4.11
4.8	Conclusions	4.11
4.9	Recommendations	4.11
4.10	References	4.11
4.11	Appendix	4.12
	4.11.1 Additional Figures	4.12
 5	Launch System Design for Access to Space	5.1
5.1	Design Objective	5.1
5.2	Abstract	5.1
5.3	Glossary	5.1

5.4	Background	5.1
5.4.1	Current Non-Man-Rated Space Vehicles	5.1
5.4.2	Current Man-Rated Space Vehicle: Space Shuttle	5.2
5.4.3	Future Concepts (Present to 2015)	5.2
5.4.3.1	Redesigned Space Shuttle	5.3
5.4.3.2	NASA Single Stage to Orbit (SSTO)	5.3
5.4.3.2.1	DC-X	5.4
5.4.3.2.2	Winged SSTO	5.4
5.4.3.3	National Aerospace Plane	5.4
5.4.4	Customer Requirements for Future Launch System	5.4
5.4.5	Determination of the Relative Importance of Customer Requirements	5.5
5.5	Concept Generation and Recommendation of Final Concept	5.7
5.5.1	Hybrid Launch System: MLV	5.7
5.5.2	Hybrid Launch Concept: Astronaut Escape Vehicle	5.9
5.5.2.1	Discussion of Concepts	5.11
5.5.2.2	Escape System Concept Selection	5.17
5.5.2.3	Configuration of the Final Escape System (Ballistic Escape Pod)	5.17
5.6	Conclusion	5.19
5.7	Bibliography	5.20

6

	LH ₂ Fuel Tank Design for SSTO Vehicle	6.1
6.1	Summary	6.1
6.1.1	Design Objective	6.1
6.1.2	Abstract	6.1
6.2	Glossary	6.1
6.3	Background	6.1
6.4	Material Selection	6.2
6.4.1	Composite Materials	6.2
6.4.2	Aluminum Honeycomb Description	6.3
6.5	Design Concept	6.3
6.5.1	Structural Concepts	6.3
6.5.2	Lamination Theory of Composite Materials	6.4
6.6	Heat Transfer	6.9
6.6.1	Overview	6.9
6.6.2	Thermal Resistance Model	6.10
6.6.3	Insulation	6.11
6.6.4	Defining the Total Insulation Mass	6.15
6.6.5	Insulation Application	6.16
6.6.6	Thermal Expansion	6.16
6.7	Diffusion Rate of Liquid Hydrogen	6.17
6.8	Design Analysis	6.17
6.8.1	Structural Configuration	6.18
6.8.2	Insulation Configuration	6.19
6.9	Thermal Expansion	6.19
6.10	Recommendations	6.20
6.11	References	6.20
6.12	Appendix: Material Properties	6.22

Feed System Design for a Reduced Pressure Tank	7.1
7.1 Summary	7.1
7.1.1 Design Objective	7.1
7.1.2 Abstract	7.1
7.2 Glossary	7.1
7.3 Background for SSTO Feed System	7.1
7.4 The Design Concept	7.2
7.4.1 Feed System Modeling	7.2
7.4.1.1 Feed System Design	7.2
7.4.1.1.1 Feed System Introduction	7.2
7.4.1.1.2 LOX Feed System Configuration	7.2
7.4.1.1.3 LOX Piping Descriptions	7.3
7.4.1.1.4 RP-1 Feed System Configuration	7.5
7.4.1.1.5 RP-1 Piping Descriptions	7.5
7.4.1.1.6 LH2 Feed System Diagram	7.8
7.4.1.1.7 LH2 Piping Descriptions	7.8
7.4.1.1.8 Feed System Assumptions	7.10
7.4.1.1.9 Error Analysis	7.10
7.4.1.2 Computer Feed System Model	7.10
7.4.1.2.1 Computer Program Introduction	7.10
7.4.1.2.2 Model Development	7.11
7.4.1.2.3 Computational Results	7.12
7.4.1.2.4 Errors	7.12
7.4.1.2.5 Future Efforts	7.13
7.4.2 Fluid Recirculation Feed System	7.13
7.4.2.1 Description	7.13
7.4.2.2 Preliminary Assumptions	7.14
7.4.2.3 Feed Line Specifications	7.14
7.4.2.4 Calculation of Pump Requirements	7.15
7.4.2.5 Disadvantages of the Recirculation System	7.15
7.4.2.6 Conclusions	7.15
7.4.3 Land Based Pressurized Fuel System	7.16
7.4.3.1 Description	7.16
7.4.3.2 Safety Concerns	7.16
7.4.3.3 LBPFS Operation	7.16
7.4.3.4 LBPFS Weight Reduction	7.16
7.4.3.5 LBPFS Weight Reduction	7.17
7.4.3.6 Deficiencies and Future Efforts	7.18
7.5 Recommendations	7.18
7.6 References	7.19

1 Vanderbilt University Mechanical Engineering Design

Seniors in the Mechanical Engineering Program at Vanderbilt University are required to take a sequence of two courses in mechanical engineering design. These courses are intended to expose the students both to the formalism of design methodology and to actual problems in design similar to those encountered by practicing engineers. The 1993-1994 academic year marks the second year in which Vanderbilt has participated in the Advanced Design Program (ADP) sponsored by the Universities Space Research Association (USRA) and the National Aeronautics and Space Administration (NASA). This program provides financial support for the class including expenses for supplies, travel, a teaching assistant, and a summer internship.

1.1 Program

The USRA ADP program promotes engineering education in the field of design by presenting students with challenging design projects drawn from actual NASA interests. In doing so, the program yields two very positive results. Firstly, the students gain a valuable experience that will prepare them for design problems with which they will be faced in their professional careers. Secondly, NASA is able to use the work done by students as an additional resource in meeting its own design objectives.

1.2 Summer Internship

During the summer of 1993, Mr. Robert G. Tryon, who was one of two teaching assistants for the 1993-1994 academic year, worked as a Visiting Summer Fellow at NASA/Marshall Space Flight Center (MSFC) through the NASA/USRA ADP. For his internship, Mr. Tryon worked in the Propulsion Systems Branch of the Preliminary Design Office (PD-13) under the supervision of Mr. Jim Thompson and placed under the direct tutelage of Mr. Robert Champion. The objective of this fellowship was to prepare Mr. Tryon for his role in assisting Professor Thomas A. Cruse organize the senior design program for the following year. This preparation was divided into two categories: developing an understanding of how the design process is applied to liquid rocket propulsion systems and identifying candidate topics for the spring semester design projects.

An understanding of the fundamental theory, hardware, and application of liquid rocket propulsion was achieved through reading textbooks and NASA documents along with discussions with NASA engineers. Mr. Tryon's specific project was a preliminary design of the feed system for the Access to Space single stage from earth to orbit (SSTO) all rocket option. A team of Langley Research Center (LaRC) and MSFC engineers are collaborating on SSTO. The LaRC team is headed by Mr. Steve Cook. SSTO is currently under consideration to replace the Space Shuttle fleet around the year 2007. Mr. Tryon's preliminary design involved issues concerning engine placement, feed line layout, feed line losses, and tank pressurization.

1.3 Fall Term (ME 202 Mechanical Engineering Design Synthesis)

The fall semester was primarily devoted to teaching elements of design methodology including such things as Quality Function Deployment, functional decompositions, Problem Understanding Forms, and project management using Gantt charts. The text for the class was The Mechanical Design Process by David G. Ullman.

The students were divided into seven groups of six students each. The groups were then presented with a product which they were to redesign. The products which were selected for this exercise included: a vacuum cleaner, an electric trolling motor, an orbital/planar sander, a gasoline-powered weed trimmer, a water purification pump, a kitchen blender, and an electric air compressor. Collectively, they were to disassemble and document the components of the existing product. Their final deliverable for the semester was an individual redesign of the product which they were given.

1.4 Spring Term (ME 203 Mechanical Engineering Design Projects)

For the spring semester, the class was divided into two sections, each of three groups. Students were assigned to these groups based on the results of questionnaires regarding their areas of skill and interest. Design projects were identified at the close of the fall semester for each of the groups and each group elected a leader who was to supervise the partitioning of work among the group's members. In late January, the class made a trip to MSFC to meet with NASA engineers in order to identify the critical issues to be addressed in the students' designs.

The sections which met on Tuesdays designed elements of launch systems. The three projects included the design of a hybrid launch vehicle to meet the Access to Space requirements, the design of an LH₂ composite tank, and a feed system design. The groups which met on Thursdays worked on design problems in the area of space applications and included the design of an automated protein crystal growth facility for growing protein crystals in microgravity, the design of a universal test facility to conduct microgravity experiments, and the design of an active stiffening system for a deployable space boom.

The class periods were used as working engineering meetings where the groups presented progress reports to the entire section. Each group member was required to give presentations on at least two occasions during the semester. Following the progress reports, the groups met individually to discuss the upcoming week and adherence to their respective Gantt charts.

Near the close of the spring semester, the entire class gave a formal presentation of their final designs with Vanderbilt faculty and a number of engineers, both from NASA and from the aerospace industry in attendance. The final written reports submitted by the students comprise the remainder of this document.

2 Universal Test Facility

2.1 Summary

2.1.1 Design Objective

To develop a highly marketable, automated test facility capable of performing diverse microgravity experiments according to NASA space station constraints.

2.1.2 Abstract

A universal test facility for Space Station Freedom is developed. In this context, universal means that the experimental rack design must be: automated, highly marketable, and able to perform diverse microgravity experiments according to NASA space station requirements. In order to fulfill these broad objectives, the facility's customers, and their respective requirements, are first defined. From these definitions, specific design goals and the scope of the first phase of this project are determined.

An examination is first made into what types of research are most likely to make the UTF marketable. Based on our findings, the experiments for which the UTF would most likely be used include: protein crystal growth, hydroponics food growth, gas combustion, gallium arsenide crystal growth, microorganism development, and cell encapsulation. Therefore, the UTF is designed to fulfill all of the major requirements for the experiments listed above. The versatility of the design is achieved by taking advantage of the many overlapping requirements presented by these experiments.

The UTF centers around eight, self-contained experimental canisters. The UTF supplies these canisters with the resources their respective experiments require (power, electricity, etc.), and is able to monitor them with two video cameras. The canister's rectangular shape is chosen to optimize volume and space within the rack system. Its features include: an ergonomic handle for easy transport and installation, an effective clamping system designed to keep the canister locked into place, an LED indicator which lights when the canister is properly inserted, and a single, universal interface for exchanging raw materials and data with the UTF.

The universal interfaces, attached to the back wall of the experimental rack, add versatility to the overall design. Consisting of a data acquisition linkage, power source, and six input / output portals for transport of vital resources, the universal interface is responsible for sustaining all microgravity experiments in the rack. More importantly, it becomes the experimenter's direct link to an experiment and all data acquisition involved.

The rack system is broken into three sections. On the top of the facility, the computer system for data acquisition is positioned and insulated from possibly harmful heat transfer derived from the experimental section. The experimental canisters, universal interfaces, and visual monitoring systems are located in the central portion of the rack. Specifically, a total of eight canisters (four on each side of the rack) are separated by two small video cameras which monitor the experiments. The bottom portion of the rack consists of two storage tanks for either the recirculation or disposal of resources, the HVAC system, and a utility section for containment of the motor and pump.

It is important to note that the facility design is, for the most part, conceptual. Specific hardware definition is reserved for our successors. We believe, however, that the design objective is entirely satisfied. The design process is made significantly less burdensome by giving our

customers the responsibility of designing the internal components of the experimental canisters which they purchase.

2.2 Glossary

camera system	- visual monitoring system for the UTF which utilizes two, independently operating, video cameras.
canister	-a self-contained unit which houses a microgravity experiment.
LED	-Light Emitting Diode
rack	-the entire unit containing the experimental facility (including the canisters).
teleroobotics	-a vital link enabling the experimenter to communicate with and monitor the experiment's progress while in the test facility.
Universal Interface (UI)	-a versatile interface which provides for all the input and output of all the Space Station supplied resources.
Universal Test Facility (UTF)	-the entire unit containing the experimental facility (including the canisters, universal interfaces, optical system, storage facility, HVAC, and utility containment of the pump and motor).

2.3 Background

In order to satisfy the "highly marketable" aspect of the design objective, several microgravity experiments are researched and identified. Based on our findings, the experiments for which the UTF would most likely be used include: protein crystal growth, hydroponics food growth, gas combustion, gallium arsenide crystal growth, microorganism development, and cell encapsulation. This evaluation is made assuming the experimenter reserves space in the rack and financially supports an experiment from beginning to end.

2.3.1 Protein Crystal Growth

The study of protein crystal growth is necessary in developing a complete understanding of the purpose and function of proteins. Because proteins play a key role in life, a comprehension of their function can elicit breakthroughs in medical research. Other fields such as biochemistry and agriculture can also benefit from a thorough understanding of proteins. Protein molecules are too small to study individually, therefore protein crystals, which are large enough to be tested, are grown. The difference between a protein crystal grown on Earth and one grown in a microgravity is illustrated in Figure 2.1. As shown in this figure, techniques used to analyze



Figure 2.1.
Comparison of a terrestrially grown protein crystal (l)
with a protein crystal grown in microgravity (r).

crystalline structure, such as x-ray diffraction, are significantly more effective on three-dimensional crystals grown in microgravity. On Earth, crystals tend to grow in two dimensional patterns.

This experiment is chosen for two reasons. First, protein crystal growth was the primary emphasis of the 1993 design effort, thus it seems a logical place to start. Secondly, the growth of protein crystals involves several unique processes. That is, protein crystal growth rounds out a list of experiments which have very diverse input and output requirements. However, since the design of components tailored to specific experiments are left to the individual scientists, the processes involved with protein crystal growth are not discussed here. It is sufficient to list the necessary inputs and outputs to and from Space Station Freedom. These include power and data transfer for the sensing and control systems.

2.3.2 Hydroponics Food Growth

NASA space exploration has reached a level where the idea of a permanent space station and/or a space colony is feasible. To make the space station self-sufficient is important to the feasibility of this mission. Part of the process of making the space station self-sufficient lies in the ability to provide its own life support. One solution to this problem is a system under development called the Controlled Ecological Life Support System (CELSS). The CELSS system is dependent on the use of higher plant species such as wheat and beans to regenerate oxygen, water, and food supplies, from different forms of wastes produced in the station. The key in developing the system lies in hydroponics. Use of hydroponics on earth is now common, but the use of hydroponics in space is a relatively new science. Since the use of hydroponics in space is untried, researchers need ways to experiment with different types of hydroponics systems in space. The proposed Universal Test Facility is able to accommodate such experiments, and thus advance the body of knowledge on this subject.

The term hydroponics describes any of several methods for growing plants without soil. In general, a hydroponics system works by utilizing a rich nutrient solution that flows through a containment structure where the plant roots have attached themselves. As the solution passes through the apparatus, the root draws from the solution the essential nutrients it needs to grow. The solution, depleted of some of its nutrients, returns to a reservoir to be stored or have its nutrients replenished.

One of the main advantages of a hydroponics system is the ability to control the growth environment. The researcher is able to control the concentration levels of: water, nutrient, pH, electroconductivity, and oxygen. Controlling these factors allows the researcher to maximize plant growth. This control also allows the researcher to alter the type of growth desired. For example, alteration of light patterns between night and day as well as modification of the light wavelength affect the amount of root and shoot growth. Experimenting with these levels will provide the best method to produce crops in space. Another advantage to hydroponics is its sanitary conditions. Since there is no soil, there is no sand or grit to cling to the roots. Also, sanitation of the entire system is simple because the containment structures and solution piping are all plastic. This feature allows the use of a cleansing solution to clean all parts of the hydroponics system. Another important advantage to researchers is the flexibility that a hydroponics system offers. Planting and interchanging of the crops is quick and simple. The ease of changing the types of plants allows the researcher to study the growth patterns of many different species. Finally, the most important advantage of hydroponics is that it is conducive to automation. It is relatively simple to program a computer to control the environment in which a plant grows. This factor makes hydroponics experiments excellent candidates for execution in the universal test facility.

The hydroponics process can be generalized to have certain requirements that are necessary in order for the system to function. These requirements are that: the system must have the ability to monitor and adjust the nutrient levels in the solution, the ability to efficiently distribute the solution, the capability of effectively transferring nutrients to the roots, and the capacity to store or recycle the used solution. The design of the UTF meets all these requirements. The facility provides the hydroponics experiment with: power, water, air, and nutrients through the universal interface. The facility's computer, utilizing researcher-written hydroponics software specific to the experiment, then monitors and adjusts the growth process. The facility can then store the used nutrient solution before it is recycled.

Figure 2.2 shows a simplified version of a possible hydroponics system for use in space racks. The original concept work was done by Steven H. Schwartzkopf at Lockheed Missiles and Space Company (reference MSC-2165). The system is internalized into one of the facility canisters. The system operates in a cycle starting from solution bladder 1 passing through the system to solution bladder 2. An air compressor forces the solution out of bladder 1 by increasing the pressure. As the solution passes through the system, sensors monitor many elements including flow, temperature, pH, and nutrient level. The solution then passes through a control manifold where the computer adjusts the levels of concentration for all the components using supplements stored internally or in the optional storage canister. The adjusted flow now enters the test chamber where it feeds the roots of the plants. Video monitoring is available to record the patterns of growth of each plant. The depleted solution returns to bladder 2 for temporary storage. When bladder 2 reaches its capacity, valves shut off the pressure to bladder 1. After bladder 1 is filled, the valve switches back to their initial positions and the process starts over again.

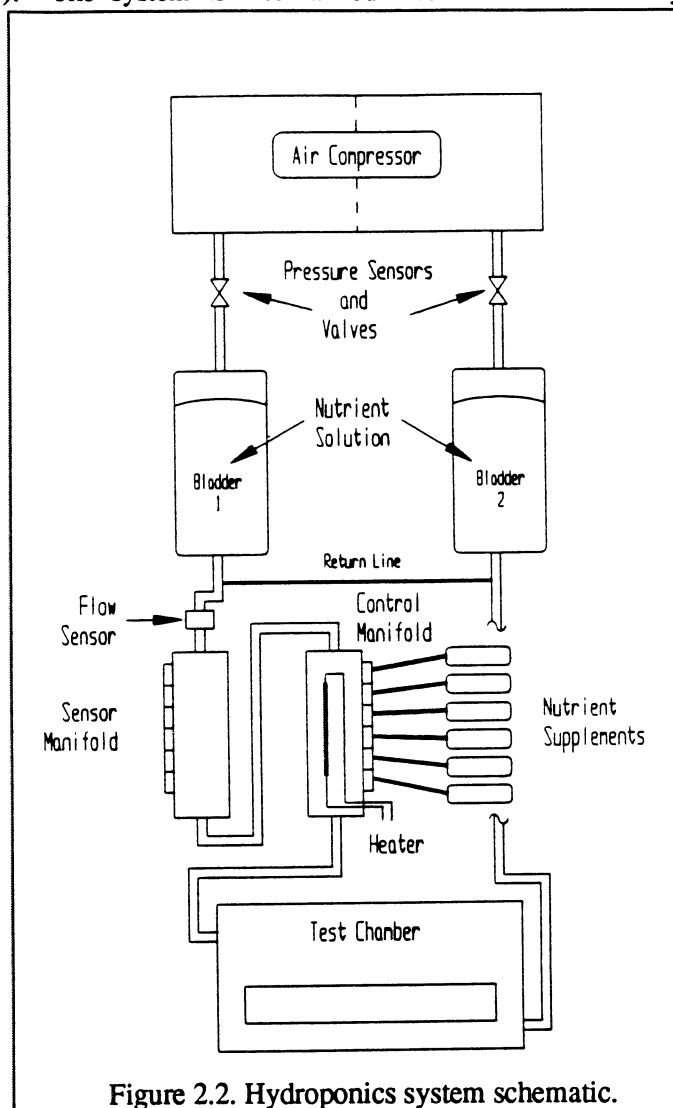


Figure 2.2. Hydroponics system schematic.

2.3.3 Gas Combustion

Gases and other substances behave very differently in microgravity than on Earth. Combustion is no exception to this principle. Microgravity causes differences in the manner by which a gas is excited. The understanding of how gases combust in microgravity is important to the development of alternative fuels for space exploration. Thus, research is ongoing on how gases and other substances combust in microgravity. The Universal test facility offers the ability to perform combustion experiments efficiently.

In general, the combustion experiment utilizes an experimental canister that can withstand the high pressure generated by combustion. The test specimen rests on a pedestal as oxygen fills the canister. The test facility's computer then prompts a pyrotechnic wire fuse attached to the specimen to ignite. During ignition and combustion, the facility monitors the entire process for later viewing by researchers. The researcher quenches the experiment by introducing argon and nitrogen gases into the chamber. The canister then releases the exhaust gases to a storage container for later disposal.

The requirements of the combustion process are that the system have: the ability to monitor the combustion process, the ability to supply and control the introduction of the igniting and quenching gases, and the capability to store the combustion reactants and products. The facility supplies the necessary video monitoring and data acquisition, thus allowing the researchers to view and document the process at a later time. The facility, through the universal interface, can control the supply of the ignition and quench gases available from the combustion canister or from the optional storage canister of the test facility. In addition, the facility provides an exhaust outlet to a storage container for future disposal.

Figure 2.3 shows the combustion process configuration. The original concept was created by Theodore A. Steinberg of Lockheed Engineering and Science Company (reference MSC-21777). The canister mounts a rod specimen from the top of the chamber. The command control system sends a signal to ignite the pyrotechnic fuse located at the bottom of the chamber. The chamber has its own data acquisition system to record the readings from various thermocouple and pressure gauges. The universal interface provides the link for the transmittal of the control signals and the recorded data. Also, a viewing port allows the facility to video record the entire combustion process. If the pressure inside the canister reaches the high pressure limit (in this case 10 MPa), a valve opens and the gases are released from the chamber. The researchers retrieve the data and the canister is ready for reuse.

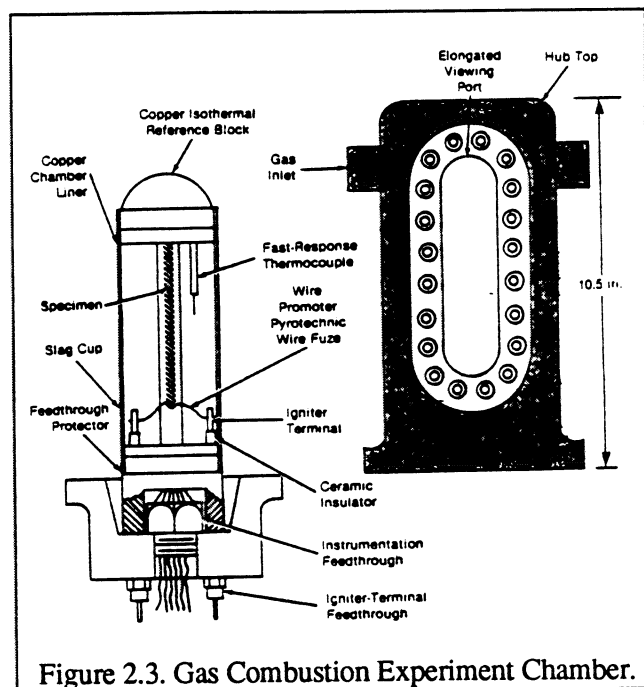


Figure 2.3. Gas Combustion Experiment Chamber.

2.3.4 Gallium Arsenide

Gallium arsenide is a group III-V semiconductor characterized by a relatively high electron mobility and larger energy band gap. This makes gallium arsenide crystals perfect for high frequency applications. High frequency GaAs has applications for: high speed computing, military hardware, biomedical research, and communications. A small brassboard circuit constructed from GaAs was operated at a frequency in excess of 2 GHz, thus demonstrating the potential of research in this field.

Because crystal impurities move along the solidification front when grown in space, and do not contaminate the crystal, the growth of gallium arsenide crystals in a microgravity environment is desirable.

Gallium arsenide crystals have already been grown in space in a "gas can" type experimental set-up. This same type of gallium arsenide growing technique can be incorporated into the Universal Test Facility.

2.3.5 Cell Encapsulation

The purpose of cell encapsulation experiments is to protect islet cells so that, when injected into the human body, the cells will not be killed by antibodies. The islet cells, which produce insulin, are being studied to develop a treatment for diabetes. Experiments done on rats using encapsulated cells on earth have achieved favorable results. Unfortunately, due to the effects of gravity, it is very difficult to

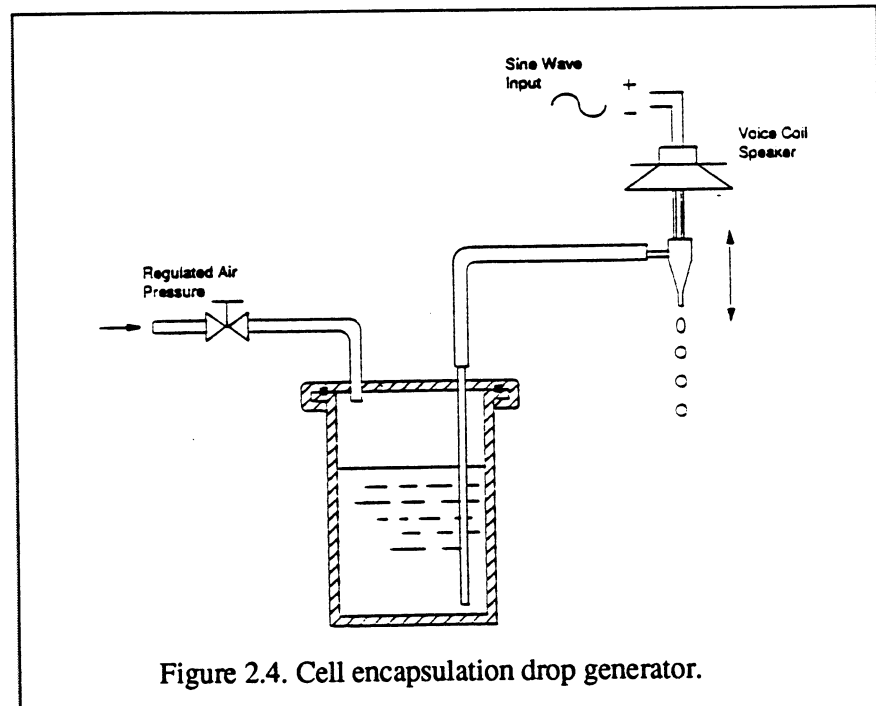


Figure 2.4. Cell encapsulation drop generator.

encapsulate cells consistently on earth. Therefore, the production of encapsulated cells needs to be investigated in space and is a perfect candidate for use within the UTF design.

Currently, cells are suspended in a nutrient solution to keep them alive. This nutrient solution is also the base for the polyanionic encapsulation process. The solution is then run through a drop generator (See Figure 2.4), and the droplets are immediately immersed in a polycationic solution. The chemical reaction between the two solutions creates the polymer encapsulation shell. Therefore, the islet cells are encapsulated in a semi-permeable membrane which allows nutrients and insulin, but not antibodies, to pass through. This experiment requires strict environmental control, therefore the entire process is controlled by computer.

It is possible to put the cell encapsulation experiment into one or more of the UTF containers. The experiment will utilize the storage sites at the bottom of the UTF. For this reason, the experimenter would probably purchase a whole rack.

2.3.6 Microorganism Development

The constant gravitational force which has influenced life on earth for the past 3.5 billion years leads biologists to speculate that many organisms utilize gravity in their normal developmental cycles. In particular, the belief that gravity plays an instrumental role in the evolution of many present-day organisms in terms of their structure and function prevails. Thus, studying the effects a microgravity environment has on these organisms, might provide insight into possible human reproduction in space.

Several reasons exist for pursuing the study of embryonic development in microgravity environments. First, biologists are interested in gravitational influence on normal development. For example, some organisms display a natural orientation in the earth's gravity. The development of eggs which rotate according to gravity is vulnerable in zero-g conditions, possibly preventing proper maturation. Scientists hope to identify common traits of development (for these organisms) in microgravity conditions.

Secondly, biologists believe that in studying microgravity experiments, there is potential for data acquisition on basic cellular processes. Therefore, the scientists hope to be able to generate information on individual cells which, again, could be applied to human embryonic development in space.

Thirdly, with the instatement of a permanently manned space station, the development of lunar and Martian bases becomes increasingly possible. Because of the complexity of such systems, it is necessary to focus now on how organisms reproduce in lunar (0.16g) and Martian (0.39g) environments. Such information will be vital to understanding how humans reproduce and develop under these conditions.

The ideal experiment is one which is self-contained, requires relatively small volume, is fully automated (with minimal power needs) and can be transported in the space shuttle's mattock locker to Space Station Freedom's experimental racks. Since several experimental microorganism systems have already flown under SSF conditions, we are confident that our canister and rack designs can ensure successful completion of the specific experiment.

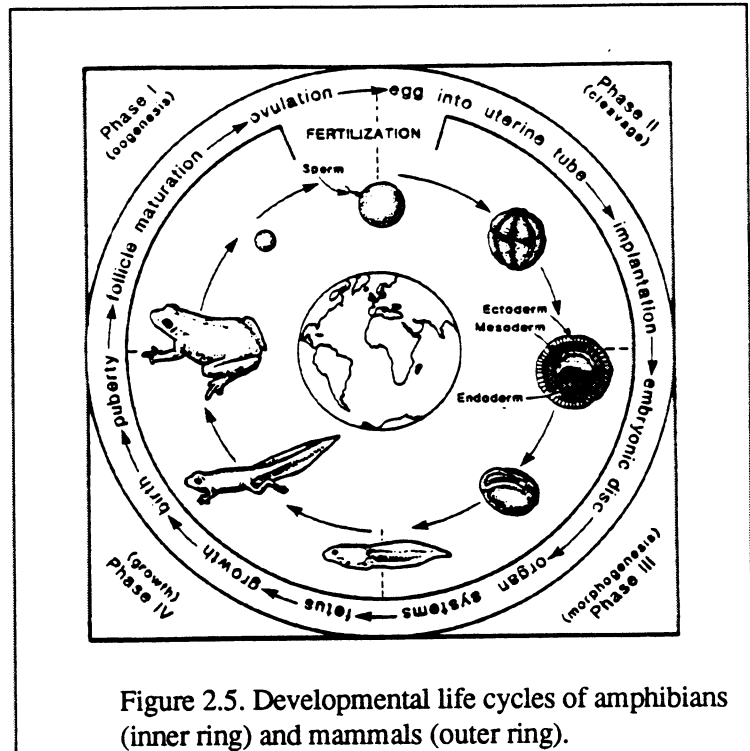


Figure 2.5. Developmental life cycles of amphibians (inner ring) and mammals (outer ring).

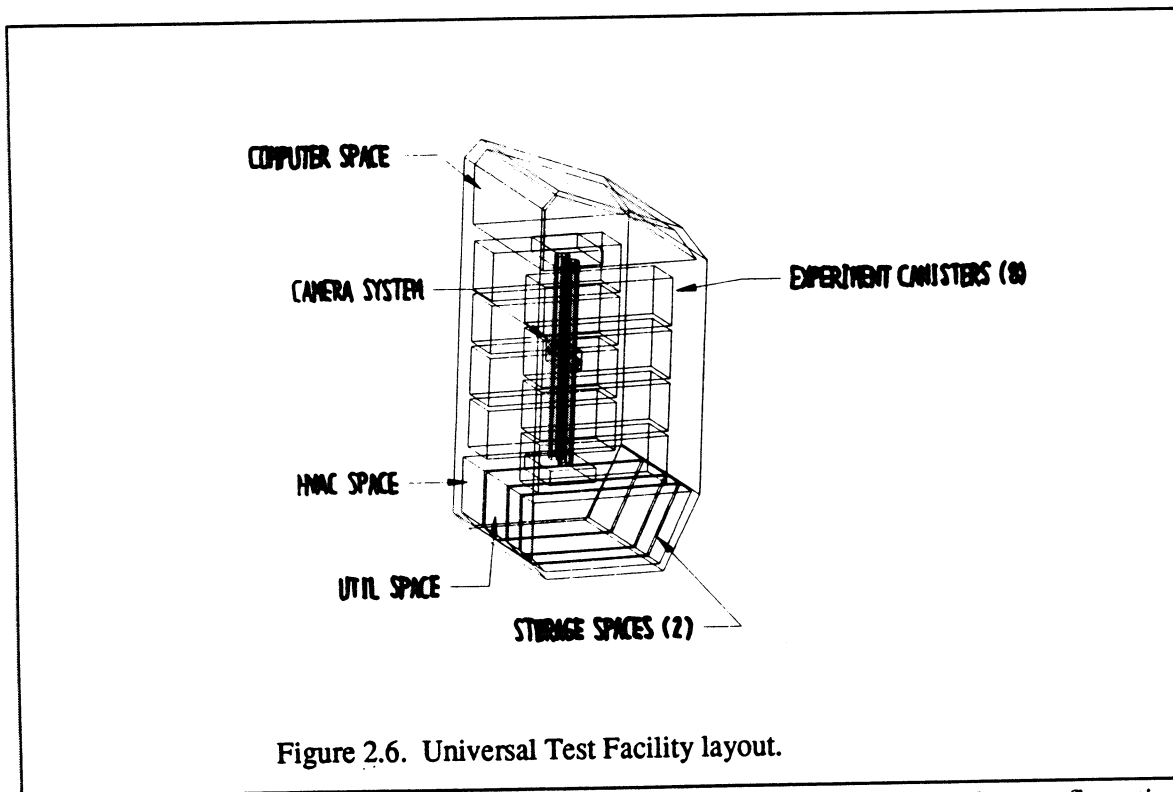
2.4 Design Concept

The design concept consists of the overall rack design, the canister design, visual monitoring system design, the universal interface design, and the telerobotics system design.

2.4.1 Overall Rack Design

The main point of the design goal is to design a Universal Test Facility (UTF) capable of performing diverse microgravity experiments. In order to achieve this broad design goal several important decisions were made in regard to the overall rack design. These decisions include:

1. Optimum component layout
2. Incorporation of auxiliary equipment necessary to perform several experiments
3. Selection of a "gas can" type experiment configuration
4. Utilization of the universal interface at each canister location to activate experiments
5. Designation of intricate plumbing system to transfer the needed fluids.



The experimental facility design chosen maximizes space and has simplest configuration. The selected rack configuration is shown in the UTF layout given in Figure 2.6. The computer and the data acquisition system are located in the top of the rack. The experiment area, located in the middle of the rack, contains the canisters, the visual monitoring system, and the universal interfaces. The experimental canisters are located along the sides of the experiment area. In the center of the experiment area is the visual monitoring system. On the back wall of the experiment area are the universal interface jacks. The bottom of the rack contains the auxiliary equipment used in performing the experiments. The rear of the rack contains the plumbing and electrical systems.

The auxiliary equipment in the bottom of the rack has three main components. These components are: the HVAC, the utilities, and the storage bays. The HVAC is used to condition the air, water, and storage fluid that is supplied to the experiments. The utility section contains the pumping and filtering systems for the air and water. Finally, the two storage bays, which are purchased and internally designed by the experimenter, have the capability to store and/or recirculate the fluids used or produced by the experiments.

In order to configure the rack to be able to handle diverse experiments, it was decided that the experiments conducted in the rack must be "gas can" type experiments. "Gas can" type experiments were chosen because they require very little human interaction with the experiment itself. However, this should not limit the type of experiments that can be conducted in the rack since the size and shape of the canister is large enough that the experimenter can incorporate his or her own experiment manipulating system, if necessary.

The use of a universal interface allows each canister location to become active without being moved. The interface supplies the air, water, power, storage fluid, and data transfer devices. When the computer determines it is time to activate an experiment, the universal interface is "turned on", and supplies the experiment with the necessary elements for it to execute properly.

The plumbing system is located in the rear of the rack. The plumbing system is able to transfer fluids throughout the experimental facility. This is accomplished with the use of pumps and filters located in the utility section, in conjunction with a series of solenoid valves. These computer controlled valves will be able to transfer fluids to and from each canister, from canister to the fluid storage site (and vice versa), or from canister to canister.

2.4.2 Canister Design

The idea of using canisters in the design of the Universal Test Facility (UTF) stems from the current use of gas can type experiments on previous space shuttle missions. This format provides the versatility that the design goal mandates. The function of the canister is to enclose the actual experiments performed on Space Station Freedom (Figure 2.7). The purpose of containing the experiments inside a canister is to avoid any fluid transfer between the experiments and the Space Station atmosphere. In the interest of versatility, the design of the inner volume of the canister is the experimenter's responsibility. The canister is simply a hollow shell whose interior workings are functioning systems developed by the individual experimenter. Since the researcher is responsible for the internal makeup of the canister, the design effort of this group centered on the issues of canister volume and universal inputs and outputs.

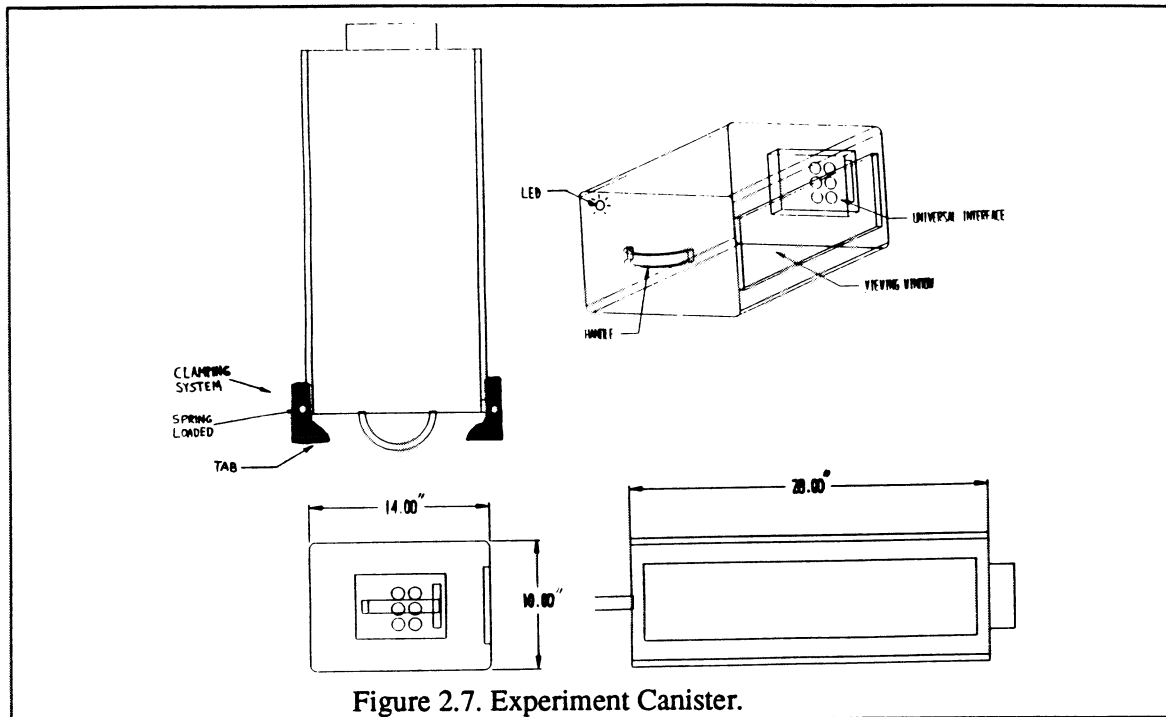


Figure 2.7. Experiment Canister.

The canister design is in the form of a rectangular box with a cross section 10 inches tall by 14 inches wide and a depth of 28 inches. These dimensions give the individual experimenter approximately 4000 cubic inches or 2.25 cubic feet of space within which to contain their experiment. The dimensions are determined from the overall rack dimensions and the total number of sites (8) desired. The large volume that the canister encloses is necessary in order to enhance the versatility of the rack. The large canister volume allows for larger experiments or in the case of a small experiment, a large canister allows more experiments per canister.

The determination of the universal inputs and outputs to the canister results from the cross section of experiments the group chose to research. There are only four essential requirements common to all six experiments that Space Station Freedom needs to provide. These four fundamental inputs consist of air, water, power and data transfer. The inputs and output connections are part of a versatile jack that is now the universal interface (UI). (See section 2.4.4). In addition to the four inputs already mentioned, the UI allocates an extra input and output for an optional fluid transfer. This extra interface offers experiments such as hydroponics an additional input, i.e. a nutrient solution.

There are several other issues addressed by the group concerning the design specifications of the canister. The first issue deals with the visual monitoring system (See section 2.4.3). In order for the researcher to visually monitor a experiment inside the canister, there has to be some kind of transparent window along the length of the canister. Figure 2.7 shows the location of this window. The second issue centers on how to anchor the canister to the rack after insertion of the experiments. To solve this problem, the group proposes a system of spring loaded clips (Figure 2.7) that snap into place when the canister is completely inserted into the rack, thus locking the canister in place. To remove the canister, an astronaut simply has to press the clips outward until they clear the sides of the canister. Small springs located on the UI aid the removal by pushing the canister out past the clips. The canister comes with a handle to aid the astronaut in carrying it. Finally, to ensure proper connection to the power source, a light on the front of the canister signals proper insertion of the canister into the interface.

2.4.3 Visual Monitoring System Design

Many of the experiments in the Universal Test Facility require frequent visual inspections. Thus, a method must be available to record and store the video monitoring of the experiments. Also, the monitoring system must allow the researcher on Earth to visualize his or her experiments. For these reasons, the facility has a camera system that records and stores the experiments progress but is also capable of interfacing with the telerobotics system (Figure 2.6).

The monitoring system utilizes two cameras located in the center of the rack. The use of two cameras allows the viewing of each of the two columns separately. The camera moves longitudinally (from canister to canister) by screw-type drives. In addition, the cameras can translate along the length of the canister by means of a track system incorporated into the top and bottom of the compartment. Thus, the cameras supply video for the entire length of each of the canister's window. Positioning control of the camera system, generally, comes from the on board computer. The on board computer receives its instructions from the software that accompanies each experiment. The researcher may control the cameras as well via the telerobotics system discussed in section 2.4.5

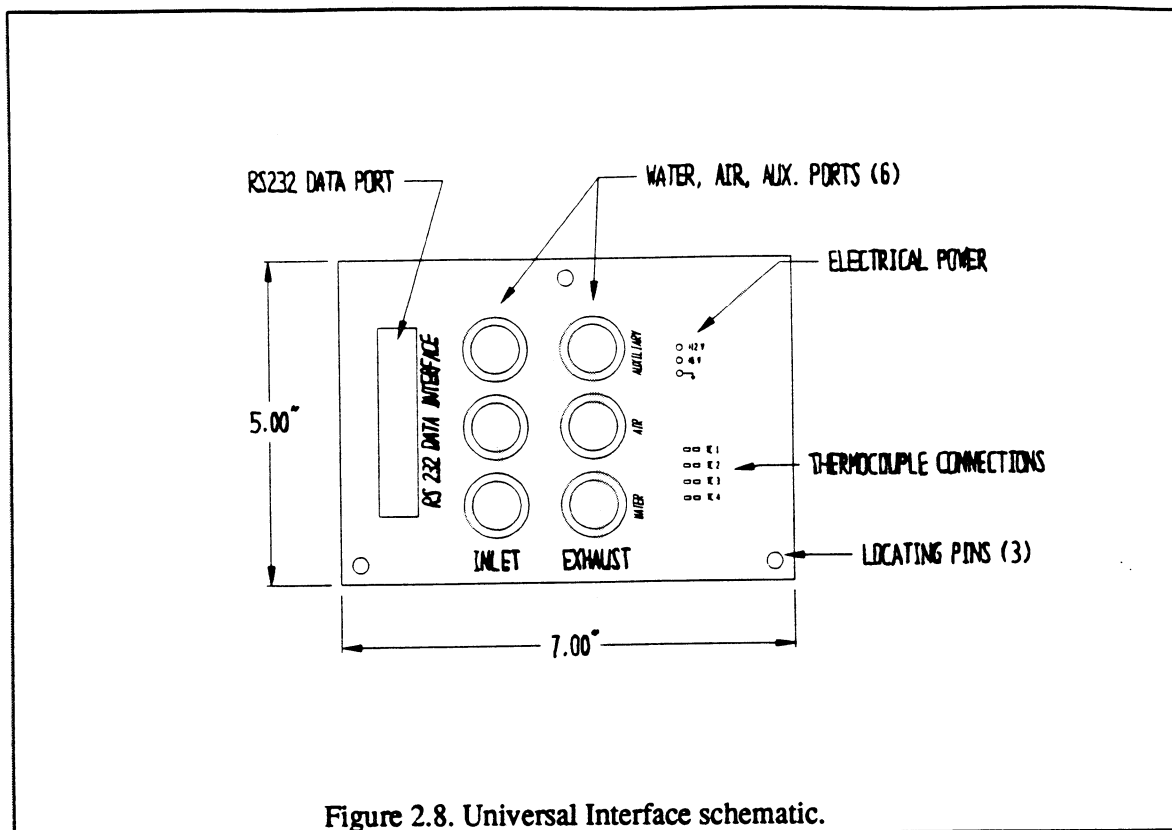
2.4.4 Universal Interface Design

To make the Universal Test Facility (UTF) more versatile, the inputs and outputs to the experiments must have a generalized format. These generalized inputs and outputs make up the universal interface. The universal interface (UI) makes the UTF more versatile. The UI provides the input and output of the resources that Space Station Freedom supplies, the resources from the storage tanks, and the data link to the on board computer. A UI lies behind each of the canisters, making all the experiments active. The decision to use a UI, making all the sites active, avoids the need for a robot to move canisters, test tubes, etc. from active to latent sites within the facility. The use of the UI allows some of the experiments which require constant access to resources to sustain the experiment.

The UI has two standard input and output jacks. These jacks are for the air and water that the Space Station supplies. In addition, the UI contains an extra input and output jack that connects the experiment to the storage canister. This connection allows the experiment to supply its own additional that the UTF does not provide in the storage canister. The connection also removes exhaust products that Space Station can not recycle to the storage canister for later disposal. The UI provides the link for power and data transfer. The data port transfers instructions from the on board computer to the experiment. Also, this port allows the use of the telerobotics system discussed in section 2.4.5. (See Figure 2.8)

2.4.5 Telerobotics System Design

The ability to communicate with the automated Universal Test Facility, while in space, is necessary for the monitoring of the experiment. For example, if an experiment is not performing as it should, the researcher will have the option to try to correct the problem in order to salvage the experiment. On the other hand, if the experiment performed successfully to completion, the researcher will be able to download the data in order to analyze the results. These examples demonstrate the need to have the ability to interact with the experiments being conducted in the Universal Test Facility from Earth. Thus, the Universal Test Facility has included a telerobotics system in order to allow the experimenter the option to interact with the experiment while it is in space.



In general, a telerobotics system connects the user to his experiment from ground control via a simple PC terminal. The connection permits the transmission of electronic data signals to and from the test facility in space. The type of data that can be transmitted ranges from new instructions from the researcher to alter variables in the experiment to the experimental data that can be downloaded to the ground by the data acquisition computer in the test facility. The link between the space station and the ground is via a direct path to the space station if in synchronous orbit or via an optional satellite link up. The telerobotics system is also used to control movement of the two monitoring cameras.

A personal computer acts as the processor for the incoming and outgoing signals. The researcher, utilizing the PC terminal, can view the experimental data, and if needed, view a picture of the actual experiment which is currently in progress. Upon viewing the progress of the experiment, the researcher can enter an interactive software program, e.g. LABview, in order to input new variables to be relayed to the experiment. This ability gives the experimenter a way to alter the experiment from the ground. Thus the researcher is given a greater sense of control of his experiment and ultimately a higher rate of success.

2.5 Conclusion

With the conceptual designs of the universal test facility complete, the design objective is satisfied. Specifically, the identification of six microgravity experiments, which our rack design is able to accommodate, makes the design "highly marketable" to researchers and industry, alike. The ability of the design to sustain multiple and diverse experiments within the same rack fulfills

another key goal. Finally, with the development of the UI, optical, and telerobotics systems, a high level of automation is reached, essential to the successful completion of each experiment.

2.6 Recommendations

Hardware identification dominates the next design phase for the Universal Test Facility. The first step should be the design of the plumbing system in the rear of the rack. The type of hose and connectors, as well as the computer controlled solenoid valves, need to be selected. Next, the HVAC system to be used in the rack should be designed. The utilities section of the rack, which includes the pumps and filters for the various fluids, should be designed in order to supply the needed pressure and volume of fluid to the experiments. Also, the data acquisition system and computer control system need to be identified. Finally, after the bill of materials has been completed, a detailed cost analysis of the rack design should be undertaken.

3 Automated Protein Crystal Growth Facility

3.1 Summary

3.1.1 Design Objective

The goal of this design project is to develop an interactive protein crystal growth facility for Space Station Freedom. This protein crystal growth facility must include a sensing device to monitor crystal growth and an electronic control system for automatic growth. Our design objective also includes the design and fabrication of an end effector to be used with the current Zymate II system that allows for fully automated protein crystal growth in space.

3.1.2 Abstract

A customer for the protein crystal growth facility fills the specially designed chamber with the correct solutions, fills the syringes with their quenching solutions, and submits the data needed for the proper growth of their crystal. To make sure that the chambers and syringes are filled correctly, a NASA representative may assist the customer. The data needed is the approximate growth time, the growth temperature, and the desired crystal size, but this data can be changed anytime from the ground if needed. The chambers are gathered and placed into numbered slots in special drawers. Then, data is entered into a computer for each of the chambers. Technicians map out when each of the chamber's growth should be activated so that all of the chambers have enough time to grow. All of this data is up-linked to the space station when the previous growth session is over.

Anti-vibrational containers need to be constructed for the high forces encountered during the lift off and the landing of the space shuttle, and though our team has not designed these containers, we do not feel that there is any reason why a suitable one could not be made. When the shuttle reaches the space station, an astronaut removes a drawer of quenched chambers from the growth facility and inserts a drawer of new chambers. All twelve of the drawers can be replaced in this fashion. The optical disks can also be removed this way. The old drawers are stored for the trip back to earth.

Once inside the growth facility, a chamber is removed by the robot and placed in one of 144 active sites at a time previously picked by a technician. Growth begins when the chamber is inserted into an active site. Then, the sensing system starts to determine the size of the protein crystal. All during the crystal's growth, the customer can view the crystal and read all of the crystal's data, such as growth rate and crystal size. When the sensing system determines that the crystal has reached the predetermined size, the robot is told to pick up a syringe filled with the correct quenchant solution and inject it into the chamber to stop the crystal growth. The chamber is then removed from the active site and placed into its original storage slot. Another chamber is then placed into the active site and the process is repeated in all of the active sites until all of the chambers have completed their growth.

After ninety days (the scheduled time between shuttle visits), the crystal growth is completed, and the old drawers are replaced with new ones. Once the customer extracts the crystals, the chambers are retrieved for future customers.

3.2 Glossary

active sites	- locations within the experimental facility where growth occurs
cap (press fit)	- removable lid on top of chamber used when removing the crystal
CCD	- (charged coupling device) miniature camera used for viewing crystals
chamber	- self-contained capsule holding solutions necessary to grow protein crystals
chromex	- fibrous high molecular weight polyethylene material
CIN	- (code interface node) a specific function in Labview
CRT	- (cathode ray tube) computer monitor display
convolution filter	- a process used for enhancing and filtering images through the use of mathematical operations
Easy Lab controller	- computer that runs the Zymate II robot
experimental facility	- part of the ISPR that contains the robot, end effector, chambers, and syringes
FFT	- (Fast Fourier Transform) process converting image data into the frequency domain for processing and analysis
growth chamber	- site within chamber where actual crystal growth takes place
image conduit	- device used to transmit crystal image to the CCD
ISPR	- (International Standard Payload Rack) modular containment vessel used on Space Station Freedom
keyway tabs	- projections on the side of the chamber which secure the chamber within the experimental facility
Labview	- data acquisition program used to develop user-interface for the control system
MicroMo	- company which supplied the motors of the end effector
PCMCIA	- standard computer interface
pedestal	- platform where the protein solution rests
PET polymer	- Polyethylene Terephthalate
pistons	- devices within the chamber used to extrude solutions into growing area of chamber
plungers	- cylindrical devices located in the active sites used to extrude solution in the chamber
precipitant solution	- solution used to instigate crystal growth
protein solution	- solution consisting of desired protein to be grown
quenchant solution	- diluted precipitant solution used to halt further crystal growth
storage sites	- locations where chambers are stored before and after protein crystal growth
Zyline	- informational source associated with Zymark
Zymark	- company which designed the robot used in our design
Zymate II	- the name of the robot

3.3 Background

3.3.1 Importance of Protein Crystals

The complete understanding of the properties of proteins will provide researchers with valuable insight into many areas which are an integral part of life. Proteins are used by all forms

of life to grow and resist disease. A better understanding of these proteins will enable medical breakthroughs (in the areas of cancer treatments and tissue transplants) to become a reality.

Protein crystals must be grown for study because individual protein molecules are too small for analysis. A protein crystal is simply a regular, repeated chain of protein molecules which is large enough to be analyzed. Certain growing conditions must be maintained to ensure the successful growth of a protein crystal. The optimum temperature range is between 4 and 25 degrees Celsius. Specific concentrations of growing and quenching solutions are required for crystal growth. These vary depending on the type of protein crystal. The length of time required for crystal growth also depends on the type of protein.

The growth of protein crystals on Earth is altered by convective effects. A two-dimensional crystal is formed by buoyancy-induced flows caused by density gradients within the growing solution. In microgravity, these convective effects are negligible and a three-dimensional crystal with an improved internal structure is produced. Computer analysis performed on crystals grown in space is superior to that performed on Earth grown crystals. Figure 3.1 compares space grown and Earth grown crystals.



Figure 3.1 Comparison of protein crystals grown in space (top) and on Earth (bottom).

3.3.2 Vapor Diffusion Method

Vapor diffusion is a common method of growing protein crystals. Crystalline material and precipitating salts are combined with a drop of solvent and suspended by surface tension over a higher concentration of the same precipitating salts. Low vapor pressure is produced by the concentration gradient in the gas-tight chamber. This procedure causes the solvent to evaporate from the suspended drop. Crystal nucleation occurs as the volume of the drop decreases and the protein concentration in the drop approaches its saturation point. Crystalline material collects around the newly-formed nuclei and forms a crystal. This growth process continues until a quenchant solution is introduced into the chamber.

3.3.3 Sensing

The sensing system for the automated protein crystal growth facility is based on the facility designed by W. Z. Zuk and W. M. Rosenblum.¹² The sensing system is designed with the observer (scientist) in mind. The primary concern for the experimenter is the system's ability to automatically initiate, monitor, and stop specimen growth successfully for up to 90 days. To fully automate the facility, there is an obvious need for the on-board computer to automatically determine the size of the crystal. A sensing system is needed to transfer details of the crystal image to the on-board computer for analysis. The computer algorithm needs to be designed so that parameters (e.g. temperature and experiment duration) which control growth can be adjusted

automatically. A manual override capability by the terrestrial operator is a desirable feature. It is also necessary to design some level of robustness into the system.

3.3.4 Robot End Effector

One part of the group's design objective is to design and fabricate an end effector to be used with the current Zymate II system that allows for reliable transportation of chambers within the experimental facility. The Zymate II robot is on loan to Vanderbilt University from NASA and is the basis of our end effector design. The current end effector on this system does not operate with our rack and chamber designs. Therefore, a new end effector design is developed that coordinates well with the entire facility. As a result of the rack and chamber designs, two procedures are performed by the new end effector:

1. Transportation of the chambers
2. Plunging of the quenchant solution.

3.4 The Design Concept

3.4.1 Protein Crystal Chamber

3.4.1.1 Previous Chamber Designs

NASA designed a chamber for its previous protein crystal programs. We incorporated many of their ideas in our design. We are using the same vapor diffusion method for growing protein crystals. Their method of containing the precipitant solution by surface tension to chromex (a plastic wool material) is retained. Included in the design is a pedestal on which the protein drop adheres.

Last year's design teams conducted extensive research and design to create a feasible protein crystal growth chamber. We incorporated much of that research and design into our growth chamber design. The same PET polymer material is used for the construction of the thin chamber walls. Keyway tabs are located on the side of the chamber to secure the chamber within the drawers of the protein crystal growth facility. The protein crystal drop pedestal consists of a thermocouple (used to monitor the temperature of the crystal) and a heating wire designed by last year's team.

Protein and precipitant solutions are pre-loaded into the chamber. These solutions are separated from each other by a partition within the chamber. These liquids are dispensed onto the pedestal by annular plungers (see Figure 3.13 in the appendix). The outer annular region contains the precipitant solution. A membrane (a high molecular weight polyethylene) initially restrains the movement of the precipitant until it is extruded at which time the resulting pressure breaks the membrane and the precipitant is permitted to flow. The precipitant flows into the chromex and clings to the chromex by means of surface tension. Fritted glass keeps the precipitant from floating into the interior of the crystal chamber and disrupting the growth of the crystal. The porous nature of the fritted glass allows the vapor diffusion method for growing crystals to occur within the chamber.

3.4.1.2 New Chamber Design

The new chamber (Figure 3.11 in the appendix) has a diameter of 0.885 inches and a height of 1.45 inches. Two annular regions contain the protein solution (inner annular region) and the precipitant solution (outer annular region). When the chamber is placed into the active site,

these solutions are automatically extruded by means of concentric cylinders located in the active site trays (see Figure 3.2).

The inner annular region contains the protein which is extruded onto the pedestal. This solution is contained in two ducts on opposite sides, each of which makes up 1/8 of the total ring (the other 6/8 of the ring is made of the same PET polymer). These ducts are 0.4 inches in length. The lower 0.5 inches of the ring is completely empty except for the annular pistons. A diagram of this configuration can be seen in Figure 3.12 in the appendix. This solid section provides a good place for the chamber to accept the force of the spring that is exerted during the insertion and during the entire cycle in the active sites. The piston configuration for this ring has a portion 1/16 inches by 1/8 inches that makes a full circle. The pistons extend 0.3 inches into the ducts during the extrusion process. The tip of the projections leaves a space of 0.05 inches between it and the top of the ring section. This correlates to 13 μ l, which must be added to the desired drop size in order to extrude the right amount onto the pedestal. Like last year's design, the protein solution is extruded through six 1/64 inch diameter holes which are obliquely machined within the mixing ring. The resulting vortex type motion and turbulent flow assure adequate mixing of the protein and the precipitant within the protein solution.

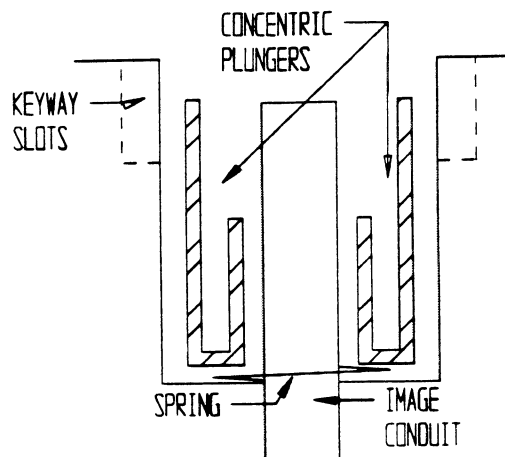


Figure 3.2 Concentric Plungers in the Active Sites

The quenching process is accomplished through the use of an external syringe (see Syringe section 3.4.1.3) interfacing with a rubber septum in the top of the chamber. The syringe also fills the growth chamber with the appropriate amount of quenchant solution. After the growth is halted, the chamber is removed from the active site and returned to the storage trays. The quenchant solution provides a safe medium for the transport of the crystal back to earth. When the protein crystal is ready to be removed from the chamber, the cap is removed and the solutions are poured from the chamber.

The 0.26 inch tunnel which runs through the center of chamber allows for the image conduit which is used to monitor crystal growth (see section 3.4.3). The wires for the thermocouple and heating element run up this conduit and hit contacts under the pedestal. The light needed to view the crystal is provided by interior lighting contained within the experimental facility (see section 3.4.2). The cap is made of a transparent hard plastic so that light can illuminate the protein crystal.

The 0.26 inch tunnel which runs through the center of chamber allows for the image conduit which is used to monitor crystal growth (see section 3.4.3). The wires for the thermocouple and heating element run up this conduit and hit contacts under the pedestal. The light needed to view the crystal is provided by interior lighting contained within the experimental facility (see section 3.4.2). The cap is made of a transparent hard plastic so that light can illuminate the protein crystal.

The chamber has specially designed grooves which allow for a simple and secure interface with the end effector gripper arms. Due to repeatability problems with the robot, the rings on the chamber's bottom are tapered.

3.4.1.3 Syringes

The design of our protein crystal growth chamber necessitates the use of a syringe to quench the crystal. A diagram of the syringe and its dimensions can be seen in Figure 3.3. An entire tray in the experimental facility is used for the storage of these quenching syringes (see section 3.4.2.2). These syringes are designed so that the dispensing of the quenchant is accomplished through the use of the plunger mechanism on the end effector (see section 3.4.5). The needle of the syringe interfaces with the rubber septum of the chamber. This connection is air-tight and secure so that the quenchant does not leak out and float throughout the interior of the ISPR. The needle is designed to prevent the liquid flow from destroying the protein crystal. Again, the syringe must have specially designed grooves which allow for a simple and secure interface with the end effector gripper arms.

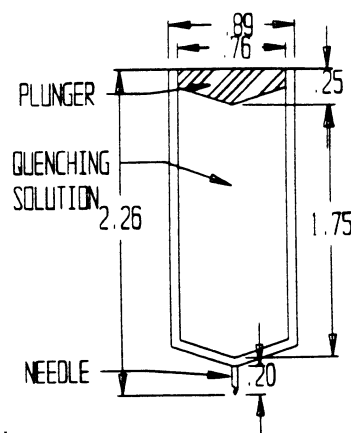


Figure 3.3 Quenching Syringe

3.4.2 Experimental Facility

3.4.2.1 Geometry

The ISPR has specific limits on its spatial dimensions. It is approximately 75 inches by 41 inches with an arc on the back which gives a maximum depth of 36 inches. For our design purposes, a certain amount of space within the ISPR is allotted for the data acquisition equipment, HVAC (heating, ventilation, air-conditioning) units, lighting and sensing equipment.

Robot accessibility to all of the chambers and syringes is a high priority in deciding on the geometry of the experimental facility. The experimental facility containing all of the chambers, syringes, and the robot approximates a circular configuration (see Figure 3.4). The radius of this circle is 16.25 inches with the chambers protruding inward 0.5 inches to allow the end effector to grip the chamber. The Zymate II robot is mounted to the back wall with its base embedded in that wall, which enables the robot to extend the entire depth of the facility. Since the robot arm rotates in a circular direction, this circular configuration is best for robot accessibility. This configuration allows for a workable robot arm length which enables the robot arm to reach all chambers efficiently and not to cause interference with chambers when the robot arm is rotating.

To facilitate the configuration of the experimental facility and the mobility of the robot, each of the drawers of the rack is angled towards the center

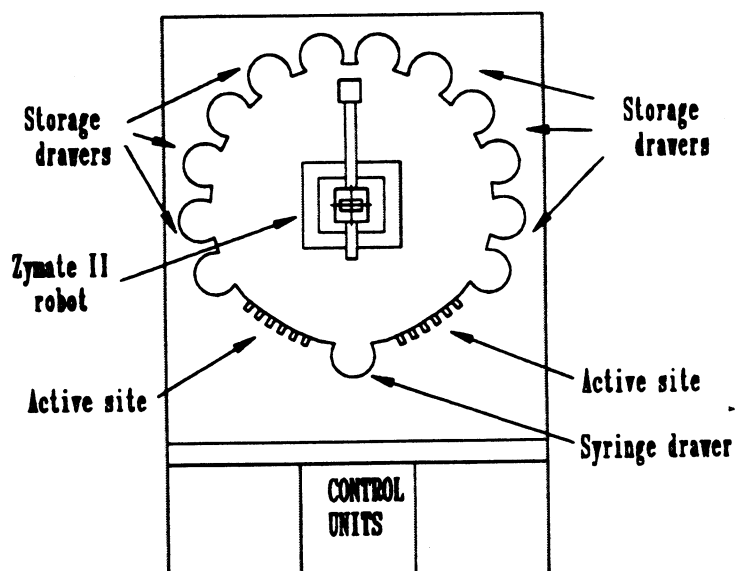


Figure 3.4 Circular Rack Configuration

axis of the Zymate II robot. Furthermore, all of the drawers are designed with the same radius of curvature which allows for secure compatibility between the chambers and the end effector. This consistent radius of curvature also aids in the mass production of the drawers. These drawers are inserted into the sleeve located in the facility and turned 180 degrees to place the drawer in the reach of the robot. The opposite action removes the drawer. A simple spring loaded lock keeps the sleeve at the proper orientation and a unique geometry keeps the drawer from moving in the sleeve after the rotation. The sleeve rotates in a cylinder cut from the rack and is kept in place by the door. Only space for the drawer is allotted in the face of the door. The drawers are designed to be air-tight. The door is 2 in. in depth and covers the front of the experimental facility. The top of the robot interfaces with the door to hold it in place securely. Also, the touch screen display for the control system is located on the door.

3.4.2.2 Active Sites, Storage Site, and Drawers

The design consists of twelve storage drawers (54 chambers per drawer), two active sites (72 slots per site), and a syringe drawer (57 syringes). Each of the twelve drawers is 3 slots across with 1.36 in. spacing and 18 slots deep with 1.23 in. spacing. The total number of storage sites is 684, which satisfies the given requirement of 500. A spring is used to keep the chamber locked in place. The drawer is based on a 5 inch diameter and 27.25 in. length cylinder with portions cut off above and below the axis (Figure 3.5 (top)). The sleeve surrounds the drawer except on the side of the chambers (Figure 3.5 (bottom)). It has a 5.5 in. diameter and a 28 in. length.

The total number of active sites is 144 (72 active sites in each shelf-Figure 3.6). Each slot is spaced 1.9 in. in each direction. The bottom of each site has two concentric cylinders for the purpose of extruding the solutions onto the pedestal and into the chromex. These cylinders are connected to a common base by a spring which is strong enough to extrude the liquid but flexible enough not to cause undue stress on the chamber (Figure 3.2). As mentioned earlier, all of the load is carried by the inner cylinder. The cylinders are not connected to the imaging conduit and the lead wires, so the contacts for the thermocouple and heating element must have a spring like quality.

The syringe drawer is located at the bottom of the circular configuration, and two active site drawers are located on each side. The syringe drawer and sleeve have a configuration very similar to the storage drawers and sleeves. The differences are that the slots are 3 by 19 and the spacing is 1.36 in. and 1.16 in. in the two directions, respectively. The base cylinder also has a larger diameter to account for the fact that the syringes are longer. Also, the spring bottom which holds the syringe in place must be formed to the syringe's dimensions and have a hole in the center to allow for the needle.

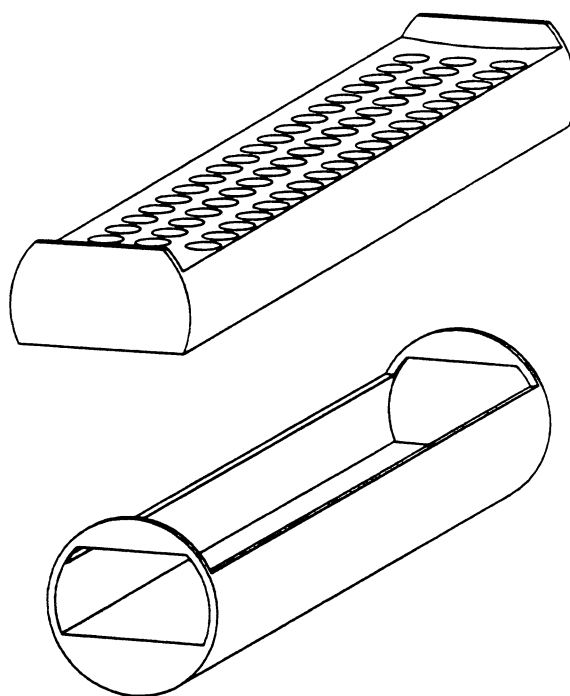


Figure 3.5 Storage Drawer (top) and Sleeve (bottom)

3.4.3 Sensing Device

3.4.3.1 Light Diffraction Method

To satisfy all of the investigator's requirements, it was necessary to consider sensing mechanisms other than the light diffraction method. The problem with the light diffraction method is that a true visual image of the crystal could not be obtained during the growth process. The light diffraction method also requires the use of pyrometric equipment which would not realistically fit within the physical constraints of the rack. Another problem with the light diffraction method is the number of media light needs to pass through prior to and after crystal penetration. Basic refraction theory explains that as the concentration of media changes, the angle of refraction differs accordingly. This is the basic principal of the diffraction method used in determining crystal size. Interference caused by the number of media involved (including the surface of the bubble and transparent shielding) will hinder the accurate determination of crystal size.

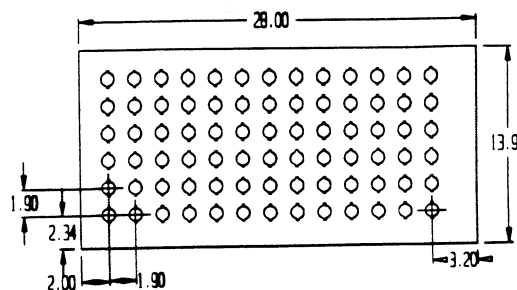


Figure 3.6 Active Site Shelf

3.4.3.2 Two Possible Sensing Methods

A CCD camera was provided by NASA for use in the crystal sensing design. An experiment was conducted using the CCD to determine whether or not the camera has a good picture quality. The optimum position of the light source relative to the camera also needed to be determined. Since it is desirable to see the start of crystal formation for crystals as small as 50 μ m, it is necessary to use magnification along with the CCD camera. Various lenses were considered and analyzed for accomplishing this task. Of the lenses available in an "Edmund Scientific" magazine, none were capable of accomplishing the magnification requirements needed to produce a large crystal image. However, a CCD microscope adapter was found which can produce magnification up to 180X. The two possible set-ups which were analyzed for use of the CCD and the microscope adapter are explained below:

1. Without Image Conduit--This configuration consists of the CCD camera connected to a microscope which is focused directly onto the crystal droplet through the in the bottom of the protein chamber.
2. With Image Conduit--This configuration consists of the CCD camera connected to a microscope which is focused onto the end of a piece of image conduit. Image conduit is a flexible, glass-like tube through which an image may be transported. The image conduit runs from a given location through the porthole in the chamber to a point just beneath the protein droplet.

According to Professor Richard F. Haglund of the Vanderbilt University Physics Department, either configuration will work. The set-up without an image conduit is best if cost is a major problem. Cost was not the only factor to be considered. Due to the large size of the CCD microscope adapter (approximately 1.5 ft long), the cameras could not be placed directly beneath the active chamber sites. Therefore, the image must be sent to a location where the microscopes can be placed. This image piping is accomplished through the use of image conduit. It has not yet

been determined where the microscopes will be placed. They will probably be located in the empty spaces around the inactive sites. Several simplifying assumptions are made:

1. Since the droplet is located in a plane parallel to the end of the image conduit, there is minimal or no refraction to distort the image.
2. There will be plenty of room around the inactive sites for the microscopes.
3. The robot will not interfere with the light inside the rack.

3.4.3.3 Selected Sensing System

The selected sensing system (see Figure 3.7) is based on the use of a CCD (Charged Coupled Device) camera which is attached to each active site. The visual image captured from each camera is digitized and processed to obtain the dimensional information which is the key factor in determining the success or failure of the sample. The primary advantage of using a CCD camera is the ability to present the actual visual image to the scientist as well as providing the crystal information to the on-board computer for automatic analysis.

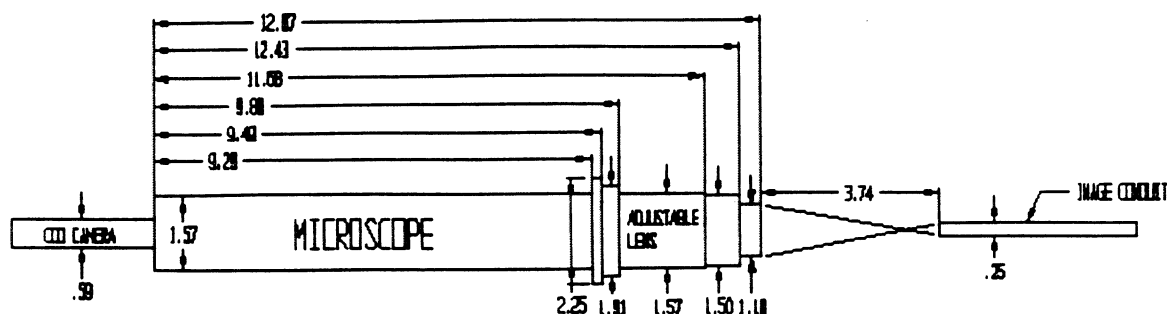


Figure 3.7 Selected Sensing Device

The first step in automatically determining the size of the protein crystal involves digitizing the crystal's image. After the digitization, the image is processed using a convolution filter, FFT (Fast Fourier Transform), and a geometric operation. The convolution filter is used to implement Laplacian filters primarily to separate the crystal edges from the background. The FFT converts the digital image from the time domain to the frequency domain which removes noise from the image. Geometric operations are performed to magnify the image to obtain an optimal result from the image analysis. The validity of using a CCD camera and digital filters for image processing is shown in various papers.^{1,2}

A simulation was conducted using the CCD camera so that we could test the imaging process and camera resolution. In order to simplify the simulation, several assumptions are made:

1. A 15 mm lens attached to the CCD camera is the only optical magnification lens used.
2. Surface of the drop is simulated using a thin plastic film.
3. Light source is positioned directly below the surface.
4. Image is digitized from an image on a VCR tape.
5. Color image is used instead of black and white.
6. Image conduit is not used in the simulation.

Note: These assumptions were made because of limited resources as well as the need to simplify the process.

3.4.3.4 Lighting within the Chamber

Accurate detection of the micron-size crystal within the growing bubble is a challenge. The image of the small crystal must be separated from the background clutter by properly contrasting the image. Light must therefore illuminate the crystal so that an image can be obtained with the CCD camera.

Several options are available for the positioning of the light source relative to the crystal and camera.:

1. The crystal growth site could be illuminated from the direction of the camera
2. The crystal could be placed between the camera and the light source (the selected method).
3. The crystal could be illuminated from the sides.

The second method is chosen for simplicity and because of spatial limitations. If the light comes from the direction of the camera, then it would be necessary to slightly enlarge the diameter of the image path to allow light to pass on the outside of the image conduit. Similarly, lighting from the sides would be achieved by "piping" light through optic fibers to the growth site. Both of the above methods, however, require the reduction of space allocated for the radial plungers and for the necessary wall thickness. Lighting the crystal from behind using the background lighting in the rack, simplifies the chamber design and provides for the best image. The chamber lid is transparent so light can pass from the light sources mounted on the walls of the rack to the crystal. Polarized light is used in order to deliver optimum contrast between the crystal edges and the background. It is assumed that background clutter does not interfere with crystal detection because only the crystal growing area lies within the focal length of the sensing system.

3.4.4 Electronic Control System

The control system is designed to have the following functions:

1. Initiate the experiment
2. Obtain and store visual information
3. Control and monitor the heating units
4. Analyze information
5. Control the mechanical manipulator
6. Supply the principal investigator (PI) with necessary information
7. Allow investigator to have control over the experiment with minimal training
8. Operate with minimal power requirement
9. Easy to maintain the components by modular design
10. Easy to re-task depending on the sample
11. Allow a multiple-user environment

The key element of this design is a strong emphasis on the use of a computer to automate this facility. The Intel 486 DX4 based laptop computer was selected to obtain maximum performance at a relatively low power consumption. Also, the computer will use Windows NT from Microsoft Corporation for its preemptive multitasking capability which allows sharing of the processor time necessary to finish the task efficiently. The computer is equipped with an image processing board, a data acquisition board, a PCMCIA removable 1.8 inch hard drive, maximum memory size, and a writable optical drive unit (instead of a floppy disk unit).

The computer is equipped with a DT 2867 integrated image processing board from Data Translation Inc. The DT 2867 was selected over other available boards because of its ability to perform two functions. This board grabs the frame (frame capture) from the analog image and processes the image with the necessary filter with minimal reliance on the main computer system. This on board processing capability is necessary since the computer needs to handle numerous tasks other than image processing. The DT 2867 is capable of handling a math-intensive convolution filter which is processed by three dedicated math processors on the board.

The user interface of this system is designed based on the need to automate the protein crystal growth facility for extended periods of unmanned operation. The user is not concerned with the computer algorithm which creates the user-friendly menus. This system allows multiple users to share the facility. This system also allows the user the ability to alter the experimental parameters on each sample.

There are two main screens

available in the user interface. The automated mode, which only displays information, is shown in Figure 3.14 in the Appendix. The manual mode allows the change of the growth temperature and the estimated time remaining in the growth process. This screen is shown in Figure 3.14 in the

Appendix. Each mode utilizes a touch screen interface with a stylus pen and a ten-key keyboard. Each scientist receives a security code which prevents the parameters of the experiment from being accidentally changed by someone else. The flow charts for the automatic and manual operation of the control system are seen in Figures 3.8 and 3.9. An overall layout of the control system is shown in Figure 3.15 in the Appendix. The system designed is based on the Labview 3.01 control system for Windows NT from National Instruments. To control each component, the code interface node (CIN) of Labview is used.

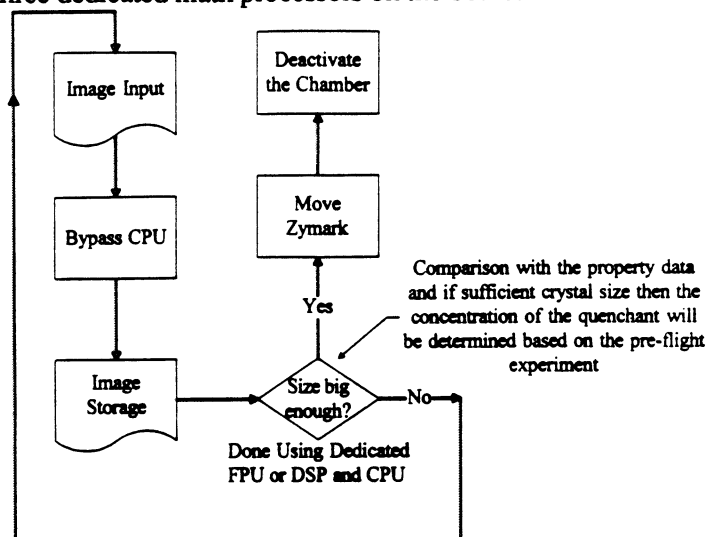


Figure 3.8 Automatic Mode

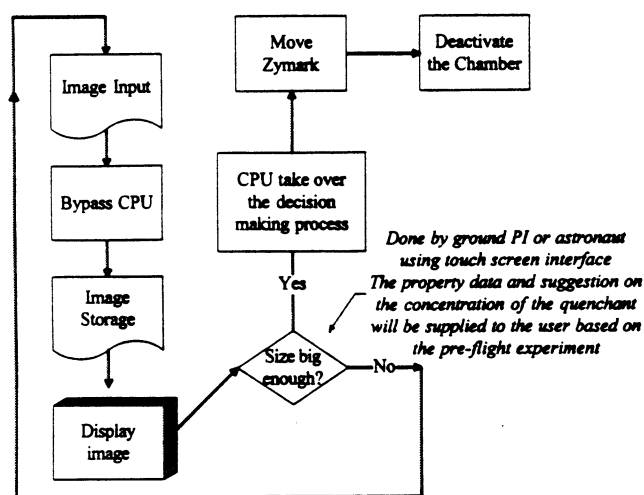


Figure 3.9 Manual Mode

CIN's are the interfaces between Labview and Pascal, C, or C++ based code. This CIN is used to control the DT 2867 image processing board, heating elements, and Zymate robot.

The graphical user interface is the same on ground and on board. The user interface is based on two different displays. These displays are the active matrix technology on board Space Station Freedom and the regular CRT on ground with the same capability. One of the displays is used to supply the user with a real time image from the CCD camera. The other display is designed as an input console using Labview.

This system is based on the use of a black and white micro charged coupled device (CCD). Images are directly deposited onto the optical storage device for further analysis. Most of the image processing, including filtering and magnification of the image, are done within the DT 2867 board. The board supplies Labview with the necessary information to control the experimental parameters. Labview determines the experimental parameters based on the pre-determined information, such as duration of experiment, maximum size of crystal and acceptable temperature range. Pre-determined information is retrieved from the PCMCIA based hard drive, which stores the operating system, as well as the experimental parameters of each sample in ASCII format. If the conditions are satisfied, then Labview initiates the CIN command to begin the deactivation of the chamber. The chamber is deactivated with a syringe containing the proper concentration of quenchant solution. Then, the Zymark robot places the chamber in a non active site for storage. To make this facility successful, it is imperative that extensive ground based simulation is done to obtain the information necessary from preflight experiment and the simulations.

Several assumptions are made to make this preliminary stage of design possible:

1. The switching system for heating, and imaging is neglected to simplify the design
2. Detailed programming of Labview is neglected
3. The Zymark robot can be controlled by using C++, C, or Pascal
4. The Programming of the DT 2867 image processing board using C++ is neglected
5. The selection of an image storage device is neglected
6. Communication with the space station and ground is done through a parallel port
7. A high capacity PCMCIA hard disk drive is available (approximately 240 MB to 320 MB)

The advantages of the current design are:

1. All the data is stored in the optical drive before any analysis is done.
2. Minimal training is necessary to operate the system.
3. It is a sufficiently fail safe system to allow multiple user environment.
4. Low power consumption is used by the laptop computer components.
5. It is relatively easy to re-task and update the system by use of PCMCIA storage device.
6. It is easy to maintain in case of component failure since it is modular.

The disadvantages of the current design are:

1. It need extensive modifications of the stock components.
2. Each component of the system must be integrated.
3. There is a high cost associated with employing the CCD cameras on each active site.
4. Extensive programming for the image processing board, the Zymark, and the switching devices for the heating and imaging elements must completed.

Recognizing the fact that this is a preliminary stage of design it is necessary to determine the validity of each component for the next stage of the design.

3.4.5 Robot End Effector

3.4.5.1 Zymate Robot

The Zymate II robot has six degrees of freedom and is operated by the EasyLab Controller. EasyLab uses seven primary commands to move the robot:

- Rotary -This controls the rotation motion of the base and has a range from 0 to 360.
- Vertical -This controls the height of the arm and has a range from 0 to 30.
- Reach -This controls the extension on the arm and has a range from 0 to 30.
- Wrist -This controls the rotation motion of the arm and has a range from 0 to 360.
- Grip -This controls the gripping motion of the gripper arms and has a range from 0 to 30.
- Syringe -This controls the syringe on the end effector and has a range from 0 to 30.
- Home -This command sends the robot back to the home position.

The above ranges are displacement values used by the EasyLab Controller; they are not distances. The use of the commands is quite simple. To extend the arm to its maximum distance the operator would type the following in the direct robot control mode or into a program; reach=30. In general, the method for using the commands is: command name=value. Two commands, grip and syringe, control the motions of the end effector.

Zyline provided information on the internal workings of the robot and end effector. There are two 6 volt DC servo motors inside the end effector housing. A circuit board is also contained in the housing that controls the electronic components of the end effector. The robot arm outputs 6 volts to the end effector in order to operate the two motors and the sensing mechanisms. By examining the end effector and its movements, it is determined that the gripper arms and syringe operate using a rack and pinion system.

The gripper arms travel at 1.07 cm/sec and the syringe travels at 1.36 cm/sec. This information is used to help determine the gear ratios for the motors in our end effector. The end effector and arm connect electrically by means of 12 pin connectors with the female receptors being on the end effector

3.4.5.2 Overall End Effector Design

The end effector is composed of two primary components: the gripper arms and the syringe plunger. The gripper arms can move linearly from an open to a closed position, and vice versa. The mechanism to provide this motion is a double rack and pinion configuration. The syringe plunger also operates in a linear manner which is accomplished through a single rack and pinion configuration (see Figure 3.10). The gripper hands are located on the center line of the robot arm. Similarly, the syringe plunger is centered between the hands with the linear travel occurring along the axis of the robot arm. The rack and pinion systems are each powered by a 6 volt motor from MicroMo. Attached to each motor is a gearhead from MicroMo to provide the necessary step down ratios needed for the system. A circuit board to control the motors and force sensors is also included in the design. Each gripper hand has a strain gauge to serve as a force sensor to control the motors. The above components are all encased in a plastic housing which will fit the arm on the Zymate II robot. The two motions can still be achieved using grip and syringe commands in the EasyLab controller.

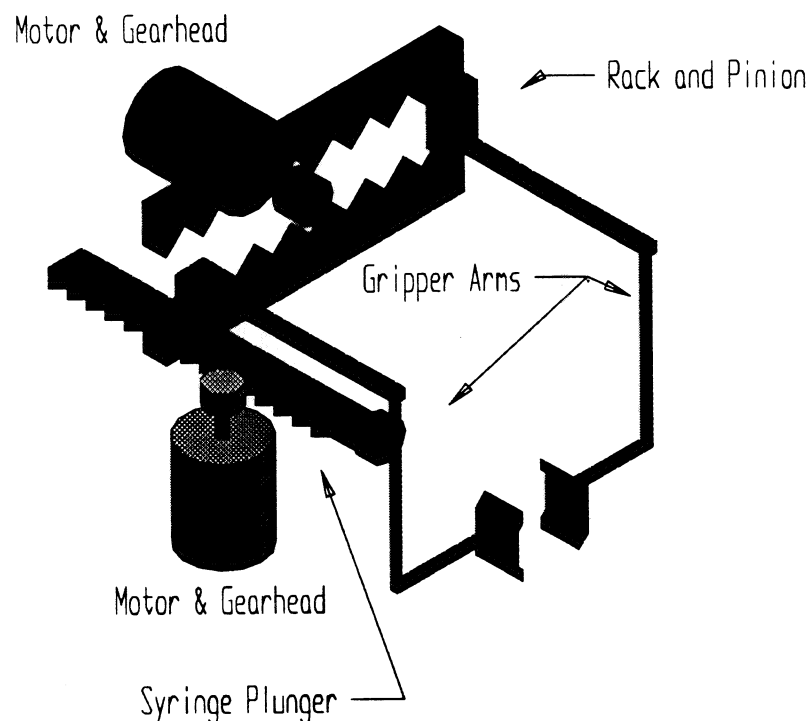


Figure 3.10 End Effector Design

3.4.5.3 Gripper Arm Design

The gripper arms serve two primary functions in the automated protein growth facility. First, the arms grip the chambers so that they may be locked and unlocked into the active and storage sites. Secondly, the arms grip the chambers and syringes so that they can be moved about the facility.

The chambers, when transported about the facility, must be locked and unlocked into the active and storage sites. This procedure requires a pushing and twisting motion to engage the chamber into the keyway (see also chamber design). The wrist and arm on the robot provide rotating and pushing motions, respectively. To utilize these movements, it is necessary to locate the center of the gripper hands along the axis of the robot arm. With this configuration the gripper hands rotate in an on-center fashion when the wrist of the robot rotates. When used with the extending movement of the robot arm, chambers can easily be inserted or removed from the sites.

The gripper arms must also be able to hold the syringes and chambers. To accomplish this task, a simple rubberized male-female notch system is used to ensure a secure fit between the hands and chamber or syringe. It should be noted that while this is an important part of the design, it is not included in the drawings. Located on each gripper hand is a strain gauge that serves as a sensor for the motion of the arms.

The motion of gripping the chambers and syringes is performed using a simple double rack and pinion design (see Figure 3.10). This mechanism is housed in Segment 1 of the end effector (see Figures 3.16 -3.18 in the Appendix). The gripper arms are attached to each of the two racks to provide the linear gripping motion of the arms.

Refer to Section 3.8.2 in the Appendix for a detailed list of the specifications on the racks and pinion used in the end effector.

3.4.5.4 Syringe Plunger Design

The plunger on the end effector is used to dispense the quenchant solution from the syringe into the chambers. The syringe plunger design closely relates to the gripper arm design. Due to the gripper arms location on the center line of the robot arm, it is also necessary to orient the plunger in a similar fashion. This enables the syringes to be plunged easily while being held by the gripper arms. The linear motion of the syringe plunger is achieved using a single rack and pinion configuration (see Figure 3.10). The mechanical components of this mechanism are housed in Segment 2 of the end effector (see Figures 3.19 - 3.21 in the Appendix).

The reader is referred to Section 3.8.2 for a detailed list of the specifications on the rack and pinions used in the end effector.

3.4.5.5 Motors and Gearheads

The movement of the gripper arms and syringe plunger is accomplished by using small DC servo motors and gearheads. Two identical motors were selected from MicroMo use in the end effector. The motors selected are used by Zymark in their end effectors and were chosen because of their small size. To achieve the necessary linear speeds for both the gripper arms and syringe plunger, two gearheads were selected from MicroMo. These were chosen because of their small size and easy compatibility with the motors. The gripper arms have a linear travel speed of 1.07 cm/sec. A gearhead with a step-down ratio of 548:1 was chosen to provide the needed rotational speed for the gripper arms. The syringe plunger has a linear travel speed of 1.36 cm/sec. A gearhead with a step-down ratio of 308:1 was chosen to provide the needed rotational speed for the syringe plunger.

A motor mounting plate was designed to enable the connection of the motor and gearhead system to the housing (see Figure 3.22).

3.4.5.6 Fabrication

Part of the original design goal was to fabricate a working end effector. Due to several unforeseen obstacles, the fabrication of our end effector design was unable to be completed. The majority of the work has been finished on the end effector. There are only a few small details that need to be completed before the fabrication can begin. First, the rest of the parts needed for the end effector would have to be ordered. Secondly, detailed calculations of the required torque for the gripper arms and plunger would need to be performed. Finally, consideration would have to be given to tolerances for the gearing components.

Several parts have already been ordered from Zymark:

- 2 MicroMo DC Motors
- 1 Wire Harness
- 1 Circuit Board
- 1 Hand Connector Housing

Refer to Section 3.8.2 for a detailed listing of the parts used in the end effector.

The determination of the step-down ratios for the gearheads was done as an approximation. It is not to say that the values calculated should be ignored, but rather reexamined before fabrication. The selection of the gearheads was done by trying to match velocities. Required torque for the gripper arms and syringe plunger was not considered.

A detailed set of machine drawings was generated for Segment 1, Segment 2, and the Motor Mounting Plate. It should be noted that these drawings do not include any tolerances for the gearing mechanisms.

Before fabrication can begin, the tolerances and spacing between the two rack and pinion systems should be considered. This is needed to prevent backlash during operation. If consideration is not given to the tolerances and spacing, binding or skipping can occur in the gear systems. For the two rack and pinion systems in the end effector, tolerances should be not greater than 0.002 of an inch for the center distance between the gears. The Precision Industrial Components Design catalog has a very complete technical section on gear tolerances and spacing. This should be referenced for finalizing the end effector machine drawings.

3.4.6 Robot Simulation

A parametric design software program was used in the design of the growth chamber and rack. I-DEAS CAD and simulation software uses solid modeling as an effective way of designing a system in 3-D. The design process can be substantially accelerated because of the increased visualization capability. I-DEAS is also used in the kinematic simulation of the overall system. Interference and motion limitations are identified at an early stage in the design and can, therefore, be taken into account.

3.5 Conclusions

3.5.1 Overall Progress

The objective of this design project was to develop an interactive, automated protein crystal growth facility. Our focus was to continue the overall design efforts of last year's design teams. Our design involved the integration and development of the protein crystal chambers, the experimental facility, the robot and the end effector, the sensing system, and the control system.

3.5.2 Chamber and Experimental Facility

The design of the chamber and facility was not a primary design goal for this year's team. However, the design of the end effector, sensing system, and control system warranted changes in the previous design. Furthermore, several details (dimensions, feasibility, manufacturability, etc.) of last year's design were not considered. This year's design tried to include these details and integrate them with the design of the other systems.

3.5.3 Sensing System

Part of the design objective was to finalize and integrate a feasible sensing system which would be able to detect protein crystal growth within the experimental facility. A visual image is required by the experimenter for evaluating the structure of the crystal. It was also necessary to produce an image that the computer could dimension (so the control system would know when to terminate growth) and store on disk for future reference. The components of the sensing system

had to be sized and arranged in such a way as to fit within the growth facility. The system which was developed integrated the use of a CCD camera, image conduit, and the digitizing part of the control system for monitoring the crystal growth. Although it hasn't been tested, we feel that the chosen design will work, or least provide a strong basis for further research in this area.

3.5.4 Control System

Another aspect of our design included the selection and integration of a computer control system which would provide a user-friendly interface between the growth facility and the multiple number of principal investigators. The control system was designed with strong emphasis on full automation of the facility while still maintaining the ability to alter the experiment. To make this design functional with minimal interference of one experiment with another, extreme care was taken when considering the security and power management system. It is also true that this control system will require more extensive study to make it reliable and realistic. This is because of the rigorous requirements placed on the system due to the sensitivity of the experiment to any variables introduced.

3.5.5 End Effector

The objective to design and fabricate an end effector to be used with the current Zymate II system that will allow for fully automated protein crystal growth in space has been met for the most part. The end effector performs two primary functions. Firstly, the end effector serves to grip the chambers and syringes. Secondly, the end effector must plunge the syringes that contain the quenchant solution. The gripping movements are achieved through a double rack and pinion mechanism. There are two gripping arms which attach to the racks and provide the means for clamping. The plunging motion is performed with a single rack and pinion system. When operating the plunger extends and dispenses the quenchant from the syringe.

There are several advantages to this design. The end effector design was arrived at because of its simple integration into the Zymate II EasyLab controller. The same two commands will still be able to be used when operating the end effector. Also, no modifications will have to be made to the robot in order for it to work with the end effector. This was an important factor when selecting a design. Limiting the number of functions that the end effector performs reduces the power requirement of the robot. This is important because of the power restrictions in space.

One part of the design objective was not satisfied. The group was not able to have the end effector fabricated. This was the result of several unforeseen obstacles. The material included in this section of the report is complete enough to have the end effector fabricated with minimal additional work.

3.6 Recommendations

3.6.1 Chamber and Experimental Facility

An optimal range of diffusion area and chamber volume that NASA had determined was mentioned last year, but our team was unable to find that information. By changing the height of the chamber or by moving the fritted glass inward or outward new ratios can be attained. These alterations would not cause serious disturbances to the chambers, the drawers, or the facility as a whole. If the chamber is lengthened, it must be remembered that the ring section must be elongated because there will be more liquid to fill the chromex space, and more syringes may be needed to account for volume change in the growth chamber.

As opposed to last year, the solutions are extruded immediately when inserted into the active sites, so the pedestals temperature will take time to attain the optimal temperature. This time lag should not cause a problem, but investigation into the heating time and the affects of the low temperature on the growth should be carried out.

The time it takes for the robot and end effector to insert the chamber into the active site has an affect on the speed which the solution is extruded into the chamber. A high velocity may not be conducive to a drop being properly placed on the pedestal. Also, the velocity of the quenching fluid may harm the crystal even if the stream is diverted. These subjects would need to be tested on actual prototypes in order to give good results.

3.6.2 Sensing

Due to the large number of cameras and other sensing equipment required, a detailed cost analysis needs to be conducted on the sensing system. A test of the system needs to be conducted to determine the reliability of the sensing equipment and its integration within the experimental facility.

3.6.3 Control System

For the future, it is necessary to implement the humidity control as well as a temperature control. The humidity control system could be learned in detail from the paper presented by L.J. Wilson of the Georgia Institute of Technology⁴. Also, as of this preliminary design of the control system, it is necessary to determine the viability of each selection based on the necessary physical and electrical requirements specified by NASA.

3.6.4 End Effector

There are a few areas that need further research and development before fabrication can occur. A detailed analysis of the speed and torque requirements for the gripper arms and syringe plunger needs to be performed. Preliminary calculations were made and appear in this report. This data should be used as a starting point for further analysis. The spacing and tolerances for the gear systems have to be calculated and integrated into the machine drawings. Also, the electrical connections of the system need to be determined. We have the circuit board that Zymark uses on their end effectors. This board should be examined so that connections for the motors and sensors can be determined. Finally, the entire end effector system needs to be qualified for use in space before it can be used in Space Station Freedom.

3.7 References

- (1) W. M. Rosenblum, J. P. Kennedy, and Brad Bishop, "Examination of protein crystals in the hanging drop using digital image capture techniques," J. Crystal Growth, 110, 171-176, (1991).
- (2) W. Z. Zuk, and K. B. Ward, "Methods of analysis of protein crystal images," J. Crystal Growth, 110, 148-155, (1991).
- (3) 1992-1993 NASA/USRA Advanced Design Program, Vanderbilt University, Chs 6-9.

- (4) L. J. Wilson, T. L. Bray, and F. L. Suddath, "Crystallization of proteins by dynamic control of evaporation," J. Crystal Growth, 110, 142-147, (1991).
- (5) Gary Walker, Electronic Technician, Mechanical Engineering Department, Vanderbilt University
- (6) MicroMo Electronic, Inc., 742 2nd Avenue South, St. Petersburg, FL 33701, (813) 822-2529.
- (7) Precision Industrial Components
- (8) Vivian Marchand, Zymark Corporation
- (9) Glennys A. Mensing, Free Electron Laser Lab, Physics Department, Vanderbilt University
- (10) Wayne Anderson, Professor, Biochemistry Department, Vanderbilt University
- (11) Craig W. Morton, Material Sciences & Engineering Group, Applied & Engineering Sciences Department, Vanderbilt University
- (12) Anthony B. Hmelo, Research Assistant Professor, Center of Microgravity Research & Application, Applied & Engineering Sciences Department, Vanderbilt University
- (13) William H. Hofmeister, Research Associate Professor, Material Sciences & Engineering Group, Applied & Engineering Sciences Department, Vanderbilt University
- (14) Richard F. Haglund, Professor, Physics & Astronomy Department, Vanderbilt University
- (15) David R. Delapp, Mechanical Engineering Department, Vanderbilt University
- (16) Joel Barnett, Mechanical Engineering Department, Vanderbilt University
- (17) Robert L. Galloway, Associate Professor, Biomedical Engineering, Vanderbilt University
- (18) Bill Gentry, Supervisor of Machine shop, Mechanical Engineering Department, Vanderbilt University
- (19) Steven W. Peterson, Assistant Professor, Mechanical Engineering Department, Vanderbilt University
- (20) Barry J. Dunn, Smart Structures Lab, Mechanical Engineering Department

3.8 Appendix

3.8.1 Figures

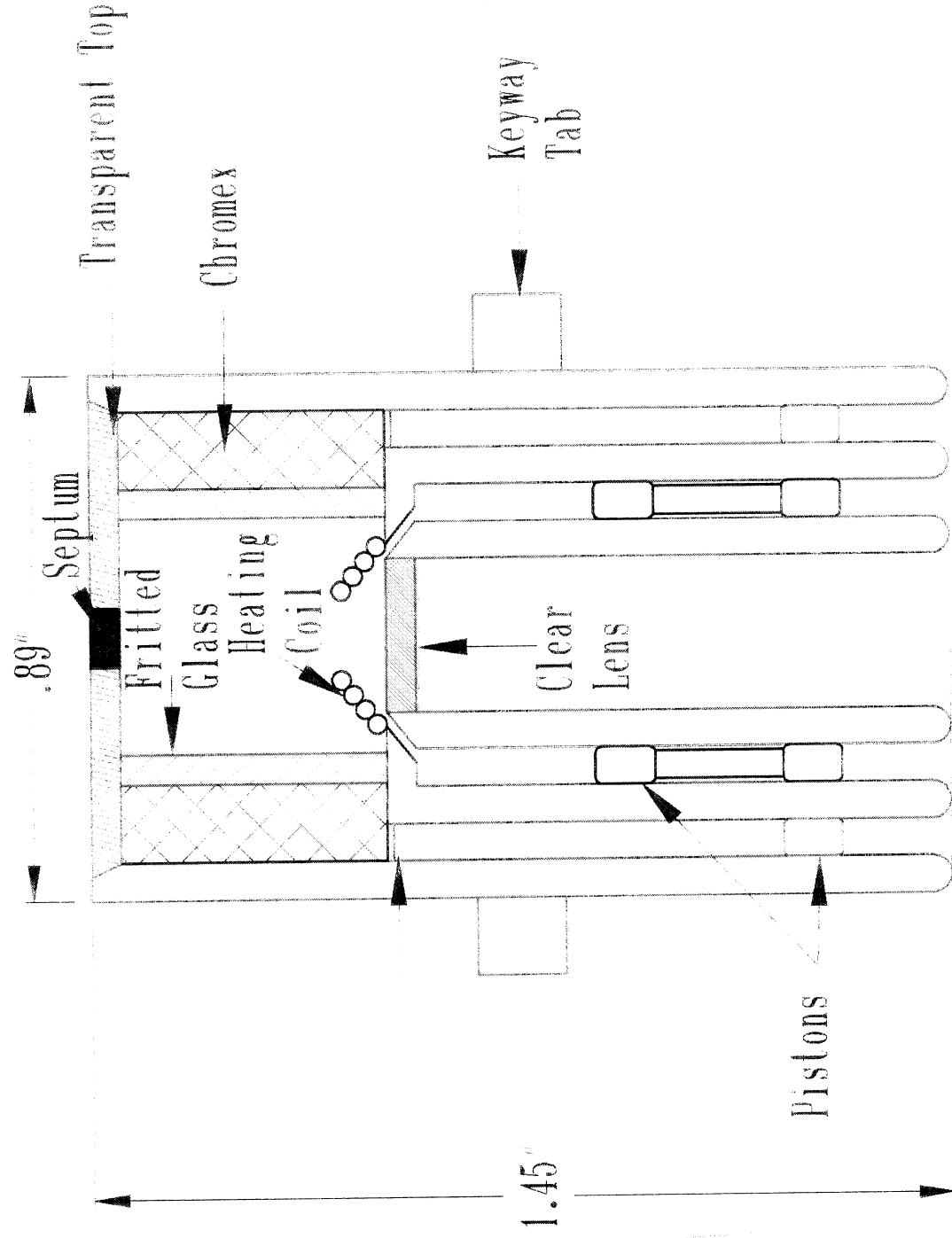


Figure 3.11 Protein Crystal Growth Chamber

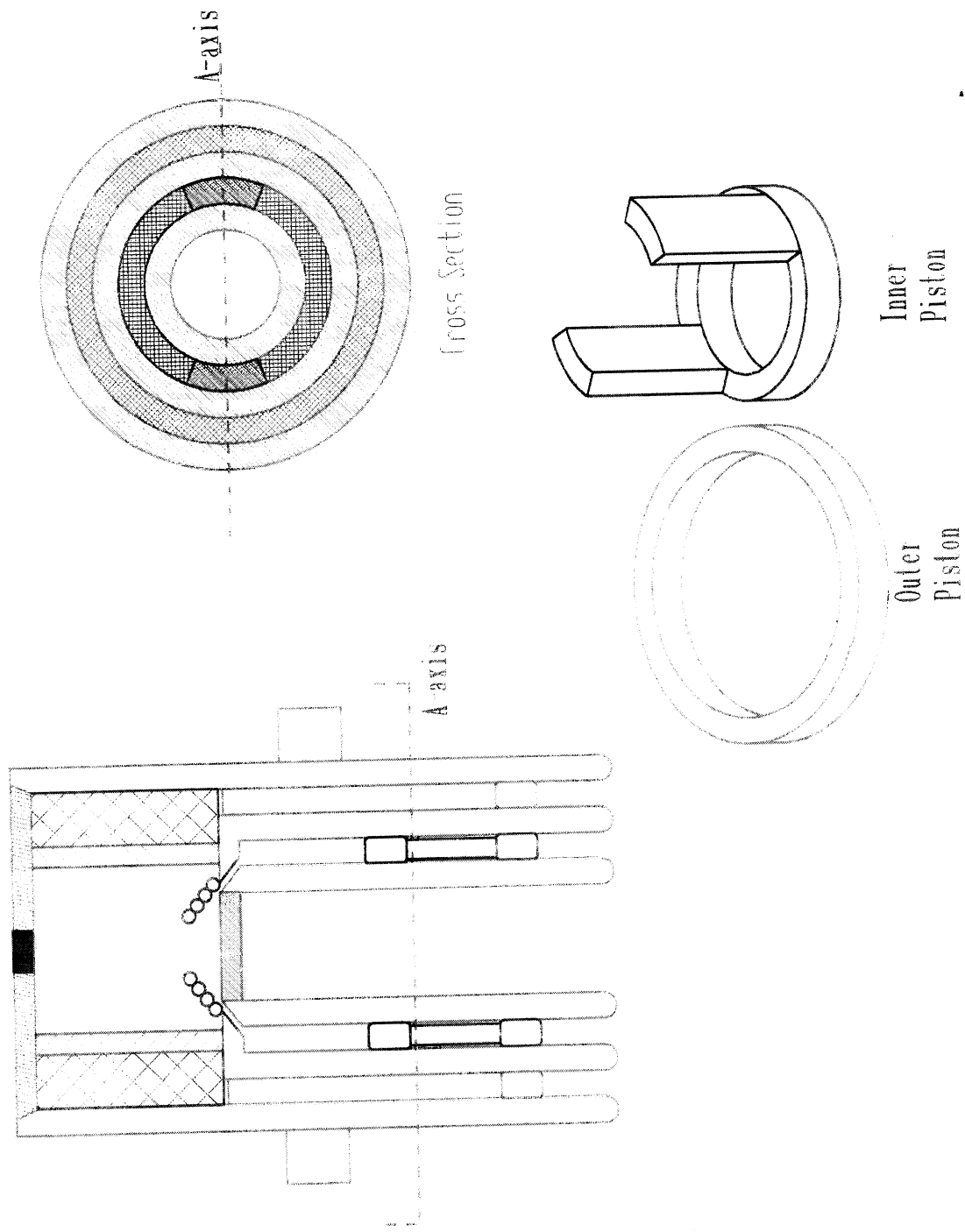


Figure 3.12 Plunger Configuration

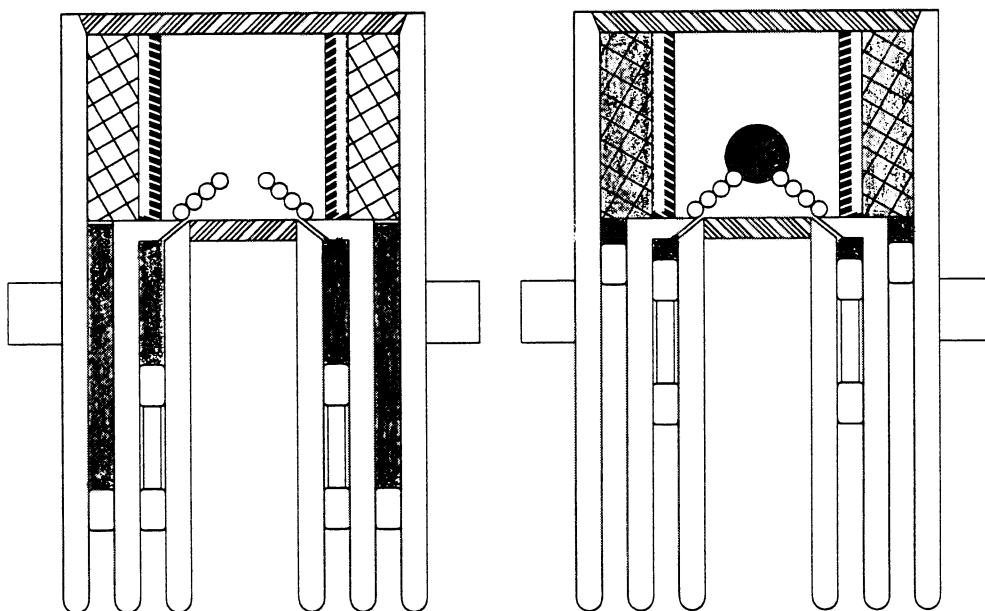


Figure 3.13 Before (left) and After (right) Plunging

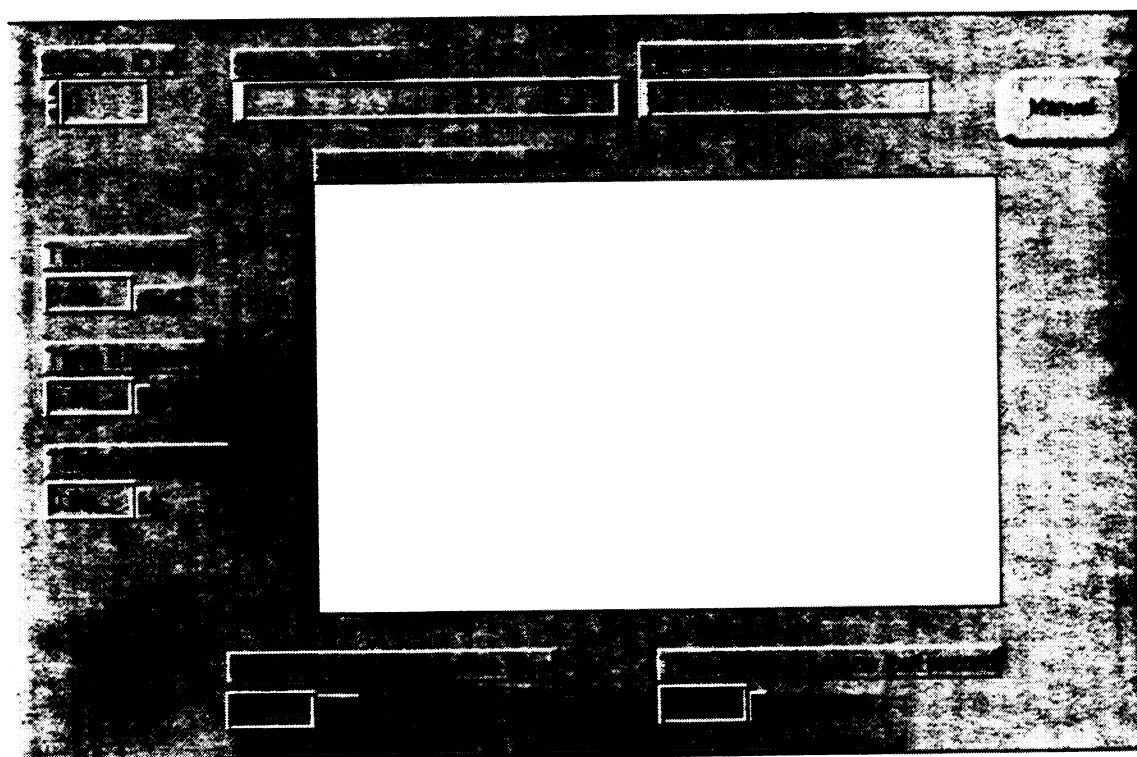
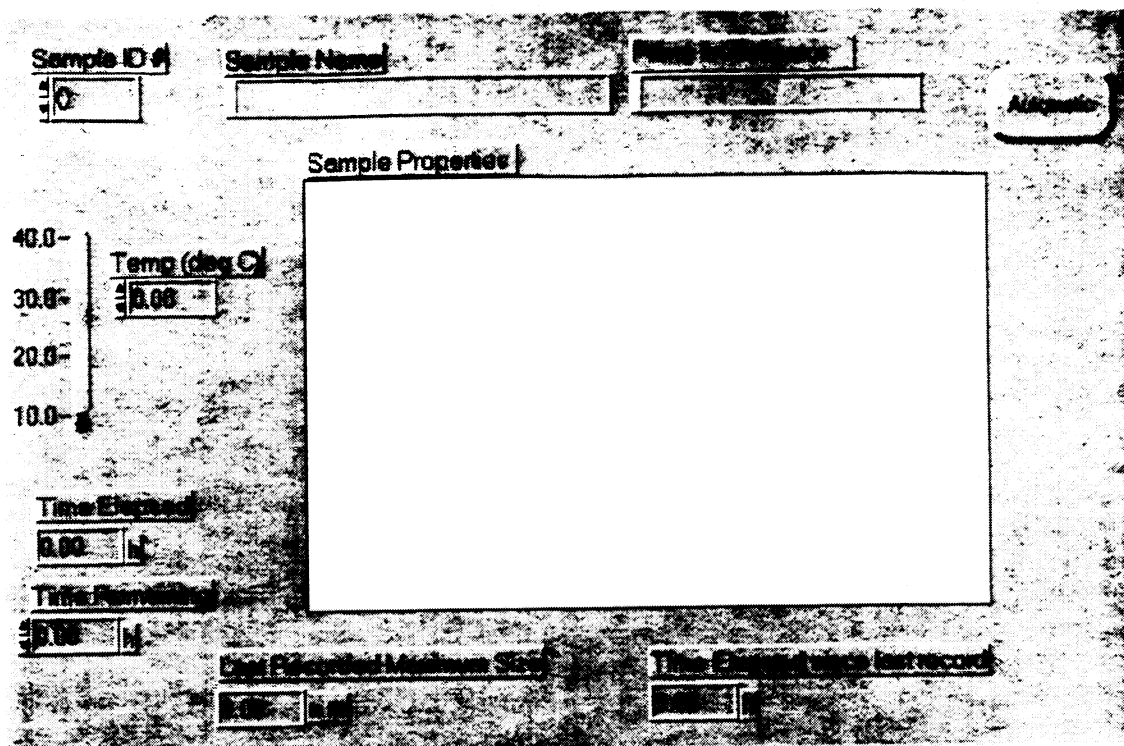


Figure 3.14 Manual (top) and Automated (bottom) Modes

ORIGINAL PAGE IS
OF POOR QUALITY

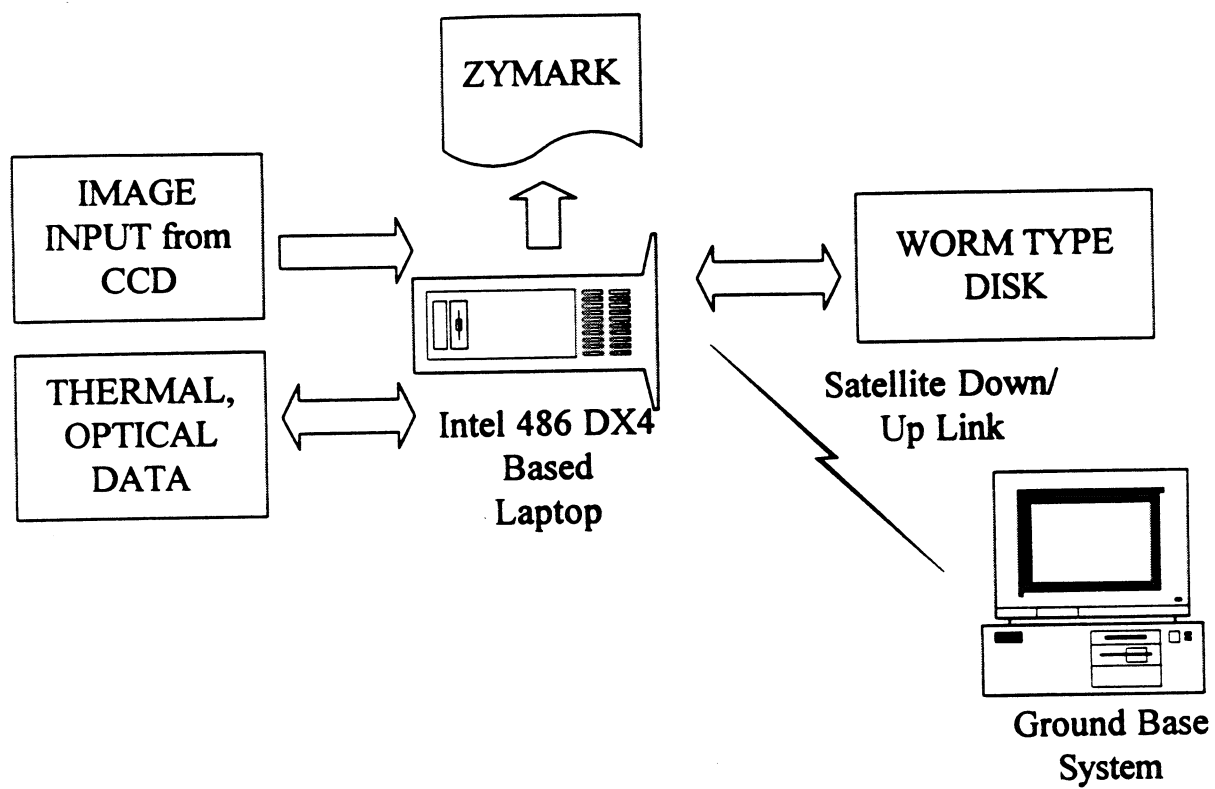


Figure 3.15 Control System Layout

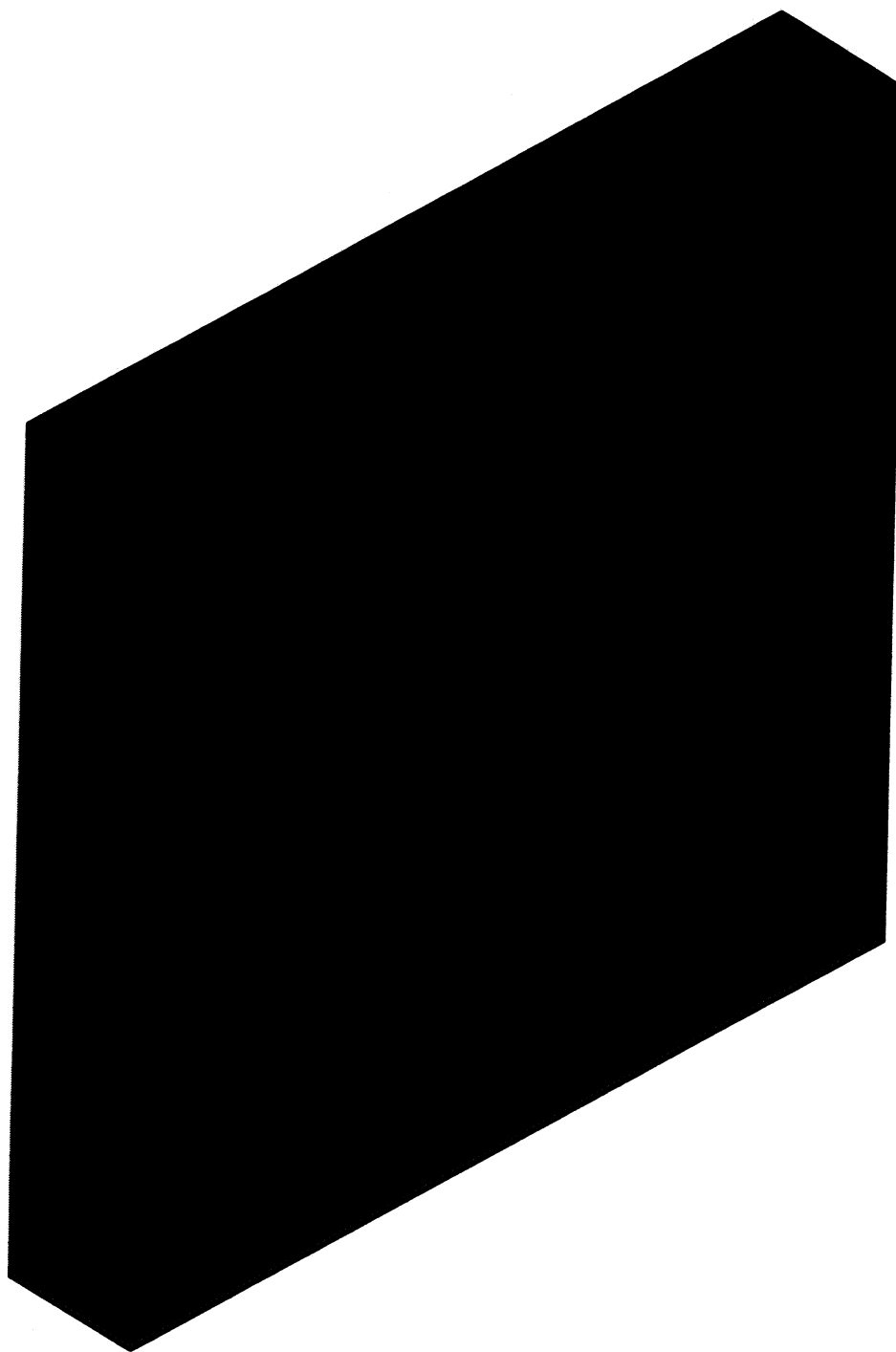


Figure 3.16 Segment 1 - Solid Rendering

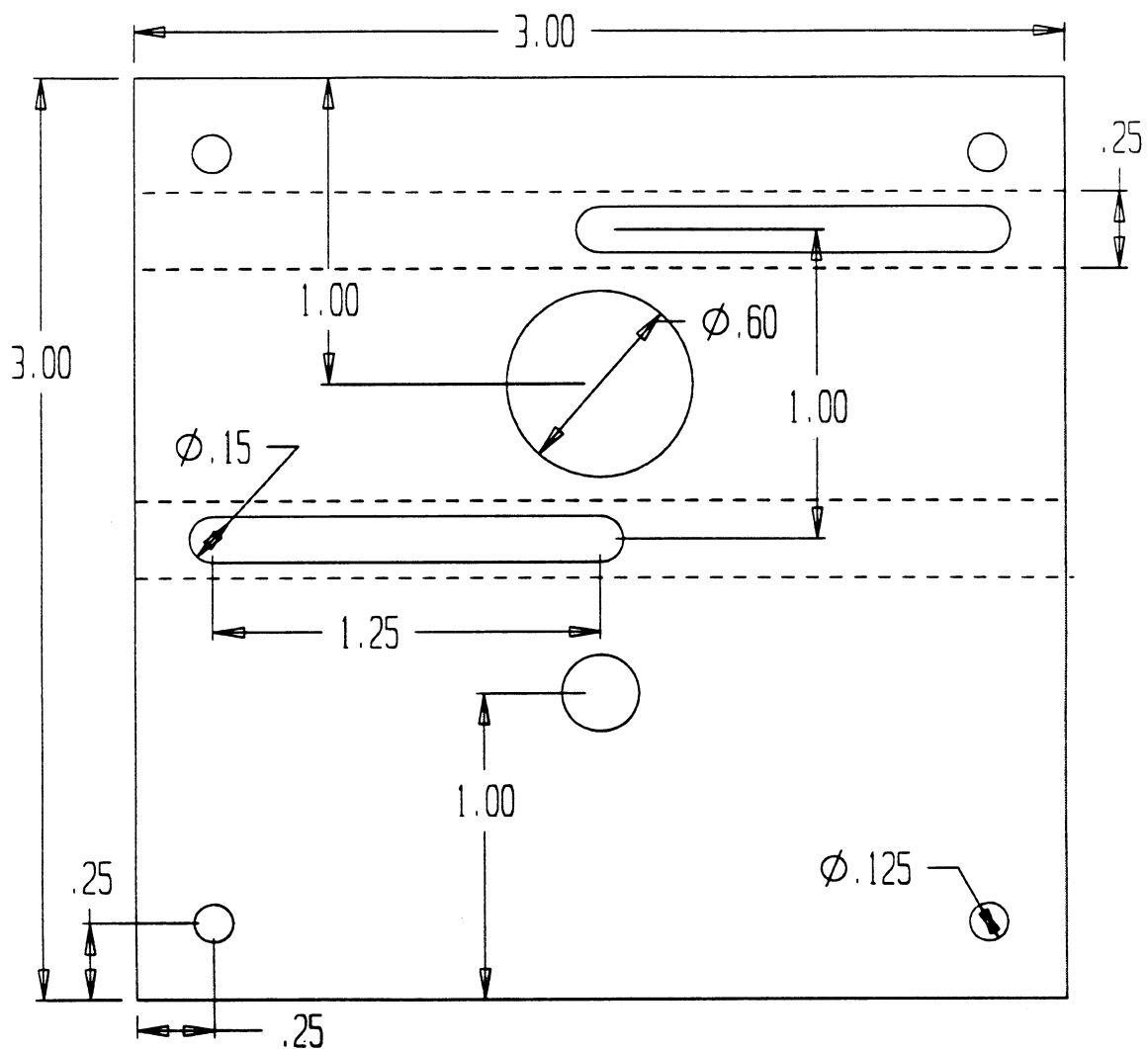


Figure 3.17 Segment 1 - Machine Drawing - Front View

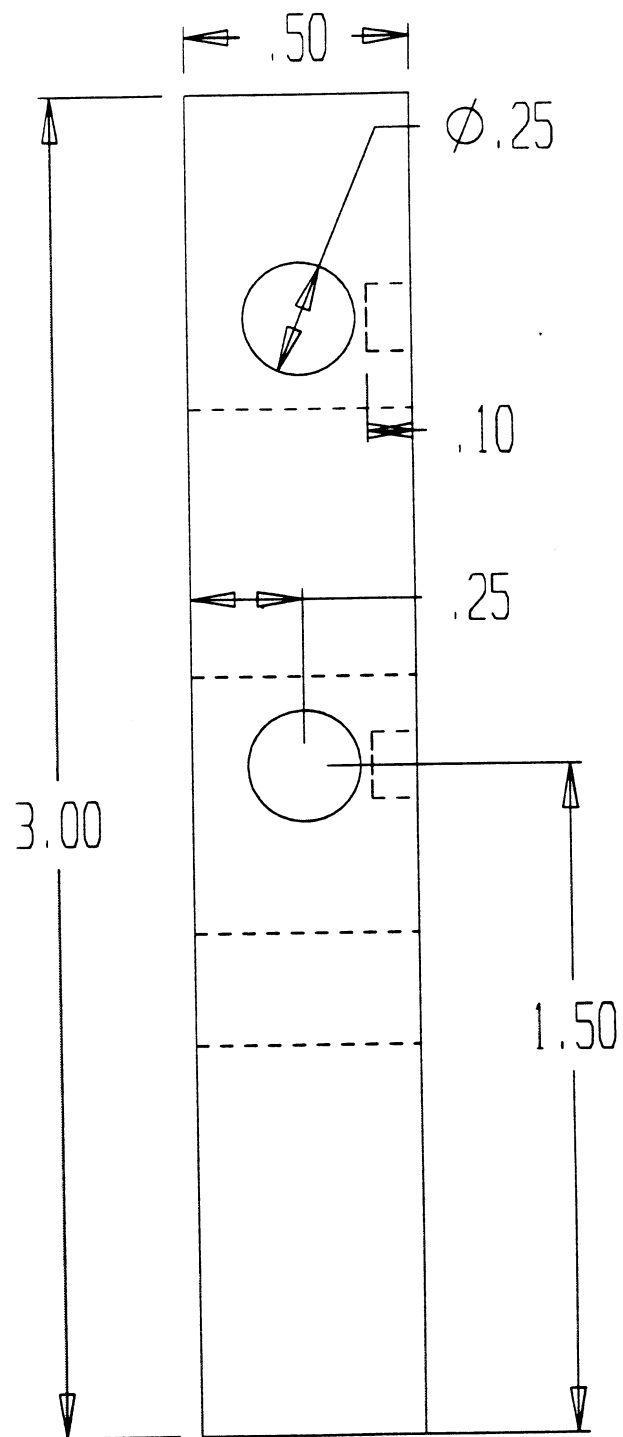


Figure 3.18 Segment 1 - Machine Drawing - Side View

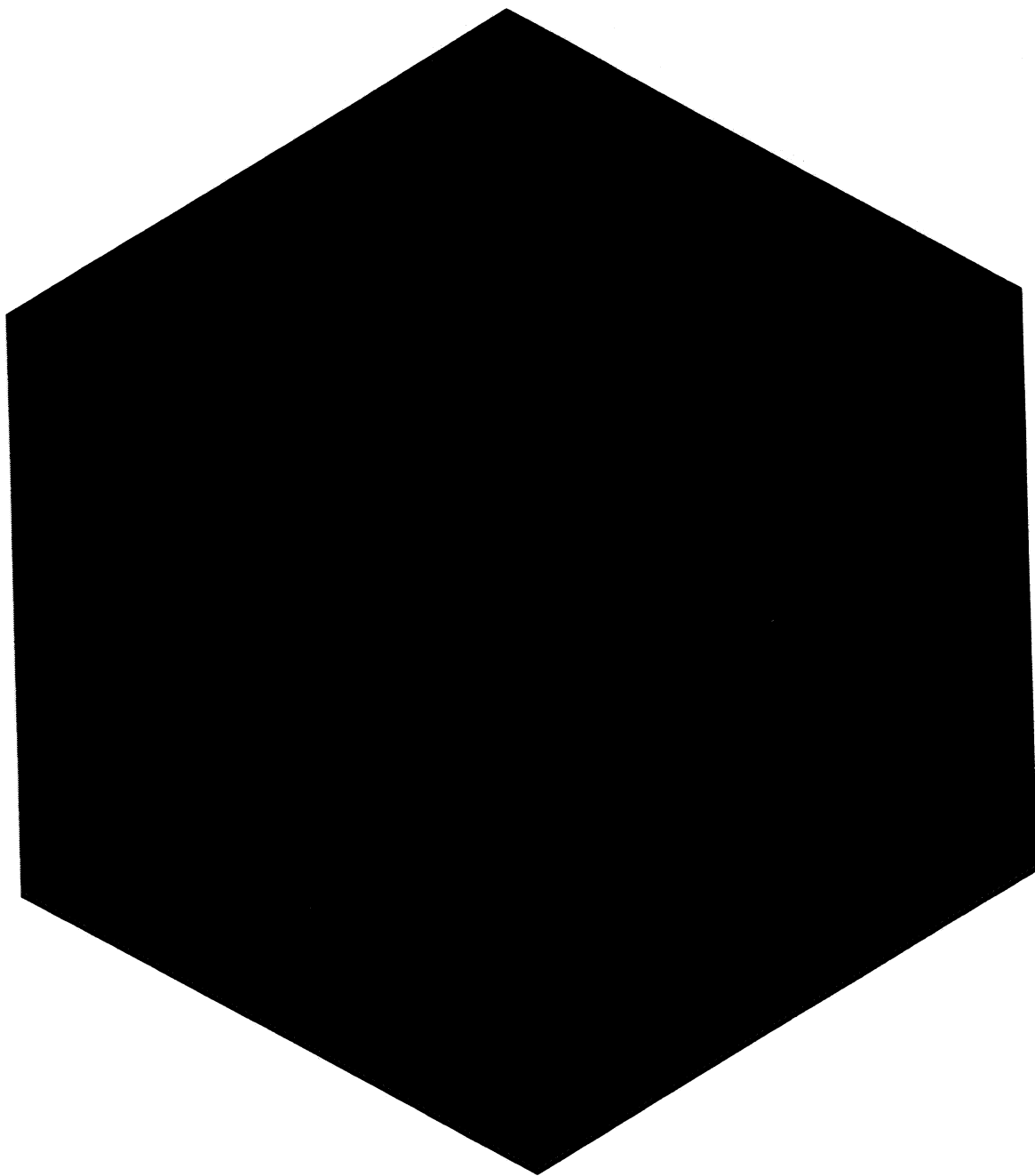


Figure 3.19 Segment 2 - Solid Rendering

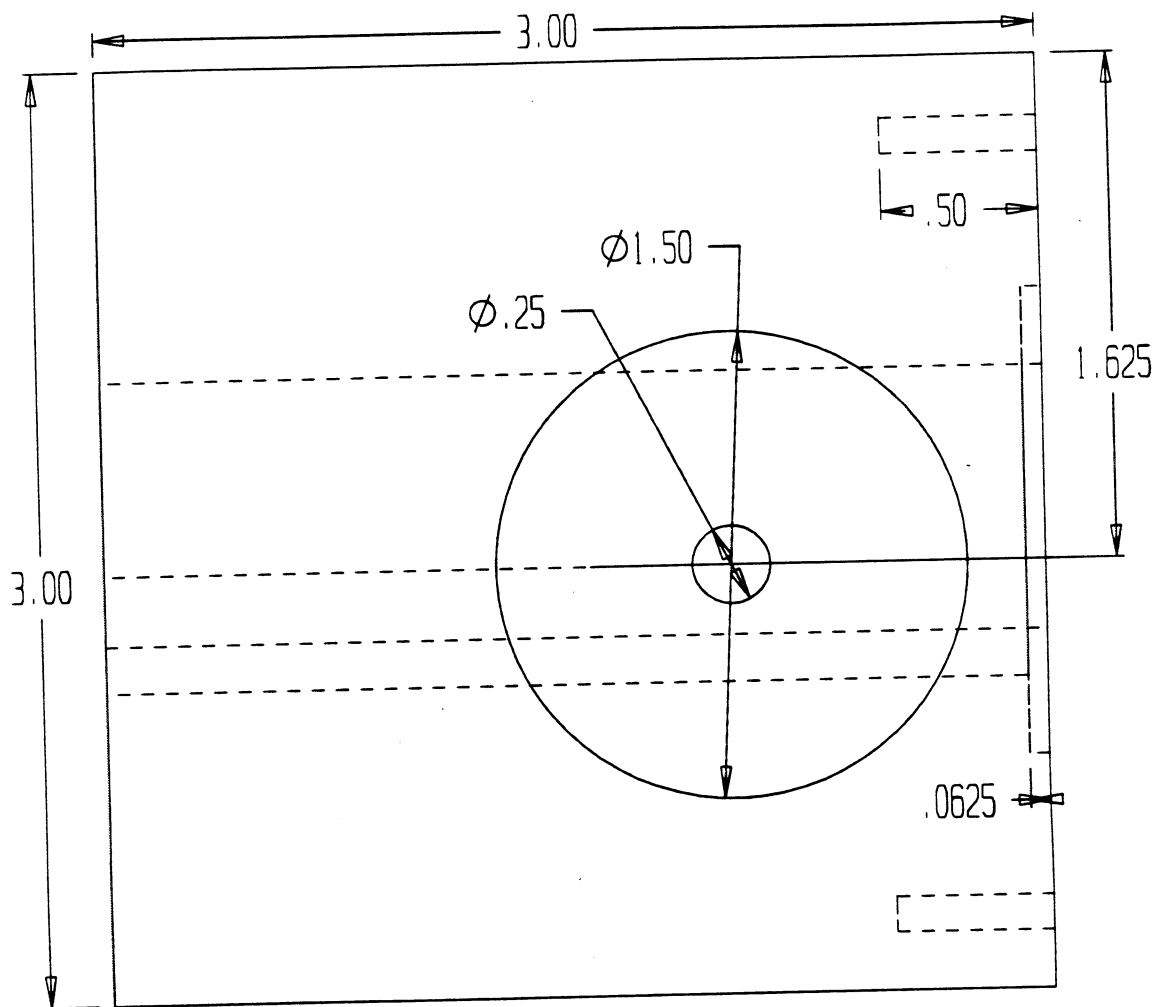


Figure 3.20 Segment 2 - Machine Drawing - Bottom View

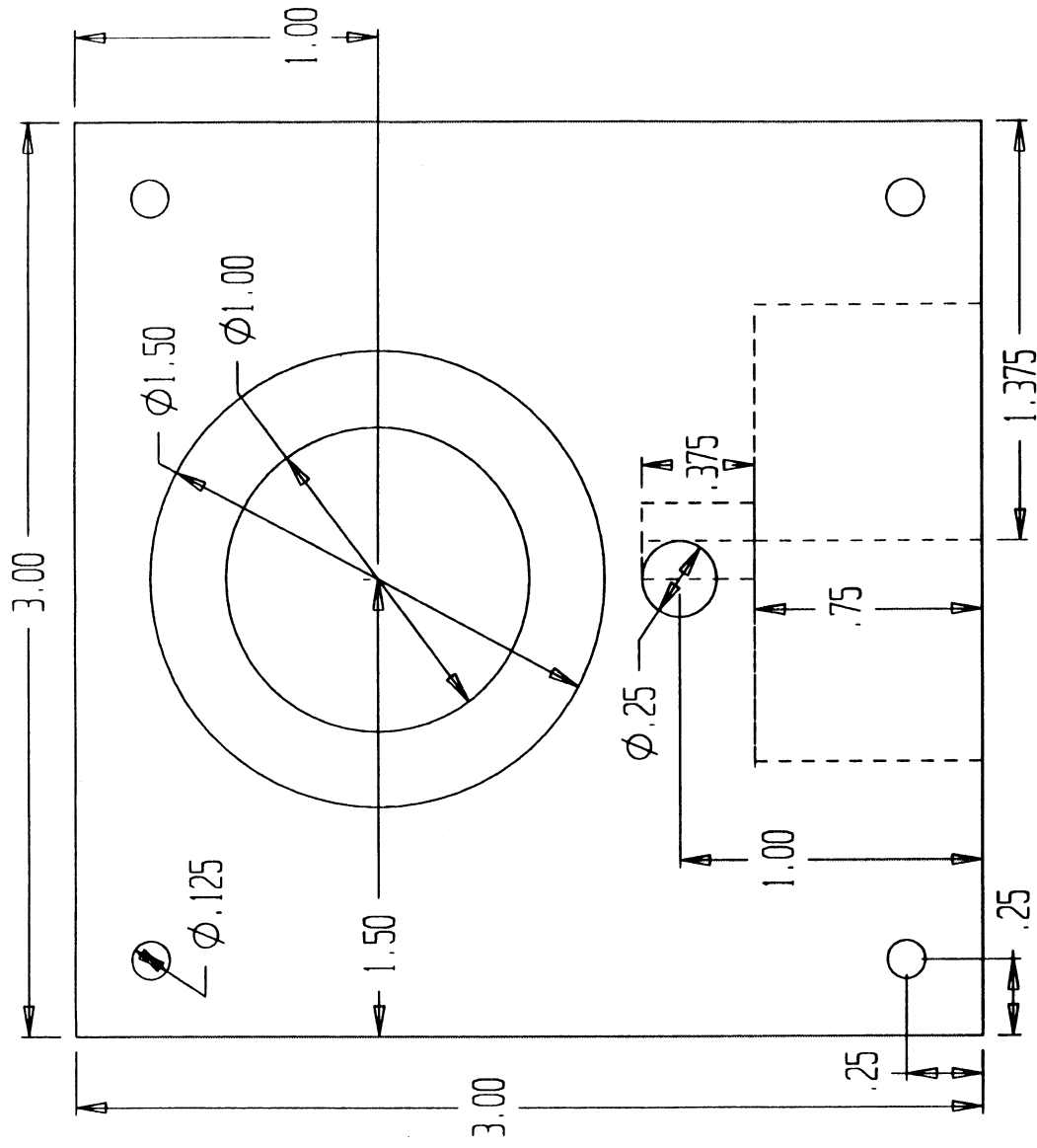


Figure 3.21 Segment 2 - Machine Drawing - Front View

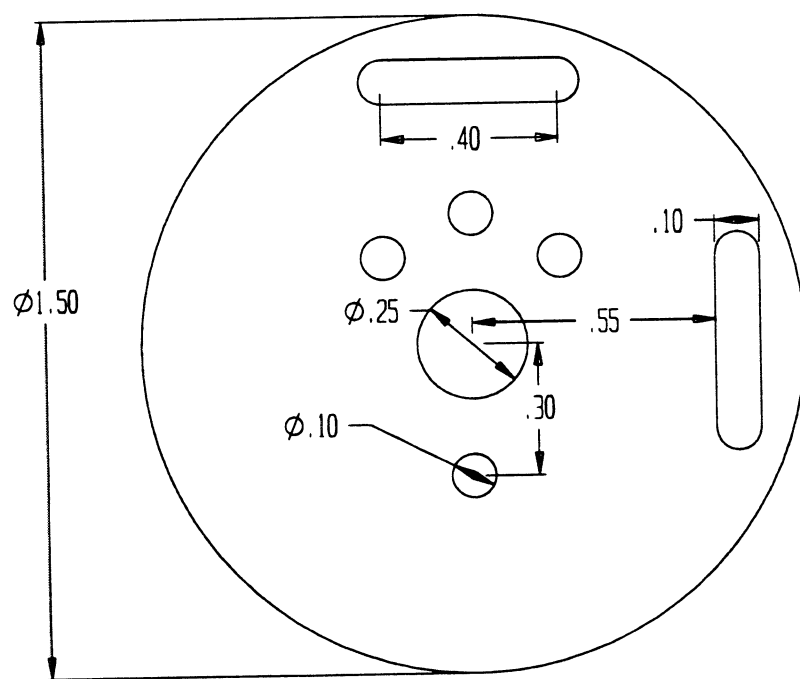


Figure 3.22 Motor Mounting Bracket - Machine Drawing

3.8.2 Bill of Materials

End Effector				
Part Number	Quantity	Price Each (\$)	Vendor	Description
36792	1	63.00	Zymark	Hand Connector Housing
39591	1	80.00	Zymark	Wire Harness
36831	1	25.00	Zymark	Circuit Board
2225T006S	2	120.00	MicroMo	DC Servo Motor
22/2	1	65.60	MicroMo	308:1 Gearhead
22/2	1	69.00	MicroMo	548:1 Gearhead
G5-21	1	-	PIC Design	Pinion Gear
AG-19	18"	68.82	PIC Design	Fine Pitch Rack
OTS	3"x3"x4"	-	-	Plexiglass for Housing
OTS	12"	-	-	1/4" Al Stock for Arms
Sensing System				
Part Number	Quantity	Price Each (\$)	Vendor	Description
G38,303	144	199.00	Edmund Scientific	Image Conduit
G52,347	144	570.00	Edmund Scientific	Microscope-180X
G52,171	144	2,975.00	Edmund Scientific	CCD Micro Camera
Control System				
Part Number	Quantity	Price Each (\$)	Vendor	Description
DT2687-60Hz	1	5,495.00	Data Translation	Image Processor
Versa 486/75 C	1	5,000.00	NEC	Laptop Computer (requires modification)
OTS	1	1,296.00	National Instrument	Labview 3.01 Software
OTS	1	1,000.00	Microsoft Co.	Visual C++ Development Kit
OTS	1	298.00	Microsoft Co.	Windows NT
SP0580-CL	1	3,495.00	Data Translation	Global Lab Image Development
PC-PA2014U	1	1,349.00	L.A. Trade	Toshiba 16MB RAM Upgrade
6M40U	1	1,200.00	Sharp	6 in. NTSC Active Matrix Monitor
OTS	1	1,379.00	IBM	15 in. Touch Screen CRT
OTS	1	N/A	Sharp	16 in. NTSC Monitor
Pantera 90	1	5,512.00	Zeos	Pentium 90 MHz Desktop computer (32 MB RAM, 2 GB HD)
N/A	2	N/A		Optical Storage Device

4 Stiffening of the ACES Deployable Space Boom

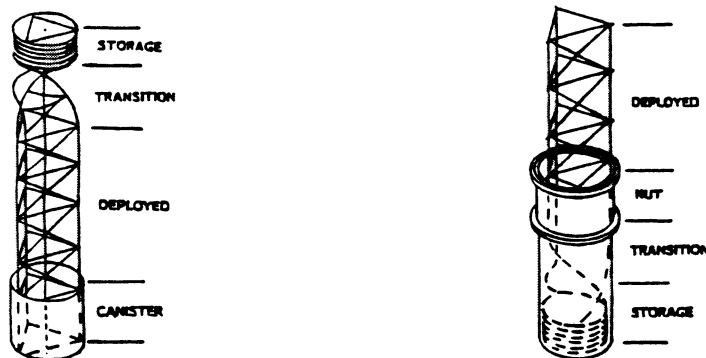
4.1 Summary

4.1.1 General Background Information

Space experiments require extremely stable and remote platforms to ensure that the experiment will operate properly. Deployable booms are used in many of these experimental platforms because of their light weight and compact size. The boom's light weight and compact size are required because of the high cost involved in transporting materials to space. Large, light structures are usually very flimsy, especially long booms. A combination of the boom's low fundamental frequencies, vibrations from the experiment itself, and vibrations at the boom's base can create conditions unacceptable for proper performance of many experiments. To make deployable space booms an effective experimental platform, the overall vibrations in the system must be minimized. One method to reduce these vibrations is by stiffening the deployable boom.

The beneficial effect of stiffening is twofold. Firstly, when the vibrational frequencies are higher, there is less energy in the system. Secondly, higher frequency vibrations are simpler to control. High performance controllers operate at high bandwidths. If the vibrational frequencies are low, it is difficult to match the controller. Therefore, if the frequencies can be increased by stiffening, the high frequency controller manipulates the system more efficiently.

The idea of using tensioned cables and spreaders, in a manner similar to a sailboat mast, allows the designers to minimize increases in both size and weight while significantly decreasing vibrations in the boom. The role of this design group is to use the concept of tensioned cables and spreaders to create an active tensioning system that will allow them to assess the effectiveness of this method to stiffen a deployable space boom.



Lanyard Deployed Boom

Nut Deployed Boom

Figure 4.1. Two Types of Deployable Booms

4.1.2 Design Objective

To design an active planar stiffening device for the existing ACES structure.

4.1.3 Abstract

The purpose of this design project was to design an active planar stiffening device for the existing ACES structure. The ACES structure was modeled using simple beam theory. Various concepts were generated about how the stiffening device should be configured in order to perform at an optimum level. The optimum configuration was selected to be a single set of spreaders located approximately 63% of the distance down the beam. Actuation was to be provided by a DC electric motor. From the test results, the design group was able to draw conclusions and make recommendations about the utility of further research into this area.

4.2 Glossary

ACES	=Active Control Evaluation for Structures
b	=length from the top to the point of maximum deflection
E	=Young's Modulus
I	=mass moment of inertia
l	=length of the boom
LMED	=Linear Momentum Exchange Device
x/l	=dimensionless length ratio
β	=weighted frequency of mode
σ	=constant

4.3 Background Information

4.3.1 Customer Requirements

The customer for this design project was defined to be the engineers at Marshall Space Flight Center in Huntsville, Alabama. Their intent was to have the group design an active tensioning system on which they could then perform control experiments. The primary contact for the definition of the customer requirements was Dr. Henry Waites. Also helping with the customer requirements were Dr. Ephraim Garcia and Mark Whorton. The final list of customer requirements is as follows:

(1) Only the first mode of vibration must be damped for a clamped, pinned beam. It follows that if that mode can be excited by the system, the system can also damp that mode by generating it 180 degrees out of phase.

(2) The amount of deflection adequate to damp the first mode of vibration is equivalent to an approximate deflection of 15 cm at the point of maximum deflection.

(3) The weight of the control device should not exceed the weight of the existing control system. The existing control system weighs eight times as much as the ACES structure or about 40 lb. The weight of the control system needs to be roughly half of this amount, about 20 lb.

(4) The cost of the system must be reasonable enough to be constructed with available funds. This limit is considerably less than the cost of the existing system.

(5) The system should be constructed so that it can be attached to the existing structure without interfering with the existing control system or the constraints defined by the building. The limiting building constraint is a hole cut into a steel floor through which the boom passes. The

rectangular opening is 26 inches by 37 inches. This opening is located 26 bays or about 12 feet from the top of the boom. The geometry of this configuration limited the length of the spreaders to just under 3.5 feet or about 1 meter.

(7) The system should not damage or harm the ACES structure during the attachment to the structure or during the testing of the control system on the structure.

(8) It is not necessary for the system to be space qualified. It will only be used as a prototype on the ACES structure.

(9) The power supply to the control system does not need to match the power supply offered by the space station. The standard spacecraft power is 27 VDC, but the system can utilize any power source available.

4.3.2 ACES Structure Background

The existing ACES structure as shown in Figure 4.2 is a 45 foot astromast boom with a 10 foot antenna attached at its bottom. The ACES structure is excited by a two axis active traverse that can simulate the firing of a positioning thruster. The current vibration suppression system consists of two sets of two-axis linear momentum exchange devices (LMEDs). An LMED is a solenoid that accelerates an attached reaction mass. The vibration in the astromast is evaluated by a laser that is bounced off of a mirror on the antenna at the end of the mast to an independent, powered gimbal mirror, back to an optical detector pad on the antenna.

TEST ARTICLE: 45 FOOT ASTROMAST BOOM
WITH TEN FOOT ANTENNA
REAL-TIME COMPUTER SYSTEM PROCESSES
37 SENSORS AND 11 ACTUATORS

1. BASE EXCITATION TABLE
2. 3-AXIS BASE ACCELEROMETERS
3. 3-AXIS GIMBAL SYSTEM
4. 3-AXIS BASE RATE GYROS
5. 3-AXIS TIP ACCELEROMETERS
6. 3-AXIS RATE GYROS
7. OPTICAL DETECTOR
8. MIRRORS
9. LASER
10. 2-AXES POINTING GIMBALS
11. LMED SYSTEM

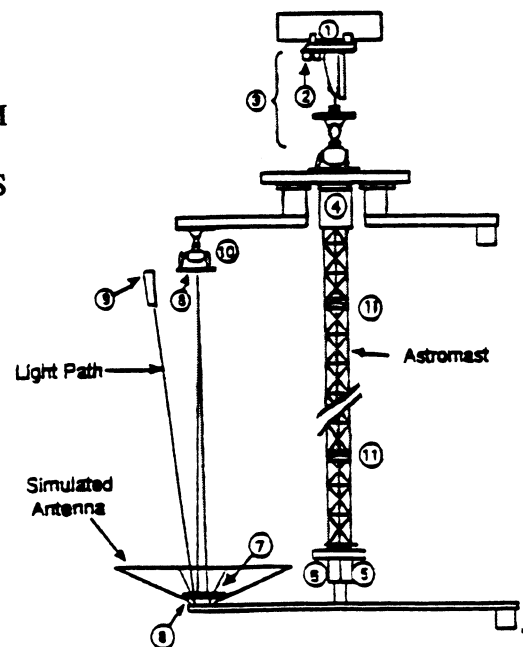


Figure 4.2. ACES structure.

The astromast boom is made up of 96 bays (Figure 4.3) that are triangular prisms 5.625 inches in height and 7.875 inches in length on each side. The overall astromast boom is a linear triple helix with a 260 degree twist from top to bottom. The fact that the astromast boom consists of over 1100 separate members made a Finite Element Analysis model an inconceivable goal for a one semester project.

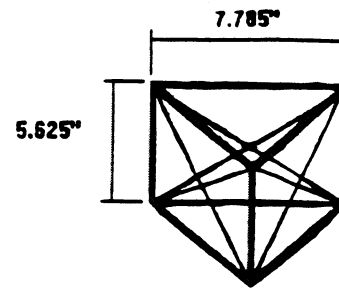


Figure 4.3. Single ACES Bay

4.4 Analysis

Due to time and logistical constraints, only the motion in one plane will be considered. Controlling the motions in one plane will sufficiently prove the viability of the tendon-spreader configuration as an active vibration suppression system.

Certain assumptions must be made in order to model the boom. The first assumption is that the boom can be modeled as an elastic, slender beam in transverse vibration. This assumption allows the use of simple beam vibration equations to determine the point of maximum deflection. The next step is to determine the appropriate mode to be damped and define the corresponding boundary conditions. The first two modes are the most critical in that they contain the majority of the vibrational energy. The first vibrational mode is the first mode of vibration of a clamped-free beam, while the second mode is the first vibrational mode of a clamped-pinned beam.

The clamped-pinned arrangement was chosen because the mass at the top of the structure is significantly large when compared to the mass of the beam. The end mass is also significantly large, however some rotational movement can be observed. These facts lead to the clamped-pinned model.

Ideally, the first mode for the clamped-free case would be damped because it contains more energy. The configuration necessary to damp this mode would have to be able to generate enough force to overcome the motion of the large end mass. The combination of weight limitations and spatial constraints prevents this from being an option.

In order to damp the first mode for the clamped-pinned case, a choice must be made between dealing with the maximum deflection or the maximum slope of that mode. While the maximum slope will occur at the bottom of the boom, the maximum deflection will occur at some point near the middle of the boom. In order to deal with the maximum slope of the mode, the spreaders must be located at the bottom and force a rotation of the entire end mass. This would require a large motor which would be capable of supplying a necessary force to overcome the rotational inertia of the bottom mass. A more realistic goal is to increase the natural frequency of the boom itself. This goal can be obtained by supplying a force normal to the boom at the point of maximum deflection.

The point of maximum deflection was determined by locating the point of zero slope. The equation for the mode shape of a clamped-pinned beam is:

$$0 = \cosh(\beta x) - \cos(\beta x) - \alpha (\sinh(\beta x) - \sin(\beta x))$$

$$\text{where } \alpha = \frac{\cosh(\beta L) - \cos(\beta L)}{\sinh(\beta L) - \sin(\beta L)}$$

$$\text{and } \beta L = 7.06858275.$$

Solving the first equation for x/l , the point of maximum deflection was found to be approximately 63 percent of the length from the top of the boom. Since the boom is 13 meters long, the point of maximum deflection is 8.2 meters from the top.¹

In order to determine a preliminary size for the motor, the relationship between tension and beam displacement was found. The configuration in Figure 4.4 was used to determine this relationship.

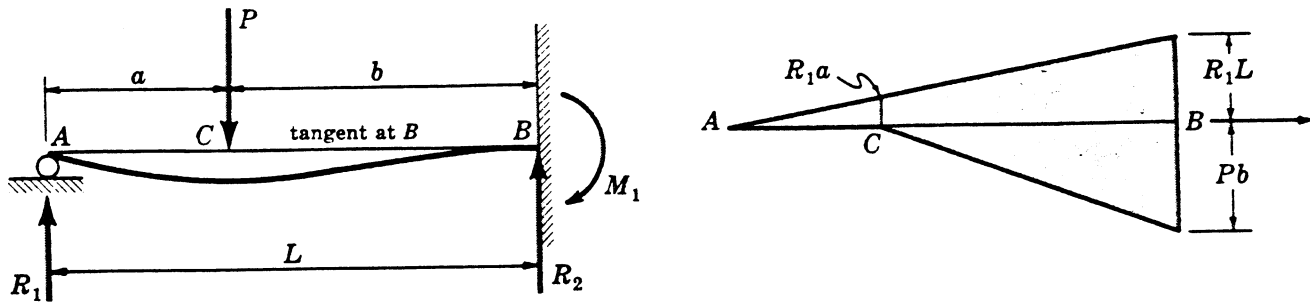


Figure 4.4. Clamped-pinned beam model and moment area diagram

Equations for the reactions at points A and B, as well as the moment at B, were obtained from the following equations.

$$R_1 = \frac{3Pb^2}{2L^3} \left(a + \frac{2}{3}b \right) = \frac{Pb^2}{2L^3} (2L + a)$$

$$R_2 = \frac{Pa}{2L^3} (3L^2 - a^2)$$

$$M_B = \frac{Pa}{2L^2} (L^2 - a^2)$$

$$EI\Delta c = abR_1 + \frac{1}{3}b^3R_2 + \frac{1}{3}b^3P$$

The following values were used for the variables in the equations:

$$L = 13 \text{ m} \quad I = 3.35 \times 10^7 \text{ m}^4 \quad b = 8.19 \text{ m} \quad E = 2.86 \times 10^{10} \text{ N/m}^2 \quad a = 4.81 \text{ m}$$

Using the reactions found above and the moment area method, the final equation relating force and displacement was determined.

$$4.7 \quad \Delta c = .003 [\text{m/N}] \times P$$

From the geometry of the system, the tension in the tendons can be directly related to the displacement at the spreader. This equation is given below.

$$4.8 \quad T = .0935 [\text{N/m}] \times \Delta c$$

4.5 Design Concept

The design concept generation phase involves both brainstorming and consideration of previous designs. The purpose of the design is functionality and reliability, so simplicity of design is a major consideration. Therefore, the customer requirements are kept in mind at all times with complex configurations eliminated in lieu of simpler, yet innovative systems.

The first step in concept generation involves examining prior designs. The present configuration of the ACES stiffening device includes linear momentum exchange devices. While this concept of damping the structure's vibration is effective, the weight of the linear momentum exchange devices comprises a large portion of the entire structure's mass. The design team is thus faced with finding an alternate design that is just as effective yet which is of lower mass. Group brainstorming resulted in a concept that seemingly fits the low-mass requirement: a spreader/tendon design. Tendons placed internal to the structure are considered, but dismissed due to the amount of motor torque necessary to produce the desired vibration damping. An external spreader design is chosen so as to reduce the power requirements of the motor and reduce the possibility of the buckling. This design requires fewer electrical considerations (the motor is the only source of energy consumption), is a fraction of the prior design's mass, and is of much lower cost.

Now that the basic design concept is selected, a means by which to tension the tendons is considered. Again, a previous design is examined. A similar design project by Barry Dunn, a graduate student at Vanderbilt University, employs linear motors in order to excite vibrational modes in a structure similar to the ACES, but on a smaller scale. Linear motors are investigated as a means of quick tendon retraction. Although these motors are ideal for the structure studied by Dunn, the very limited motor travel is not suitable for the length of tendon retraction required for the substantially longer ACES structure. In addition, the linear momentum of the motor mass introduces additional vibrational modes that need further damping. The design group is thus faced with finding a method that is capable of retracting several inches of tendon in a short time. A high torque, high speed DC motor attached to a spool is chosen. It must be capable of high angular accelerations. The cost of such a motor is less than that of a linear motor and does not contribute to vibrations in the plane of study.

Spreader material must also be considered. Brainstorming the problem yielded several possibilities. A thin wooden dowel, metal rod, plastic rod, and graphite rod were considered. Wood dowels are strong enough in tension and compression, but any bending might result in fracture. Metal rods are adequate in this area yet are high in mass. Plastic rods are difficult to break, yet bend far too easily and would lead to inaccurate force transmissions. Therefore, graphite rods were chosen for their extremely high yielding point, stiffness, and low mass. In addition, Dunn's project used the same graphite rods (manufactured by a kite company) with excellent results.

Also adopted from Dunn's project is the tendon material. DuPont Spectra kite string is used with a test strength of 500 lb., more than adequate for the forces required.

Installing tendons on the ACES structure introduces the problem of exerting forces via the spreaders on the structure, presenting the possibility of local buckling. The use of a mounting plate alleviates this problem. The mounting plates for the LMED's were used as a pattern for a spreader mounting plate. A machine drawing for the mounting plate can be found in Figure 4.10 in the appendix.

4.6 Active Tensioning Mechanism

The active tensioning system of the ACES structure consists of a motor that alternately tensions opposing sides of a continuous tendon running down opposing sides of the structure. The force from the tendons is translated to the structure by a set of spreaders located along the beam. The system can be divided into five main parts as illustrated in Figure 4.5.

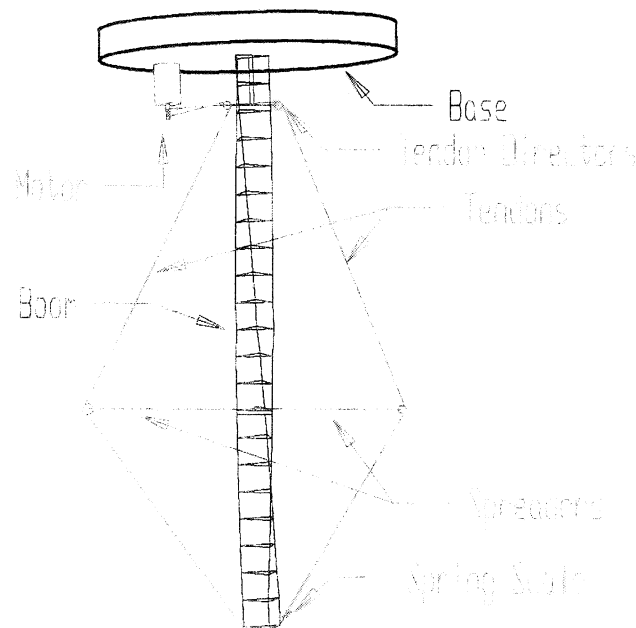


Figure 4.5. Active tensioning mechanism

The system is driven by a DC electric motor. The motor is mounted to a counterweight that is connected to the baseplate. A spool is attached to the shaft of the motor and the tendon wraps around the spool and exits at both the top and bottom of the spool.

The tendon that is used in the tensioning system was chosen for its light weight and low elasticity. A logical choice for the tendon in this case was high performance kite string. The tendon selected is braided DuPont Spectra with a breaking strength of 500 lb. It has approximately three percent stretch before breaking and is very lightweight. We should never encounter any tensions exceeding ten percent of the yield strength. Therefore it is reasonable to assume that there is negligible stretch in the tendon, ensuring consistent and instantaneous response of the system to an active control device.

The dimensions of the spreaders were defined by the spatial constraints of the building surrounding the ACES structure as well as material considerations. At approximately 11 feet down from the base of the structure, the boom passes through a steel floor.

The hole in the floor is 26 inches by 37 inches. This geometry defined the length of the spreaders. This length was 96 centimeters from the centerline of the boom. Therefore, the total length of the spreader assembly would have to be 192 cm.

The other constraint on the length of the spreaders was available material. The material used for the spreader arms is a blend of fiberglass and graphite. The longest available length was 32.5 inches (82.55 cm). This meant that to assemble a 192 cm rod, two full sections and a short section would have to be connected. This extra section would weaken the system considerably so it was decided to use a spreader length of 82.5 cm from the centerline of the structure.

Low friction pulleys in which the tendons would ride were mounted on the ends of the spreaders. It was decided to use only a normal force to damp vibration, so pulleys had to be used to prevent a moment from being applied to the structure.



Figure 4.6. Main structural constraint.

The spreaders were mounted to the structure by the use of a mounting plate. The spreader rods connected through a specially designed clamp that attached to the plate with one bolt. The use of only one bolt allows the spreader to be correctly directed with respect to the structure when mounted. Both the plate and the clamp are shown in Figure 4.8.

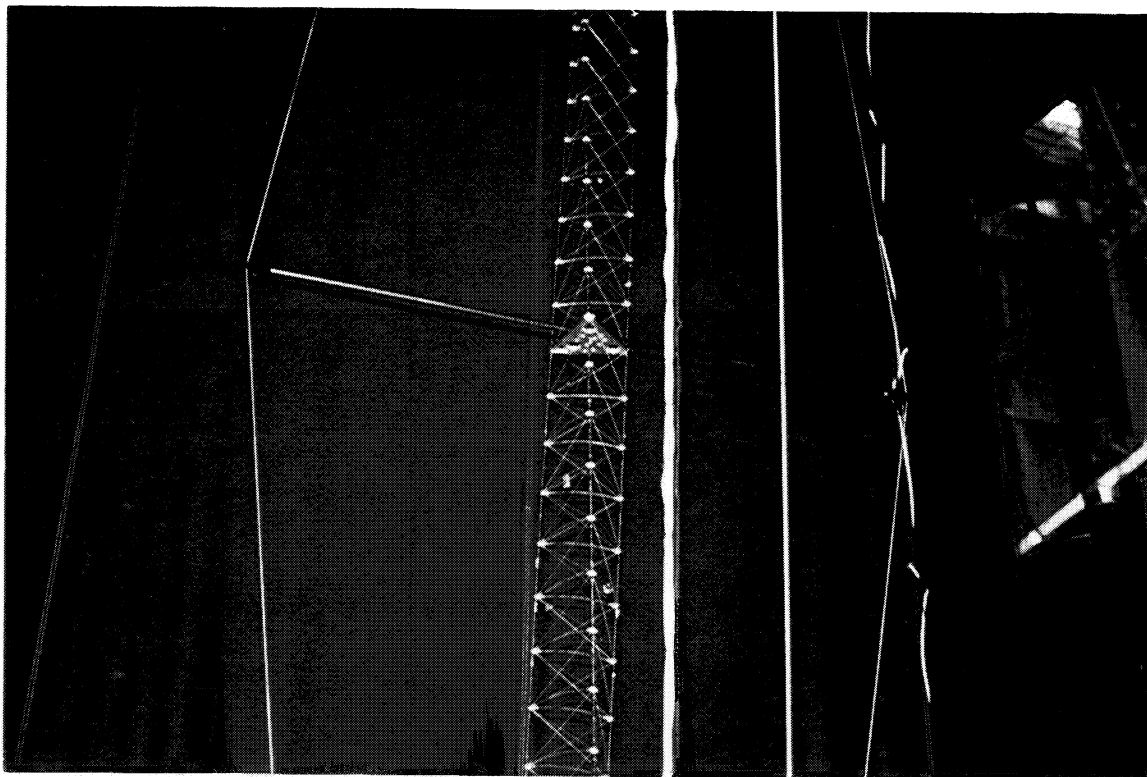


Figure 4. 7. Spreader assembly.

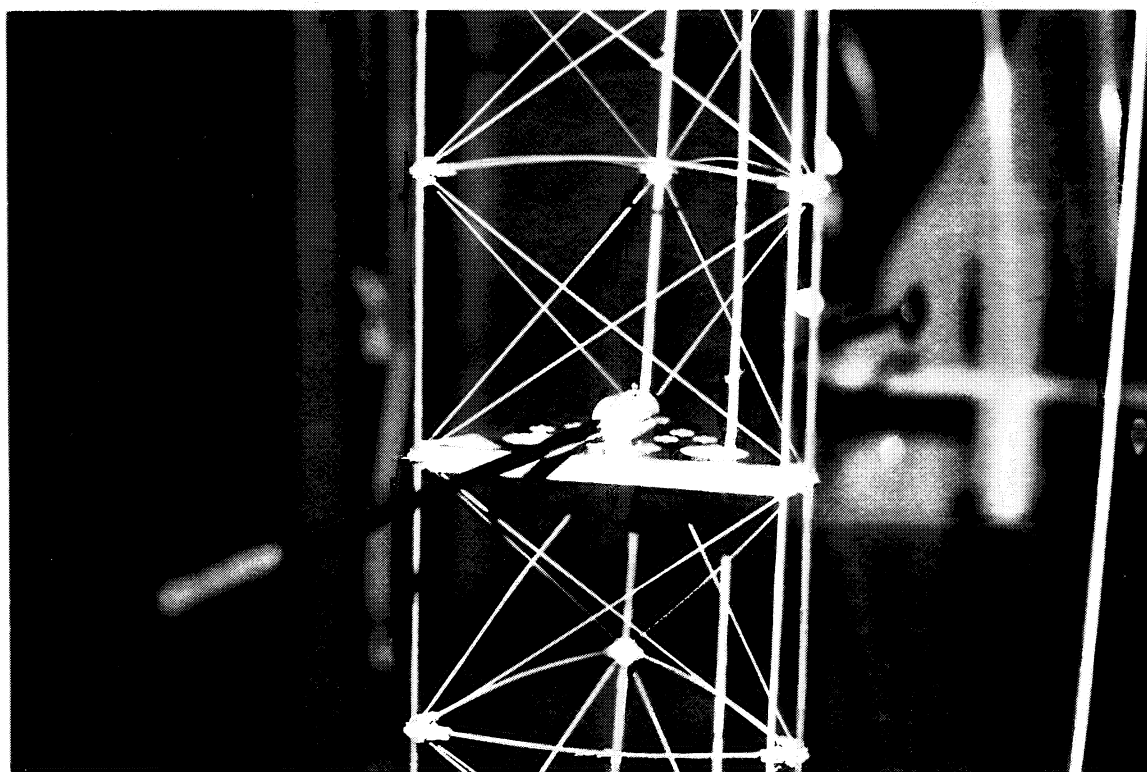


Figure 4.8a. Spreader mounting plate assembly

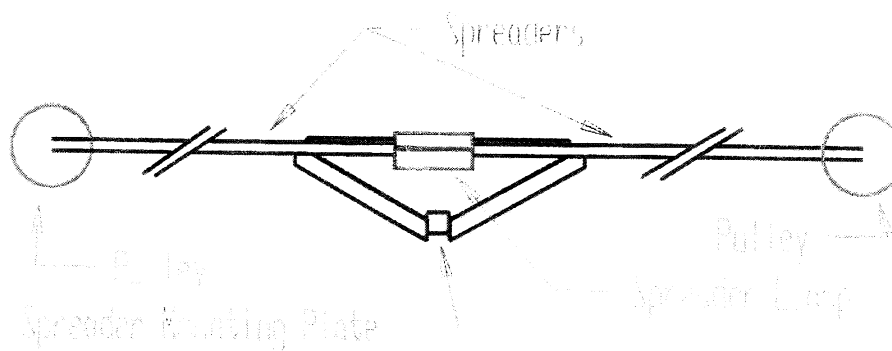


Figure 4.8b. Spreader mounting plate assembly drawing

Two different mounting mechanisms were used to attach the tendon to the bottom of the structure. On one side, a strap of webbing was used. This was ideal because it allowed for nondiscreet adjustments in tendon length, enabling the static tension in the tendons to be adjusted. On the other side, a spring scale was mounted between the structure and the tendon, showing the amount of static tension in the system. The bottom mounting system is shown in Figure 4.9.

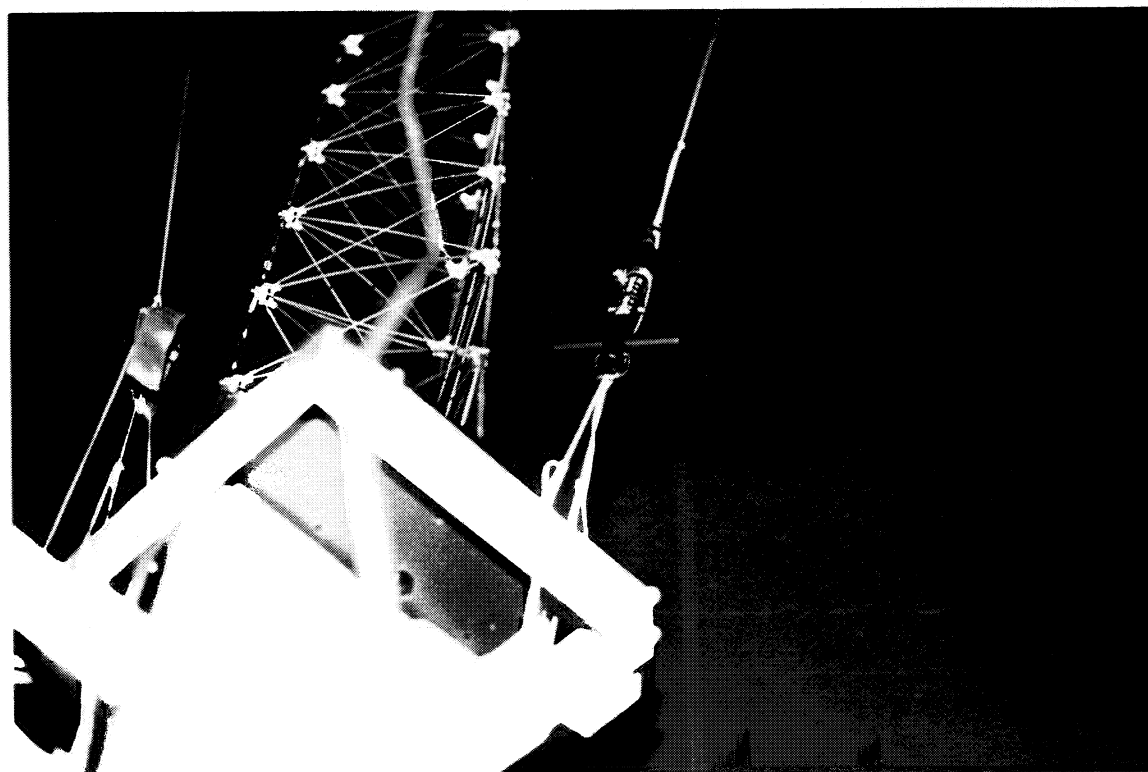


Figure 4.9. Bottom mount with strap and spring scale

4.7 Testing

The original goal was to be able to excite the first mode of the clamped-pinned case. However, due to equipment considerations discovered after mounting, it was decided that this was not feasible. Consequently, the system was evaluated under static tension. The natural frequency within the plane of the tendon system was noticeably higher.

4.8 Conclusions

The frequency of the structure in the plane considered was markedly higher than the frequency in the orthogonal plane. This was due to the static tension applied by the system. Therefore, the conclusion can be drawn that the tendon system has stiffened the structure. No conclusions can be drawn as to the effect of the active tensioning system since the active system was never operational.

4.9 Recommendations

There are many problems associated with the current tensioning system design. Many of these are relatively simple hardware considerations. Others involve major theoretical overhauls and significant design changes. One of the main problems with the design of this system is the difficulty of trying to design a system to fit a structure that is not readily accessible. This led to some fitting problems with the hardware.

It is imperative that all of the pulleys are mounted in the same plane. If the pulleys do not line up correctly, the tendon will slip out of the track. A way to alleviate this problem would be to design an adjustable system which could be properly aligned after the system is mounted.

Another improvement to the system would be to utilize stronger pulleys, possibly with deeper tracks. The existing pulleys are rated at 4.4 kg, hardly enough to withstand active tensioning. Deeper tracks or a tendon guide would help to keep the tendon from jumping out of the track.

When considering the overall purpose of the system, it would stand to reason that to remove energy from a system, it should not be necessary to input energy into that system. This is especially important in space where energy must be conserved as much as possible. An electronically-controlled variable-damping clutch could be a viable alternative.

The application of the system is crucial to the design considerations. It is possible that the reduction of end mass motion is critical to some applications. A possible alternate system could be designed that utilizes moments. These moments would be produced by fixing the tendons on the ends of the spreaders and crossing over the boom. This configuration would control the motion of the end mass.

4.10 References

- (1) Inman, Daniel J., "Engineering Vibrations" p. 335 Table 6.4.

4.11.1 Additional Figures



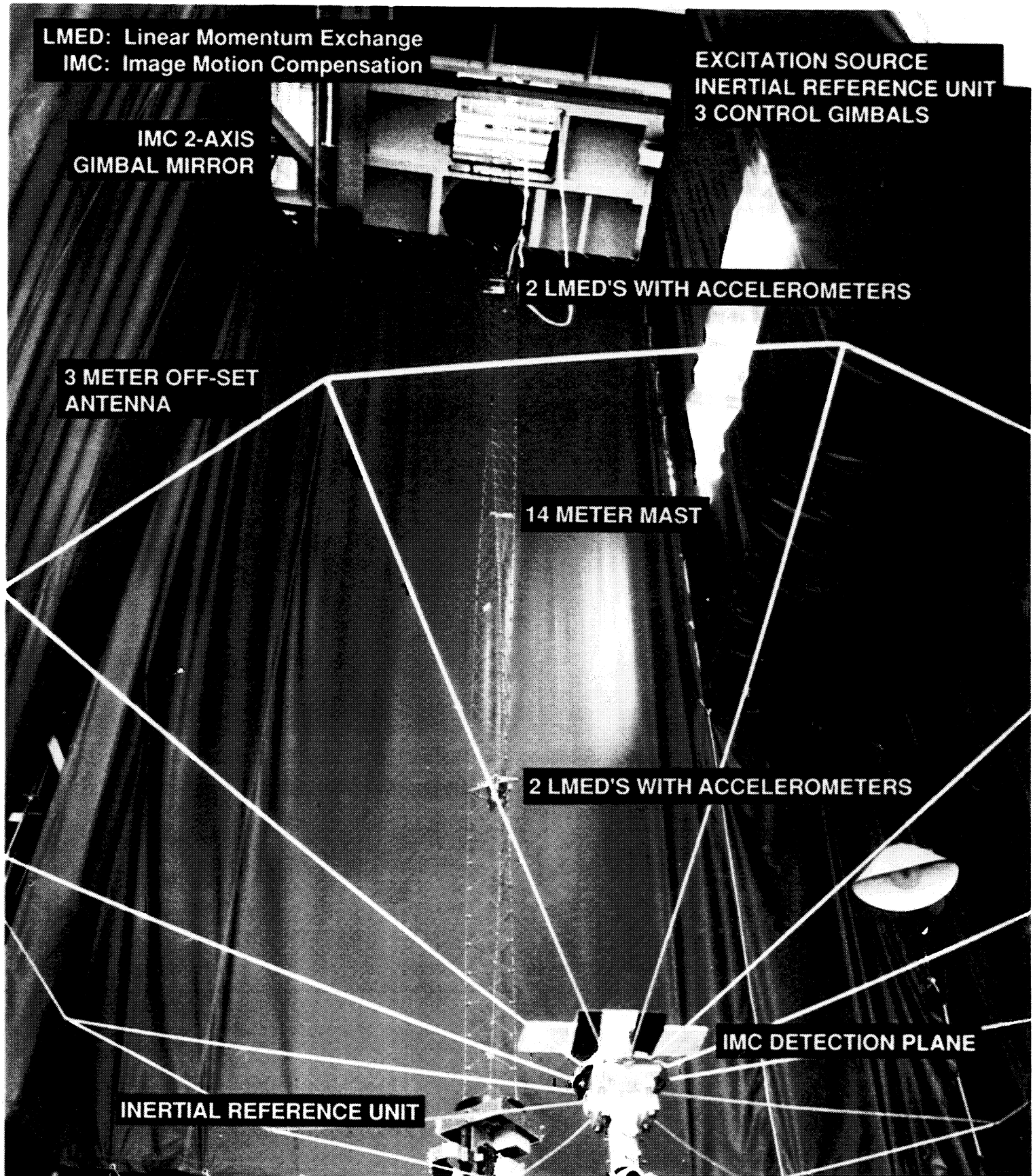


Figure 4.11. ACES structure and previous control system

5 Launch System Design for Access to Space

5.1 Design Objective

Design a hybrid launch vehicle which maintains the current crew survivability rate while reducing reliability in favor of lower cost.

5.2 Abstract

Here, a hybrid launch system is developed. The hybrid launch system combines the lower operating cost advantage of a non-man-rated SSTD MLV with the crew survivability advantage of a ballistic escape pod. Ultimately, it was found that a non-man-rated MLV is configured the same as a man-rated MLV and offers no significant savings in operational cost. However, addition of the proposed escape system would increase the crew survivability rate of the SSTD while incurring only a small cost per pound payload penalty.

5.3 Glossary

Term	Definition
DRLS.....	Down Range Launch Site abort
LEO.....	Low Earth Orbit
MLV.....	Main Launch Vehicle
NASA.....	National Aeronautics and Space Administration
NASP.....	National Aerospace Plane
RTLS.....	Return to Launch Site abort
SSTD.....	Single Stage To Orbit

5.4 Background

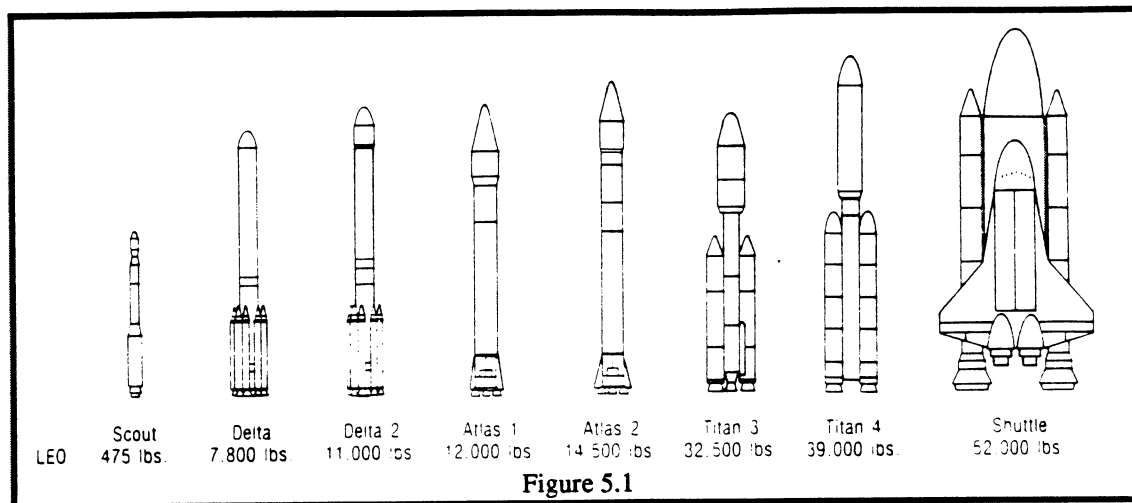
The primary needs for the United States space program through the next two decades are to provide access and support for Space Station Freedom, to deploy and service Earth-orbiting satellites, and to deploy deep space exploration satellites. To meet these needs, approximately 900,000 pounds of payload will have to be carried into LEO (OTA¹, 1990). Currently available launch systems can meet these needs.

Launch systems are separated into two categories: man-rated and non-man-rated. Man rated systems are more expensive to design, build, and support because they require redundant life-support systems on board. The cost per pound payload for a man-rated system can reach \$20,000 compared to \$3,000 for a non-man-rated system (OTA¹, 1990).

5.4.1 Current non-man-rated space vehicles

Currently there are five families of non-man-rated MLV's capable of placing payloads into LEO. Schematics of these systems and their LEO (100 to 350 miles) payload capabilities are shown in Figure 5.1. The overall reliability of these launch systems ranges between 88 and 95 percent (OTA¹, 1990).

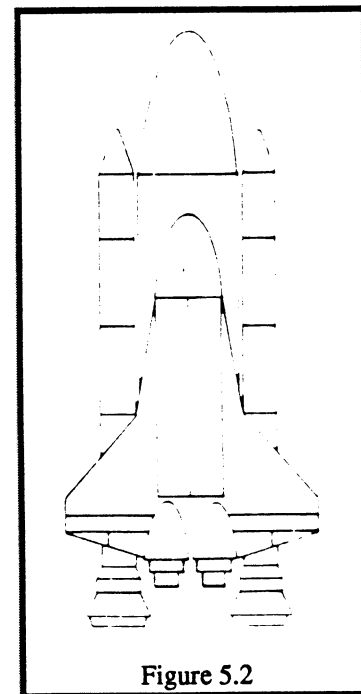
failures of the Atlas and Titan systems resulted in their temporary grounding; however, the Scout, and Delta systems still offer flexible payload capacities and serve as economical payload delivery options.



5.4.2 Current man-rated space vehicle: Space Shuttle

The Space Shuttle was designed in the early 1970's with its first flight in 1981. Figure 5.2 shows the current Space Shuttle configuration. It is a partially reusable system in that the orbiter glides back to earth after each mission, while parts of the propulsion system are jettisoned during ascension to orbit. The Shuttle can deliver 52,000 pounds of payload and a crew of seven to LEO using liquid-fuel main engines and SRB's.

The major advantage of the Shuttle is its flexibility to be used as a cargo carrier, research platform, and recovery vehicle. One major disadvantage of the Shuttle is its complexity which has driven its operational costs above initial projections. Furthermore, it was anticipated that the turnaround time between missions would be approximately 60 days, but because the Shuttle is only partially reusable, excessive maintenance often requires twice as much time. Another major factor is that safety parameters for hundreds of systems must be satisfied before an orbiter can launch. This system complexity is such that a single malfunction can delay a mission. Launches may also be delayed because of poor weather conditions at the launch site or any of the landing sites (Asker², 1993).



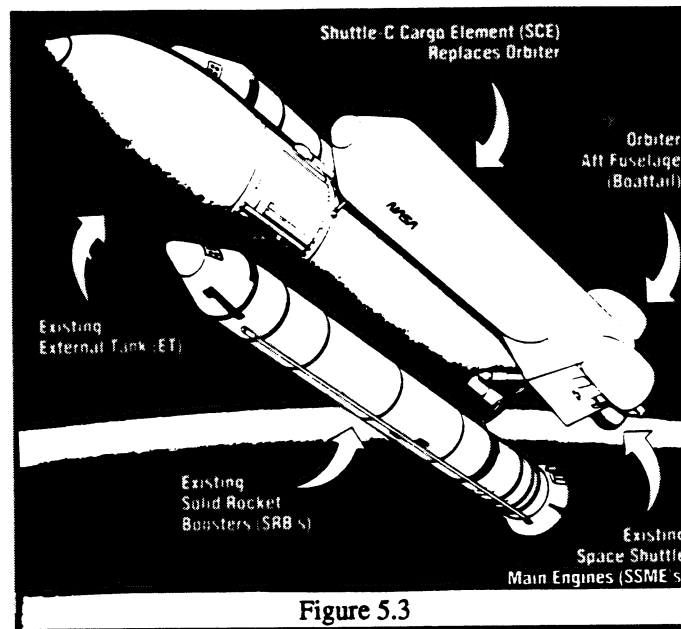
5.4.3 Future concepts (Present to 2015)

NASA engineers emphasize the importance of meeting the future (to 2015) United States space program needs, discussed in Section 5.3, with a less expensive, more reliable launch system capable of carrying a payload of 25,000 pounds and a crew of eight to LEO (Brown³, 1994). Three general concepts have been studied with respect to NASA's future needs: a redesigned Shuttle system, an SSTO transport, and the NASP.

5.4.3.1 Redesigned Space Shuttle

A new shuttle system would use the current design with modifications resulting from technical improvements. Possible improvements are:

- Replace the SRB's with liquid-fuel engines
- Make the Shuttle a totally reusable system
- Replace computers and controllers with new, more reliable systems
- Use state-of-the-art, light-weight materials for the body and engines
- Build an unmanned version of the Shuttle with a payload capacity of 155,000 pounds (Figure 5.3).



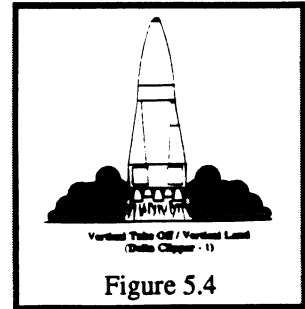
Although the modified Shuttle would use proven technology and would take advantage of existing ground support facilities, the man-rated version of the modified shuttle would be as complex and costly as the existing Shuttle.

5.4.3.2 NASA Single Stage To Orbit (SSTO)

The SSTO system is totally reusable, powered by liquid-fueled rocket engines, and capable of reaching LEO. Because the SSTO system is totally reusable, the high maintenance costs of repairing partially reusable parts, like those used in the Space Shuttle (see Section 5.4.2), are eliminated. Two SSTO configurations are the DC-X (Delta Clipper) and the winged SSTO.

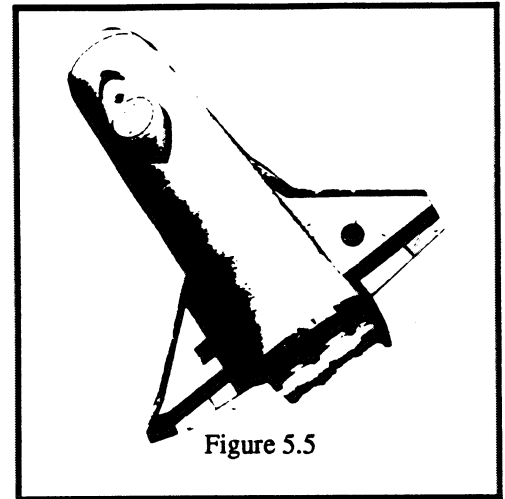
5.4.3.2.1 DC-X

The DC-X is a vertical takeoff and vertical landing vehicle that uses existing propulsion technology. A scale model of the DC-X was built and tested during the summer of 1993. Figure 5.4 is a schematic of the DC-X. Anticipated advantages of the DC-X are significant reductions of operating cost and its ability to land on any flat surface. However, researchers have not proven these advantages experimentally, nor has the DC-X demonstrated its ability to deliver a sizable payload.



5.4.3.2.2 Winged SSTO

The winged SSTO (Figure 5.5) is a vertical takeoff, horizontal landing vehicle with a design payload capacity of 25,000 pounds. The major difference between the SSTO and the Space Shuttle is that the SSTO neither has SRB's nor an external fuel tank. Five liquid-fuel engines supply the necessary thrust to lift the vehicle to LEO.



5.4.3.3 National Aerospace Plane

The NASP would take off horizontally from a runway, climb to an altitude of 100,000 feet and a speed of Mach 3, and finally switch to supersonic ramjet engines or rocket engines to propel to LEO. However, there have been no successful tests to prove the ramjet engine technology. The following section outlines the customer requirements that any future launch system (i.e. DC-X, winged SSTO, or NASP) will need to meet.

5.4.4 Customer Requirements For Future Launch System

Before any trade studies or design changes were proposed, customer requirements were determined for the future launch system. The customer requirements are used in the selection process for the final launch system. Customer requirements were grouped into five categories: crew safety, system reliability, ability to abort, system robustness, and the overall structure of the system. Some of the customer requirements are only important in the case of catastrophic failure of the MLV (e.g. explosions, multiple engines out, structural failure) which prohibits an RTLS abort or a DRLS abort maneuver. These customer requirements are marked *catastrophic* throughout the following paragraphs. Non-catastrophic failures allow for the MLV to be salvaged through an RTLS or a DRLS maneuver, while catastrophic failures require that the crew escape and sacrifice the MLV.

The safety of the crew during a mission is a major concern to NASA. The major customer requirements for crew safety are:

- Separation of the crew from the MLV (catastrophic)
- Separation of the crew from the MLV without injuries (catastrophic)
- Return of an incapacitated crew if necessary (catastrophic)
- Easy recovery of the crew (catastrophic)
- Backup life-support systems.

The two customer requirements for system reliability are:

- High reliability (i.e. > 0.98) of the MLV
- Mature, proven technology.

The threat of major (e.g. multiple engines out, life-support failure) and minor (e.g. single engine out) system failures, structural failure, and explosions makes it necessary for a crew to be able to abort a mission at any time. The six customer requirements for the ability to abort are:

- Abort at zero-zero (zero altitude and zero velocity)
- Abort in route to orbit
- Abort in orbit
- Abort during re-entry
- Separation of crew from MLV at high speeds (catastrophic)
- Easy separation from the MLV (catastrophic).

The term “system robustness” refers to the MLV’s ability to perform many different operations and handle changing circumstances. The overall MLV must be robust so that the need to abort is minimized. The six customer requirements for robustness are:

- The MLV can adjust itself to minor system failures
- The MLV is weather tolerant
- The MLV is modular to allow simple transformation between manned and unmanned missions
- The crew compartment is easily accessed
- The MLV’s complexity is lower than current level.

The MLV’s structure includes the shape and size of the vehicle and its performance capabilities. The customer requirements for the MLV’s structure are:

- Minimal weight and size of the system
- Lower operating costs than the current system.

5.4.5 Determination of the relative importance of customer requirements

Following Ullman⁴ (1992), we used a pairwise comparison to determine numeric weightings for each customer requirement. These weightings were used for the final concept selection. Before any comparisons could be made, the mandatory customer requirements were identified as:

- Abort at Zero-Zero
- Abort en route to orbit
- Abort during re-entry
- Get the crew away alive.

Performance Comparison		Abort zero zero	Abort in route to orbit	Abort during re-entry	Get crew away alive	Vehicle reliability	Fault recovery	Mature technology	Access to flight controls	Return incapacitated crew	Minimal weight and size	Weather tolerant	Vehicle simplicity	Ease of recovery of crew	Modularity	Self contained life support	Get crew away without injury	Abort at high speeds	Ease of separation	Low cost	Access vehicle easily	Abort in Orbit	Weighting
Abort zero zero		1																					1
Abort in route to orbit			1																				1
Abort during re-entry				1																			1
Get crew away alive					1																		1
Vehicle reliability						1																	1
Fault recovery							1																1
Mature technology								1															1
Access to flight controls									1														1
Return incapacitated crew										1													1
Minimal weight and size											1												1
Weather tolerant												1											1
Vehicle simplicity													1										1
Ease of recovery of crew														1									1
Modularity															1								1
Self contained life support																1							1
Get crew away without injury																	1						1
Abort at high speeds																		1					1
Ease of separation																			1				1
Low cost																				1			1
Access vehicle easily																					1		1
Abort in Orbit																						1	1
Total																							100.00%

Figure 5.6.

Because the remaining customer requirements are not mandatory, their relative importance was calculated in the pairwise comparison. The five most important requirements are:

- Return an incapacitated crew 11.03%
- Get crew away without injury 11.03%
- Abort at high speeds 10.29%
- Separate easily 9.56%
- Have high vehicle reliability 9.56%.

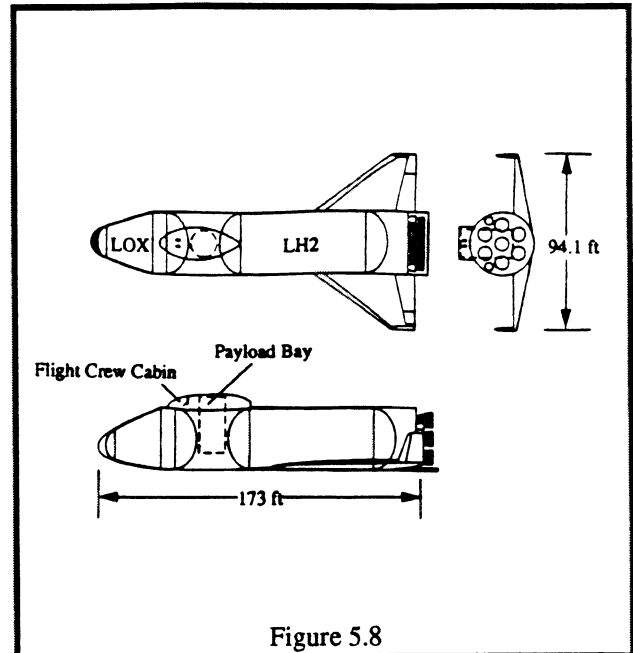
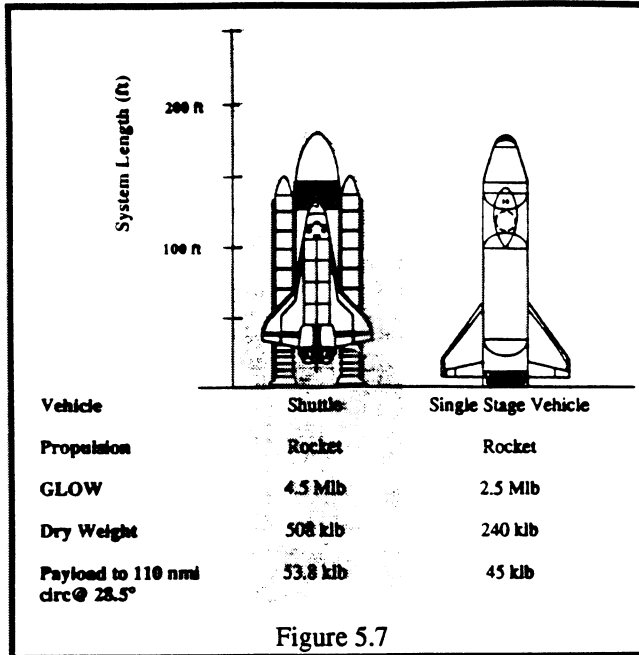
The remaining weightings are listed in Figure 5.6.

5.5 Concept Generation and Recommendation of Final Concept

We chose a hybrid launch system to achieve NASA's future goals as stated by Brown³ (1994). The two main parts of a hybrid launch system are the MLV and the modular astronaut escape system. Abort techniques such as RTLS and DRLS can be used in single engine out and dual engine out situations. These situations are not classified as catastrophic, thus the astronaut escape system remains in contact with the MLV until the abort maneuver is complete. However, in the case of a catastrophic structural failure, malfunction, or explosion, the astronaut escape module will separate from the MLV and transport crew members to a safe location on Earth. One advantage of the hybrid concept is that system reliability of the MLV can be sacrificed in favor of reduced cost while the crew survivability rating is improved due to the astronaut escape system. Also, the modular astronaut escape system can be removed from the MLV for unmanned missions.

5.5.1 Hybrid launch system: MLV

Following Advanced Technology Team (1993), the NASA winged SSTO concept (see Section 5.4.3.2.2) was selected as the hybrid launch system's MLV. Figure 5.7 shows the proposed SSTO vehicle as it compares to the Space Shuttle, and Figure 5.8 shows the general dimensions of the SSTO vehicle. Key features include:



Basic shape: Winged lifting body
 Propulsion: Rocket powered
 Takeoff: Vertical
 Landing: Horizontal
 Dry weight: 240,000 pounds

Payload (manned): 25,000 pounds (@ 28.5° to LEO)
 Payload (unmanned): 45,000 pounds (@ 28.5° to LEO)
 \$/lb payload (manned): \$1,995
 \$/lb payload (unmanned): \$1,240
 Turnaround time: 68 hours
 Development cost: \$661.4 Million

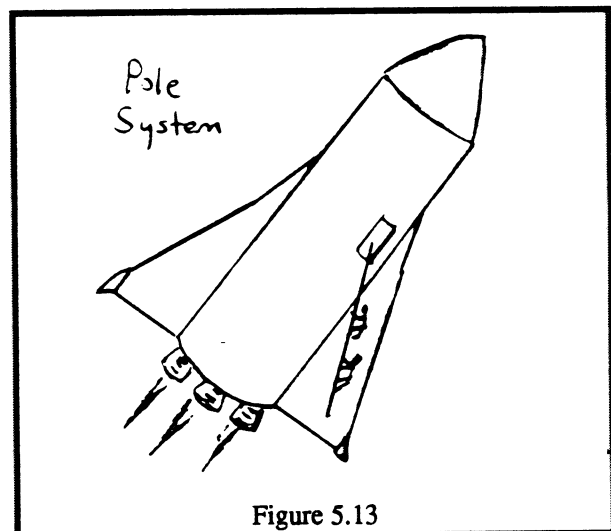
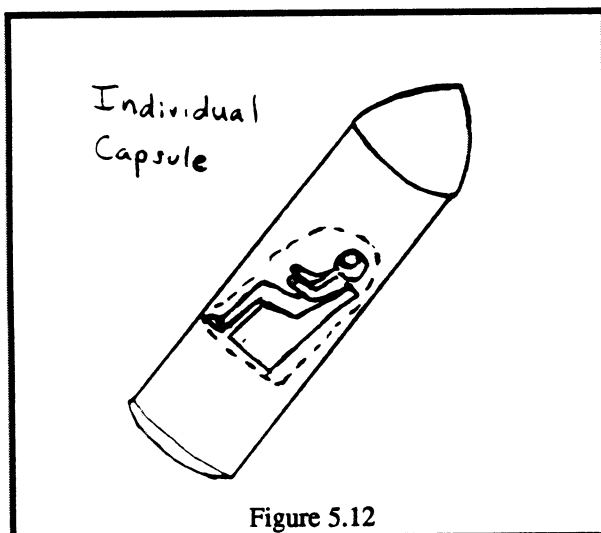
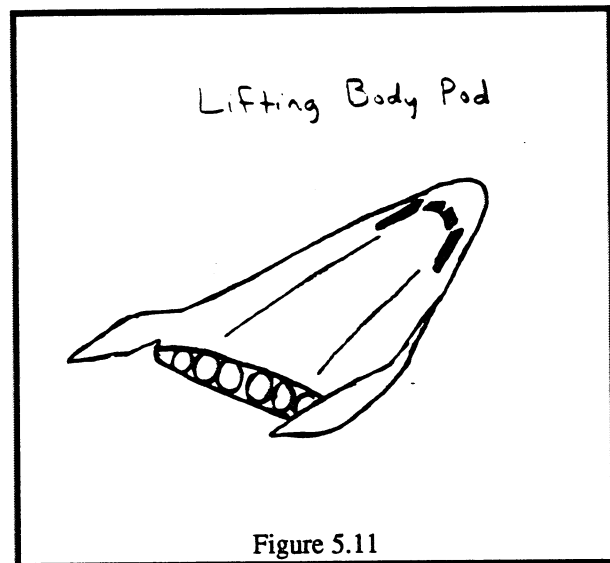
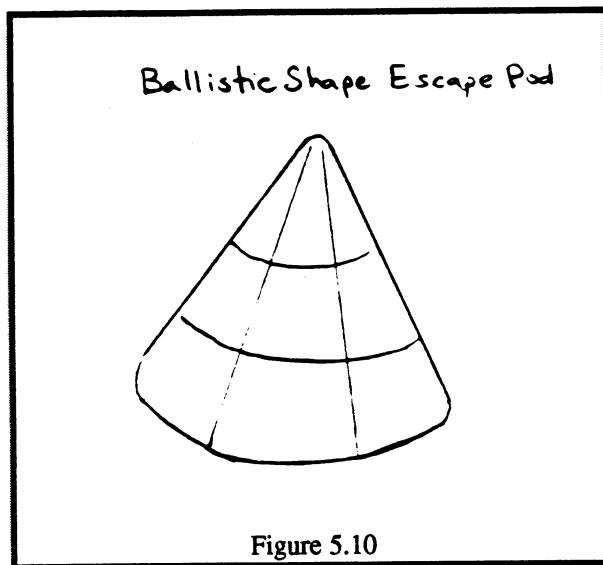
The SSTD rocket is designed for:

- Average of 43 flights a year
- Reduced ground support
- Rapid turnaround
- Minimum manpower
- Minimum infrastructure
- Mission flexibility
- Robustness/Automated Flight

5.5.2 Hybrid launch concept: Astronaut Escape Vehicle

With the winged SSTO concept selected as the MLV, concept generation was only necessary for the hybrid launch vehicle's escape system. Accordingly, a more detailed customer requirement list was compiled with respect to the astronaut escape vehicle (Figure 5.9).

Four general escape systems were selected for further evaluation: the ballistic shaped escape pod (Figure 5.10), the lifting body pod (Figure 5.11), the individual capsule (Figure 5.12), and the currently employed pole system (Figure 5.13). The escape system holds a crew of eight astronauts.



Final Concepts

Customer Requirement	Weighting (%)
Vehicle Reliability	9.6
Fault Recovery	7.4
Mature Technology	3.7
Access to Flight Controls	2.2
Return Incapacitated Crew	11
Minimal Weight and Size	6.6
Weather Tolerant	3.7
Vehicle Simplicity	6.6
Ease of Crew Recovery	7.4
Modularity	5.2
Self Contained Life Support	0.7
Get Crew Away Without Injury	11
Abort at High Speeds	10.3
Ease of Separation	9.6
Low Cost	2.2
Access Vehicle Easily	0.7
Abort in Orbit	2.2

Figure 5-9

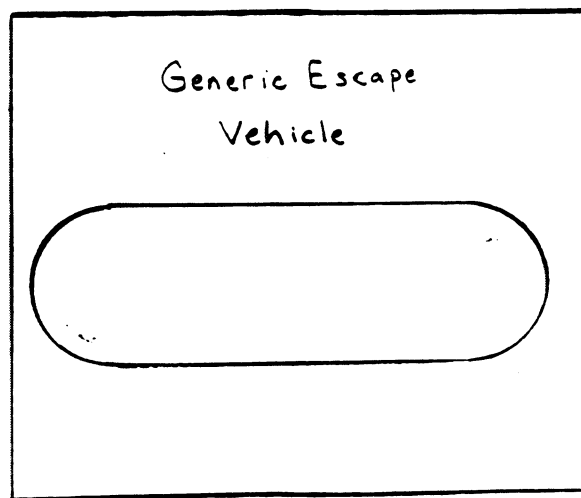


Figure 5-14

5.5.2.1 Discussion of concepts:

The final escape system must be capable of completing five main task:

- Zero-zero abort
- Separation from the SSTO MLV
- Returning to earth
- Landing
- Integration with the SSTO MLV.

Specific concepts were generated to complete each of these tasks. Throughout the following discussion, the shape in Figure 5.14 represents the escape system because the exact appearance and characteristics of the escape system have not yet been determined.

Figure 5.15 illustrates concepts for the zero-zero abort task. Figure 5.15a is a schematic of a zero-zero abort in which the escape system is shot horizontally from the MLV and lands in a body of water. The ocean near the launch pads at Kennedy Space Center and Vandenberg Air Force Base may serve as the body of water. With the proper orientation and reasonable velocity, the water should dissipate some of the escape system's impact momentum. Figure 5.15b is a schematic of a zero-zero abort in which an inflatable airbag / parachute (Gottschalk⁵, 1993) system is used. The parachute slows the descent of the escape system, and the air bag serves as a shock absorber during impact. Figure 5.15c and 5.15d are schematics of zero-zero abort concepts which both require an initial thrust in the vertical direction to give the escape system the extra height necessary for a gliding descent (Figure 5.15c) or a floating descent (Figure 5.15d). Figure 5.15e illustrates a zero-zero abort concept in which a slide is used to move the escape system away from the MLV.

Figure 5.16 illustrates concepts for the task of separating the escape system from the MLV. For all concepts included under the task of separation, the connecting joints between the escape system and the MLV are first severed with pyrotechnics. Figure 5.16a is a schematic of separation using the detonation force of a lumped mass of explosives stored under the bottom side of the escape system. The concept illustrated in Figure 5.16b uses a small solid rocket motor to propel the escape system away from the MLV, while the concept illustrated in Figure 5.16c uses liquid propellant transferred from the MLV prior to separation to power a small engine.

Figure 5.17 illustrates concepts for the task of returning to Earth. Figures 5.17a and 5.17b illustrate the concepts of gliding back to earth with and without propulsion, respectively. Figures 5.17c and 5.17d illustrate the concepts of floating back to earth with and without propulsion, respectively. Propulsion adds an element of control to the crew on the return trip.

Specific concepts for the landing on land, on water, or in either place. Finally, the concepts for integration of the escape system into the MLV are illustrated in Figure 5.18. Figure 5.18a illustrates the escape system being fully integrated into the MLV. The partially integrated escape system, illustrated in Figure 5.18b, uses the shape of the MLV as well as part of the escape system, with part of the escape system protruding from the MLV body. Figure 5.18c illustrates the non-integrated concept where the escape system rides on the back of the MLV and is in full view.

Figure 5-15c

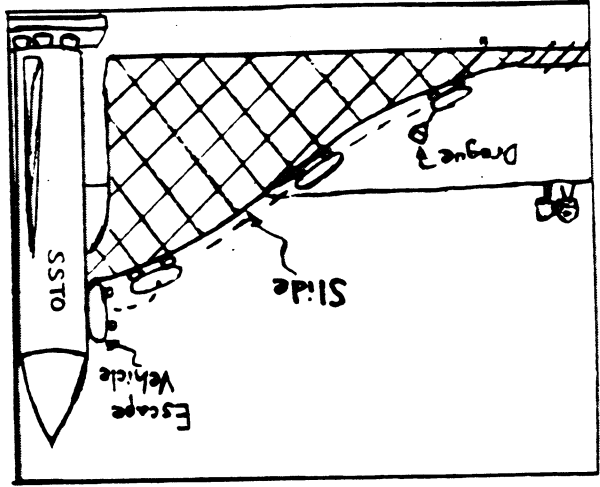


Figure 5-15d

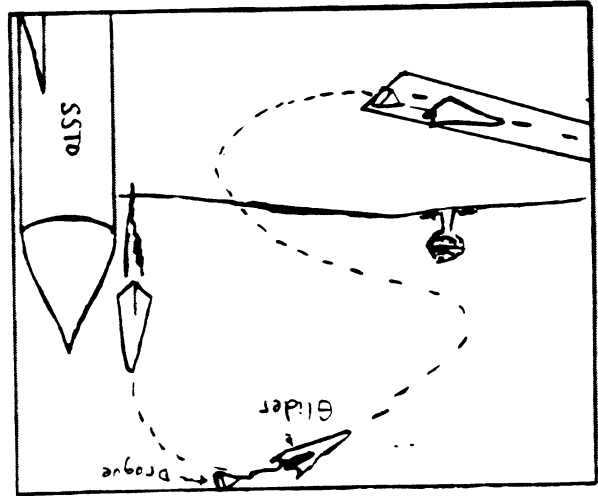


Figure 5-15e

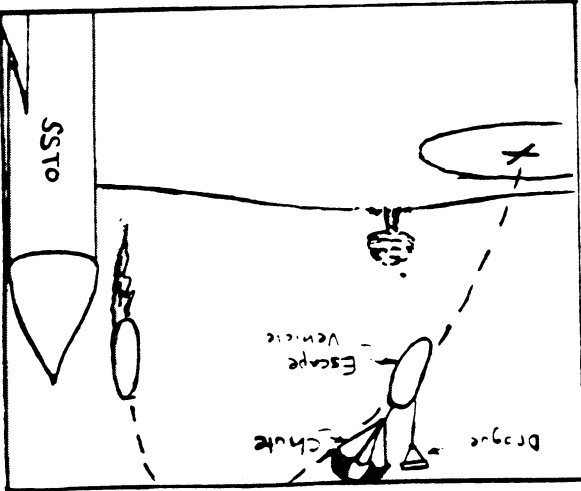


Figure 5-15a

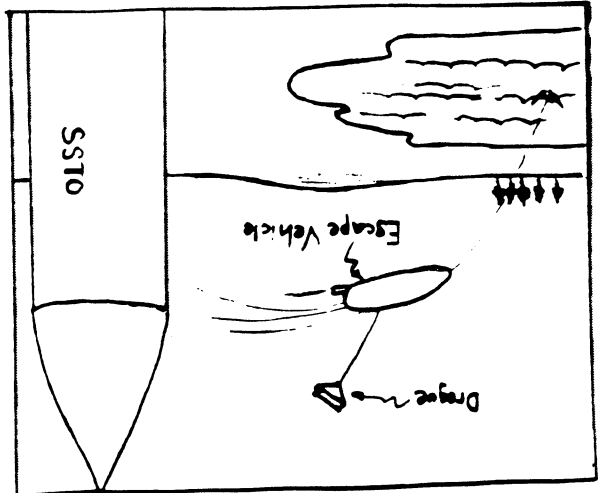
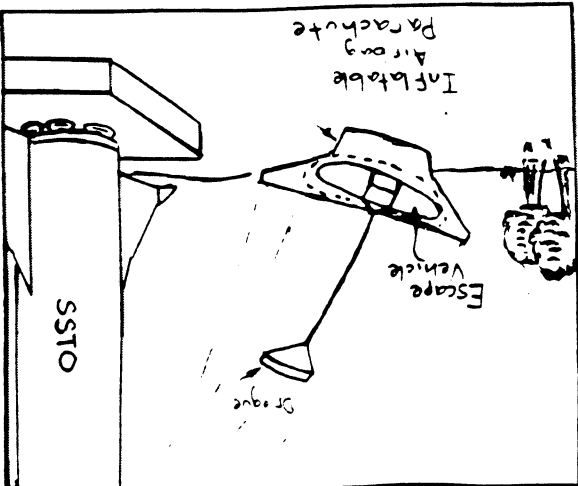


Figure 5-15b



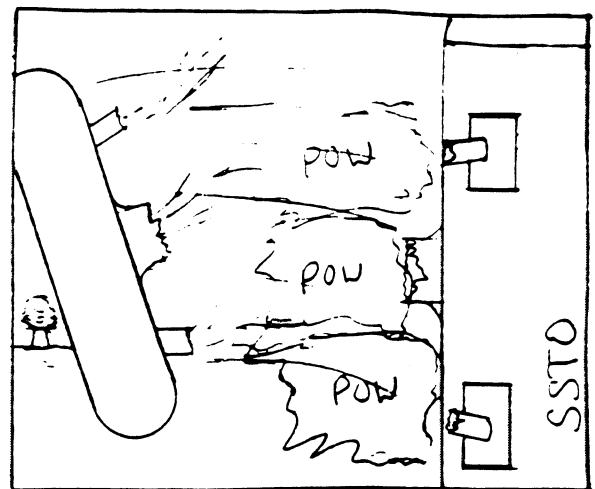
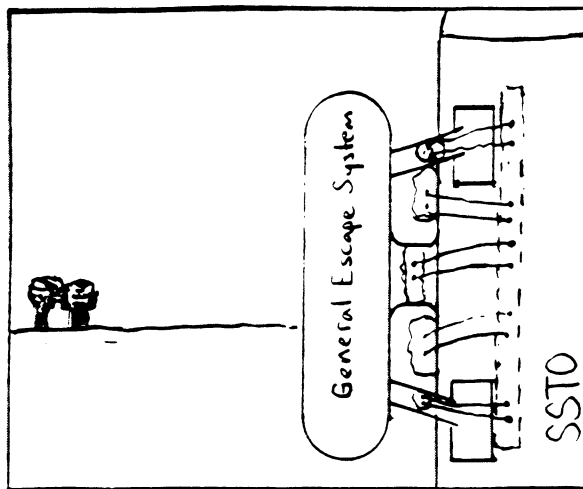


Figure 5-16a

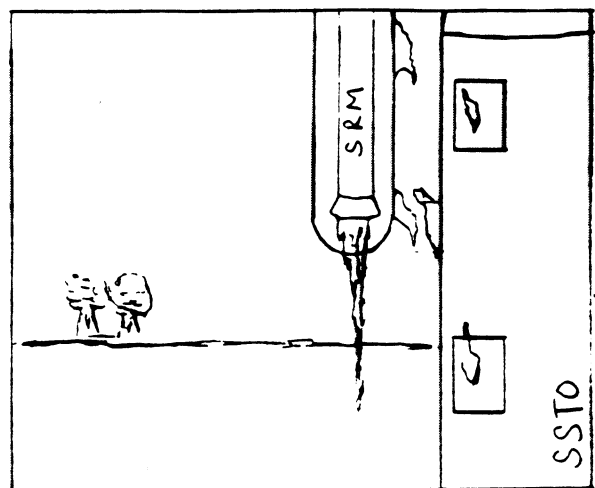
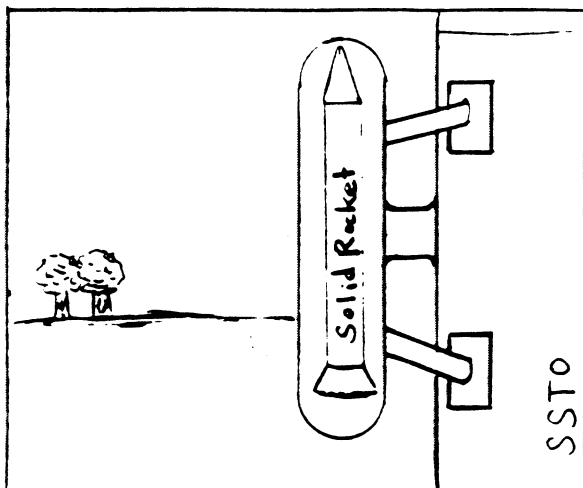


Figure 5-16b

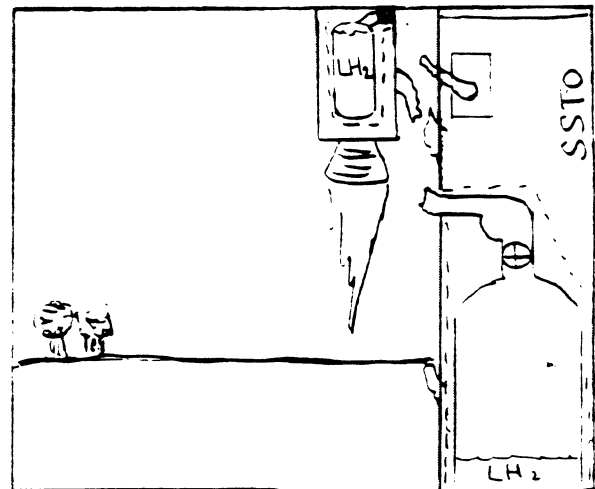
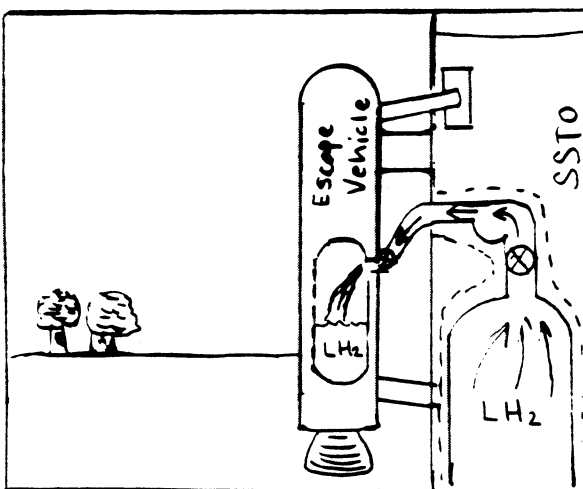


Figure 5-16c

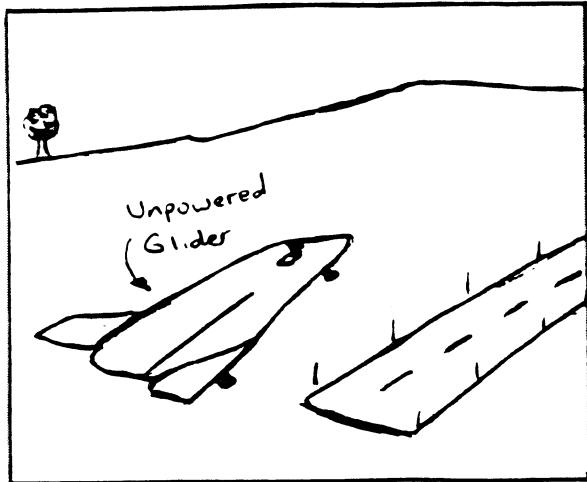


Figure 5-17a

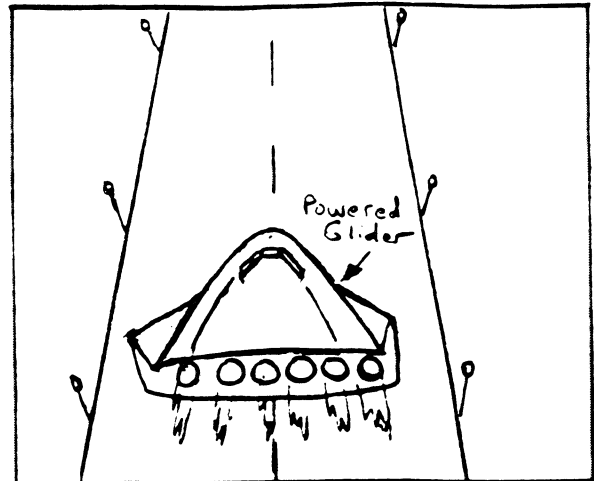


Figure 5-17b

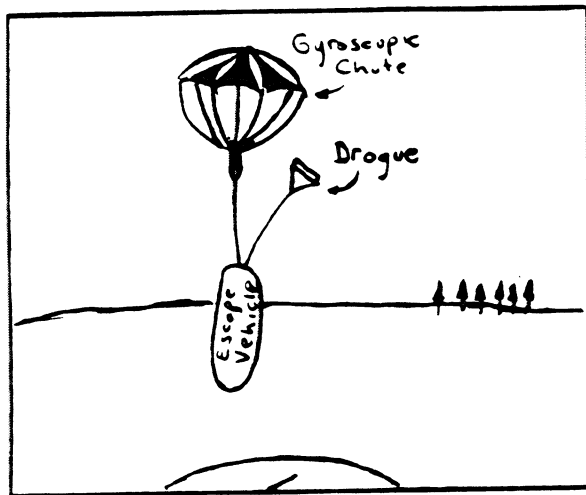


Figure 5-17c

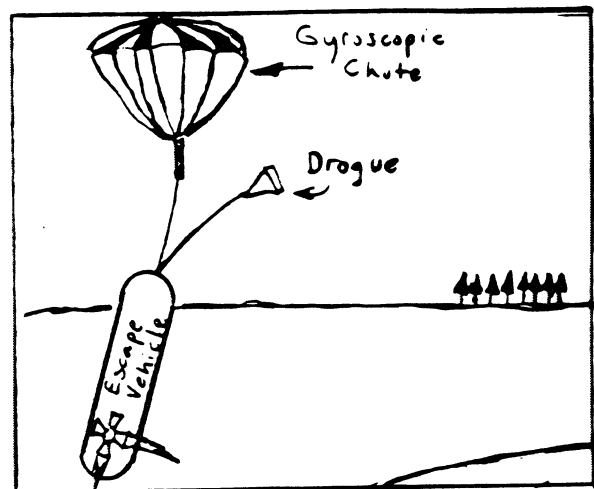


Figure 5-17d

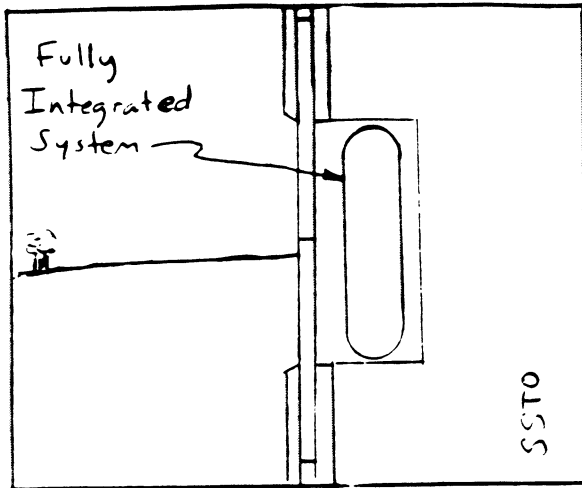


Figure 5-18a

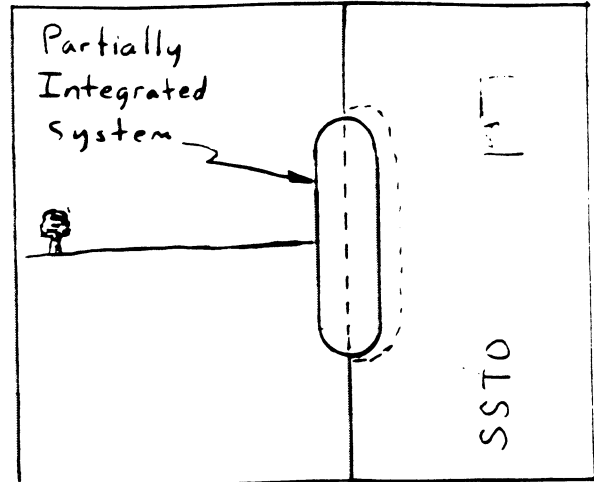


Figure 5-18b

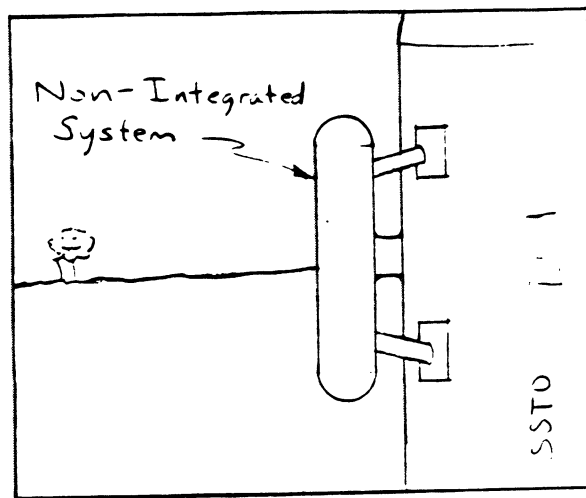


Figure 5-18c

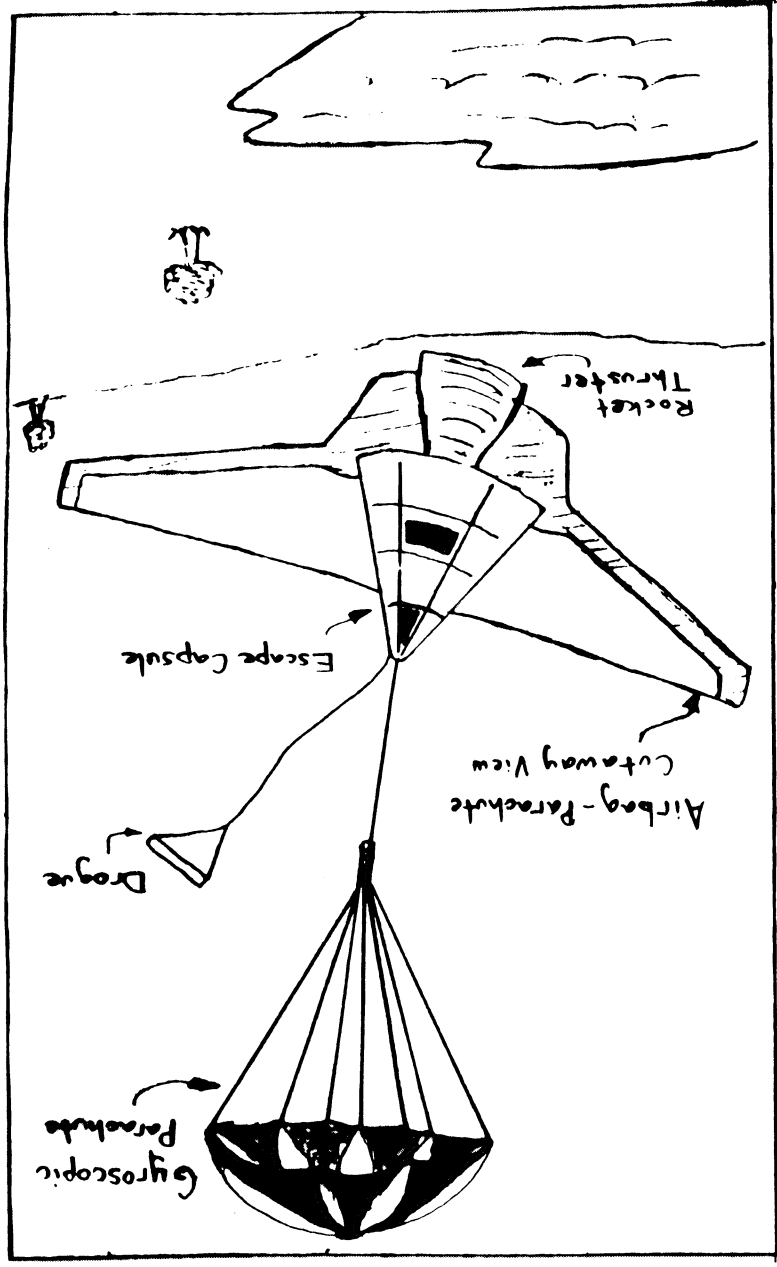


Figure 5-19b

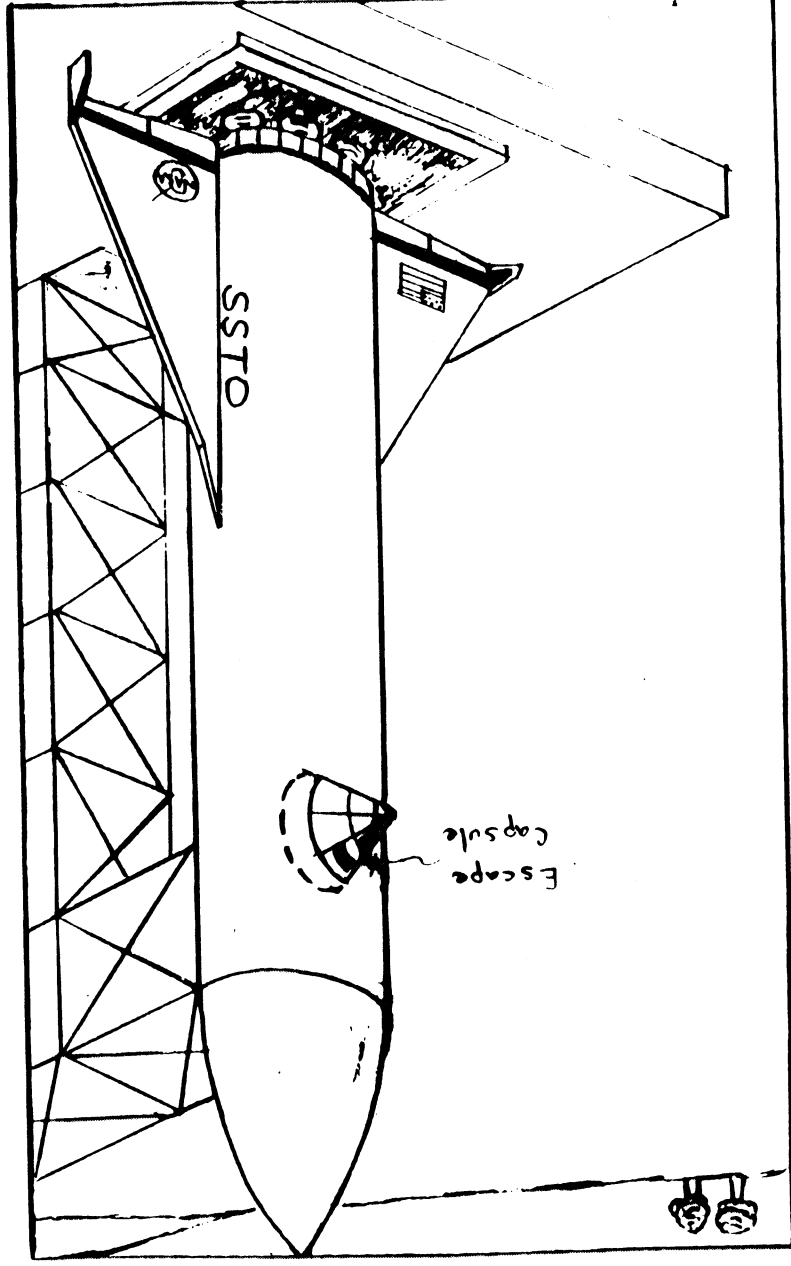


Figure 5-19a

5.5.2.2 Escape system concept selection

The pole escape system concept (see Figure 5.13) was excluded from further evaluation because it cannot realistically satisfy all of the crew safety customer requirements listed in Figure 5.9 for each of eight crew members attempting to escape from the MLV during a catastrophic failure. The remaining three general escape systems (see Figures 5.10, 11, and 12) utilize specific concepts for each of the following tasks: zero-zero abort, separation from the SSTO MLV, return to earth, landing, and integration into the SSTO MLV. These specific concepts for each escape system are listed under their respective tasks in Tables 5.1a, 5.1b, and 5.1c.

For each escape system; the ballistic shaped escape pod, the lifting body pod, and the individual capsule, the specific concepts for completing each task were compared to one another using the decision matrix method (Ullman⁴, 1992). The decision matrix provides a means for scoring concepts in their ability to meet the detailed customer requirements for the escape system listed in Figure 5.9. One decision matrix was used to select the best concept for each of the five tasks for each escape system in Table 5.1. The best concepts for each task were combined to give one best configuration for the ballistic shaped pod, lifting body pod, and individual escape capsule systems. These concepts are listed in Table 5.2. Finally, these three configurations were compared in a decision matrix to determine the best overall escape system design. The characteristics of this final escape system are listed in Table 5.3.

5.5.2.3 Configuration of the final escape system (ballistic escape pod)

The ballistic escape pod is illustrated in Figure 5.19. Figure 5.19a shows the pod in its integrated position with the MLV, and Figure 5.19b shows the pod with all of its subsystems exposed. The escape pod uses technology currently employed in the F-111. As with the F-111, the MLV is controlled from the pod which serves as the cockpit.

The dimensions and weight of the escape pod are the minimum necessary for eight crew members, life-support systems, and flight controls. The pod (see Figure 5.20) has a bottom diameter of 14 feet, top diameter of 8 feet, and height of 5.5 feet. Six crew members sit facing forward in two rows of three while the pilot and co-pilot have access to flight controls. The pod is partially integrated into the MLV and is intended to be occupied only during the flight to orbit and re-entry. Once the astronauts reach orbit, they will leave the escape pod to conduct their mission in other compartments of the vehicle. The escape system weighs approximately 13,000 pounds; this value is based on information in Chacko⁸ (1969) and Gottschalk⁵ (1993).

Separation from the MLV is accomplished with a small, onboard rocket motor which uses self contained fuel to provide the 13,000 pounds force thrust necessary to propel the escape pod forty feet from the MLV in one second. Forty feet was determined to be a safe distance from the vehicle for any possible MLV orientation during a catastrophic failure. Pyrotechnics, similar to those used by the Space Shuttle for SRB separation, are used to sever the connections between the escape pod and MLV.

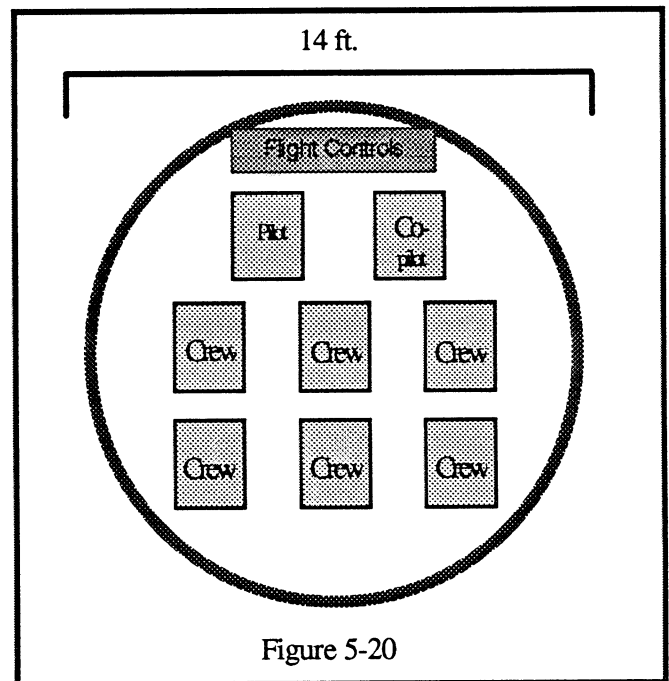


Figure 5-20

The zero-zero abort concept (see Figure 5.15b) uses a deployable drogue and an inflatable airbag / parachute (Gottschalk⁵, 1993). The drogue is a two foot diameter, rotating, flexible dragmill parachute. The drogue is made entirely of Kevlar and weighs 0.5 pounds (Design News⁷, 1984). The drogue is used to reduce the speed of the escape pod and more importantly to stabilize its descent. The fully inflated airbag / parachute (see Figure 5.21) is forty two feet in diameter, seventeen feet tall, and weighs 500 pounds including the weigh of the inflation system (Gottschalk⁵, 1993). The airbag inflates in 1.5 seconds, and its large surface area creates a drag force which slows the descending pod. The airbag reduces the impact between the pod and the ground by venting 180 cubic feet of air through three, eight inch relief valves. Conventional parachutes would not have sufficient time to deploy at an altitude below five hundred feet; therefore, the zero-zero abort concept is also utilized for any aborts within the altitude range of zero to five hundred feet.

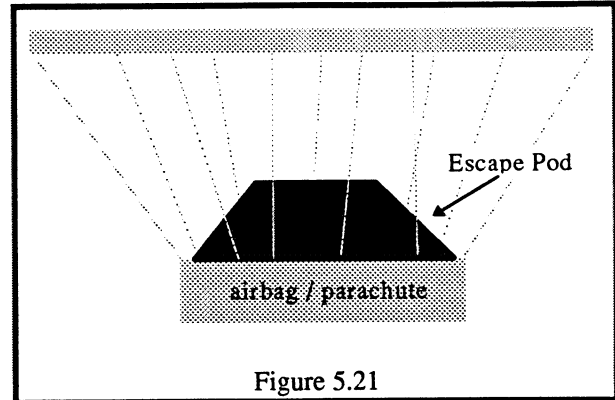


Figure 5.21

For aborts at altitudes greater than five hundred feet, a ringsail parachute is used along with the drogue and the inflatable airbag / parachute (see Figure 5.19c). First, the drogue is used to reduce the pod's speed to Mach 0.46. Upon reaching Mach 0.46, the ringsail parachute is deployed and reduces the pod's speed to 23 feet per second (Phillips⁶, 1991). At 500 feet, the airbag / parachute is inflated, and the pod descends to Earth. Air remaining in the airbag after impact allows it to serve as a flotation device in the case of a water landing.

Ballistic Shaped Escape Pod

Zero-zero	Separation	Return to Earth	Landing	Integration
Lake	Detonation	Float	Land	Fully Integrated
Parachute	Stored Propellant	Float with propulsion	Water	Partially Integrated
Airbag/Parachute	Shared Propellant		Both	Fully Exposed
Slide				

Table 5.1a

Lifting Body Escape Pod

Zero-zero	Separation	Return to Earth	Landing	Integration
Lake	Detonation	Glide	Land	Fully Integrated
Glide	Stored Propellant	Glide with propulsion	Water	Partially Integrated
Airbag/Parachute	Shared Propellant		Both	Fully Exposed
Slide				

Table 5.1b

Individual Escape Capsule

Zero-zero	Separation	Return to Earth	Landing	Integration
Lake	Detonation	Float	Land	Fully Integrated
Parachute	Stored Propellant	Float with propulsion	Water	Partially Integrated
Airbag/Parachute	Shared Propellant		Both	Fully Exposed
Slide				

Table 5.1c

Best Configuration For Each Concept

	Final Ballistic Pod Concept	Final Lifting Body Concept	Final Individual Escape Capsule Concept
Zero-zero abort	Airbag/parachute	Airbag/parachute	Lake
Separation	Stored fuel	Stored Fuel	Stored Fuel
Return to Earth	Float back	Glide back	Float with propulsion
Landing	Land and water	Land and water	Land and water
Integration	Partial Integration	Fully exposed	Fully Integrated

Table 5.2

Final Escape System Concept

Overall Shape	Ballistic Escape Pod
Zero-zero abort	Airbag/parachute
Separation	Stored fuel
Return to Earth	Float back
Landing	Land and water
Integration	Partial Integration

Table 5.3

All of the final escape system concepts described for the task of separation, zero-zero abort, landing, and integration are based on mature technology. Mature technology has the advantage of minimal development cost and proven reliability. Furthermore, the escape pod is modular which allows it to be removed from the SSTO MLV for unmanned flights, thus increasing the payload capacity of the SSTO.

5.6 Conclusion

The escape system will take the place of the cockpit in the current NASA SSTO configuration. The volume of the proposed escape pod is 846 cubic feet, while the volume of the current NASA SSTO is estimated to be 1100 cubic feet. Because the volumes of the two cockpits are relatively close, and the current NASA SSTO will have similar surrounding structure, it is valid to assume that the current NASA SSTO cockpit weighs nearly the same as the 13,000 pound proposed escape pod. Therefore, the weight penalty (1000 lbs.) of the escape pod is only due to its parachute, airbag, and propulsion systems. This lowers the payload capacity of the NASA man-rated SSTO to 24,000 pounds. For unmanned missions, the 14,000 pound modular escape pod is removed from the MLV giving the SSTO a payload capacity of 38,000 pounds. The SSTO vehicle uses a man-rated design for all missions, manned and unmanned, because according to Ryan⁹ (1994), no quantitative cost advantage exists for a non-man-rated SSTO over a man-rated SSTO as originally hypothesized in Section 5.3.

Although Ryan⁹ (1994) estimates that no cost saving are achievable through non-man-rating the MLV, the final ballistic escape pod system can be integrated into the MLV with a minimal cost per pound of payload penalty and will increase the crew survivability rate of the launch system. The major accomplishment of this study was the development of a ballistic escape pod which can be integrated into the current NASA SSTD configuration. It is possible that the addition of the escape pod to the current NASA SSTD would increase the launch vehicle's crew survivability rate to the desired 0.9999.

5.7 Bibliography

- (1) Office of Technology Assessment, Congress of the United States, Access to Space, The Future of U.S. Space Transportation Systems, (Washington:GPO, 1990)
- (2) Asker, J.R. "Radical Upgrades Urged To Cut Shuttle Cost" Aviation Week and Space Technology, 29 Nov. 1993: 42-4.
- (3) Norman Brown, personal interview, 24 Jan. 1994.
- (4) Ullman, David G. The Mechanical Design Process, New York, McGraw Hill, 1992.
- (5) Gottschalk, Mark "Inflatable Delivery Vehicle Replaces Parachute" Design News, 22 Feb. 1993: 171-2.
- (6) Phillips, Edward "USAF Evaluates New Parachute / Airbag System For F-111 Crew Escape Module" Aviation Week and Space Technology, 16 Dec. 1991: 49- 50.
- (7) "Sandia Labs Test Rotating Recovery Parachute Design", Design News, 19 Nov. 1984: 34+.
- (8) Chacko, George Reducing the Cost of Space Transportation, American Astronautical Society, 1 1969.
- (9) Dr. Robert Ryan, personal interview, 15 Mar 1994.

6 LH₂ Fuel Tank Design for SSTO Vehicle

6.1 Summary

6.1.1 Design Objective

Design a minimum weight liquid hydrogen fuel tank for the NASA SSTO vehicle that is constructed from composite materials.

6.1.2 Abstract

This report will discuss the design of a liquid hydrogen fuel tank constructed from composite materials. The focus of this report is to recommend a design for a fuel tank which will be able to withstand all static and dynamic forces during manned flight. Areas of study for the design include material selection, material structural analysis, heat transfer, thermal expansion, and liquid hydrogen diffusion. A structural analysis FORTRAN program was developed for analyzing the buckling and yield characteristics of the tank. A thermal analysis Excel spreadsheet was created to determine a specific material thickness which will minimize heat transfer through the wall of the tank. The total mass of the tank was determined by the combination of both structural and thermal analyses. The report concludes with the recommendation of a layered material tank construction. The designed system will include exterior insulation, combination of metal and organic composite matrices and honeycomb.

6.2 Glossary

B-AL Boron Aluminum Composite
B-EP Boron Epoxy
ET External Tank
GL-EP Glass Epoxy
GR-EP Graphite Epoxy Composite
LH₂ Liquid Hydrogen
MSFC Marshall Space Flight Center
SSTO Single Stage To Orbit
TC Thermal Conductivity
TR Thermal Resistance

6.3 Background

The current LH₂ tank design is based on the configuration of the Space Shuttle's external LH₂ tank. The technology used for the Space Shuttle ET dates from the 1970's. The current design effort illustrates the gains possible using state-of-the-art technology.

MSFC has completed a preliminary design of the LH₂ tank for the SSTO vehicle. The tank structure is designed to contain 244,794 lb. of fuel and withstand all static and dynamic loading during all phases of SSTO operation.(Graham¹) Conservation of weight is of primary consideration and is the main focus in this design effort.

6.4 Material Selection

6.4.1 Composite Materials

A major area of focus for the design of the LH2 Fuel Tank was the material selection process. It was decided early in the design process that an effort would be made to use *composite* materials in an effort to reduce the weight of the tank from that of NASA's baseline design.

Composites are defined as "those materials that contain a reinforcement (such as fibers or particles) supported by a binder (matrix) material." (*Composites*², pp. 27) The fibers of the material are designed to carry the majority of the applied load while the matrix binds the fibers and transfers the load between fibers. Composite materials are designed specifically for high directional stiffness-to-weight and strength-to-weight ratios. The primary design criterion for the structural analysis used in this project was stiffness-to-weight ratio, since it was decided that the tank design was a stiffness limited design. Therefore, the material selection process focused on those materials with a high ratio of stiffness-to-weight. The following table is provided for comparison of different materials. (*Comparison*¹², pp. 79-241)

Table 6.1 Material Properties.

Material	Density (lbm/in ³)	Modulus (10 ⁶ psi)	Stiffness/Density Ratio
Gr-Ep	0.057	40.0	702
B-Ep	0.073	30.0	411
B-Al	0.100	28.0	280
Gl-Ep	0.075	5.0	67
Titanium	0.183	18.5	101
Aluminum	0.102	10.8	106
Steel	0.292	30.0	103

*note: composite moduli are for unidirectional composite, longitudinal direction

Research into composite materials led to the decision to use two types of composite materials, graphite-epoxy (Gr-Ep) and boron-aluminum (B-Al). Gr-Ep is made from high modulus graphite fibers bound in an organic epoxy matrix. B-Al is a metal-matrix composite using boron fibers as reinforcement to an aluminum matrix.

Beyond the high stiffness-to-weight ratios of the two materials, Gr-Ep and B-Al were chosen for other important reasons. Gr-Ep was chosen since it is a proven material and can be easily manufactured. A pressure vessel such as a fuel tank can be made from Gr-Ep using a filament winding process, where the composite material is wound about a mandrel, maintaining the fiber as continuous throughout the material. A composite made from continuous fiber is highly desirable for its high strength and fracture toughness characteristics. B-Al was chosen specifically to provide a barrier to hydrogen diffusion. A design issue that was of important consideration was maintaining the volume of hydrogen fuel with minimum leakage or diffusion through the container walls. A metal barrier such as aluminum was necessary to insure hydrogen diffusion was kept to a minimum.

6.4.2 Aluminum Honeycomb Description

In addition to Gr-Ep and B-Al, aluminum honeycomb was used to provide additional stiffness to the tank structure. The honeycomb was used to provide spacing between the layers of composite materials to increase wall stiffness. Aluminum honeycomb was chosen since it is a proven material and is extraordinarily lightweight. Using a hexagonal cell arrangement, a cell size of 7/8 inch, a cell wall thickness of 10 mils, and Al 2024 as the base material, the honeycomb material density was calculated as follows (See Figure 6.5): (Hackman³, pp. 12.5)

$$\rho_c' = \frac{3 \cdot t_c \cdot \rho_c}{s} \quad \text{Eq. 6.1}$$

t_c = cell thickness = 0.01 in
 s = cell size = 7/8 in
 ρ_c = density = 0.100 lbm/in³

The density of the honeycomb was found to be 0.00343 lbm/in³ or 5.92 lbm/ft³. This density was used to determine the honeycomb's contribution to the weight of the final tank design.

6.5 Design Concept

6.5.1 Structural Concepts

The PUF (Section 6.12) shows that one of the most important criteria in the design of the LH₂ tank is structural stability. The first step in performing a structural analysis is to determine the spatial requirements of the tank. Graham and Luz⁹ (1993) give the required outer diameter of the tank as 331 inches and the total internal volume of the cylindrical section of the tank as 39,422 ft³. Due to the possibility of changing the tank wall thickness (t), the total length of the tank will be considered variable (Graham²) as long as the outside diameter is not increased nor the total fuel volume decreased. A large change in orbiter vessel length may cause a significant change in the location of the center of gravity that could effect vehicle control, but this will not be considered due to the relatively small length changes expected and the preliminary nature of this effort. There will be a small weight penalty involved with the extra vehicle length that will also not be accounted for.

The tank will be subjected to various pressures, axial loads, and bending moments that result from the hydrostatic pressure of the hydrogen, dynamic flight loads, and applied loads due to the structure of the tank. The loads were given in (Graham³) with values of

$$\begin{aligned} F_{\text{axial}} &= 3,850,000 \text{ lbf} \\ M_{\text{bending}} &= 170,000,000 \text{ in-lbf} \\ P_{\text{ultimate}} &= 49 \text{ psig} \end{aligned}$$

The combined axial load and bending moment represent the critical dynamic buckling load couple that the tank experiences in its lifetime. These values are not absolute and could possibly change during refinement of the vehicle design, but will be used for all further calculations in the present work. NASA

uses a 1.4 factor of safety on all loads in the design of man rated vessels (Graham¹) and this effort will use the factor in all subsequent structural calculations.

For simplicity, only the cylindrical portion of the tank will be considered. A feasible design of this portion of the tank should lead to the conclusion that the remainder can also be constructed of composite materials, but proof of this is beyond the preliminary aspect of this design. The portion of the tank under consideration is noted in Graham and Luz⁹ (1993) as the top barrel, middle barrel, and bottom barrel. All comparisons with NASA's designs will be done only with this section of the tank.

The primary goal of this design effort is weight reduction as explained in section 6.3. Initial computations suggested that the tank would be stiffness limited rather than strength limited due to the extremely high axial load and bending moment as compared to the relatively low internal pressure. Therefore, the primary determining factor in the choice of composite materials to be considered in the tank design was the fiber direction stiffness to weight ratio. Numerous materials were considered as explained in section 6.4.1, but were reduced to two materials: a 50% fiber, Boron-Aluminum metal matrix composite and a High Modulus Graphite Epoxy, strictly on their fiber direction stiffness to weight ratio. However, different combinations of these materials were considered. Since the organic composite was believed to be insufficient to prevent diffusion of the hydrogen, it was determined that the tank required at least one layer of the metal matrix composite to be a feasible design. But, since the graphite epoxy has a higher fiber direction stiffness to weight ratio, it was postulated that the best arrangement could possibly be a combination of the metal matrix composite as the inner skin, an aluminum honeycomb sandwiched in the middle, and a graphite epoxy composite as the outer skin. This arrangement would theoretically give the best configuration in that the metal matrix would be located at the inner wall, giving high transverse strength and a sufficient barrier to hydrogen diffusion. The aluminum honeycomb would serve to increase the buckling resistance by increasing the moment of inertia of the tank walls in the same way that the flange increases the moment of inertia of an I-beam. The outer layer of graphite epoxy serves to increase the stiffness of the tank by its high stiffness to weight ratio. To test these assumptions a theoretical buckling analysis was performed on the following material configurations:

- 1) one metal matrix skin
- 2) two metal matrix skins separated by honeycomb
- 3) metal matrix inner skin, honeycomb middle, and graphite epoxy exterior skin

6.5.2 Lamination theory of composite materials

The most notable difference between composite materials and isotropic materials is the presence of fibers intimately bonded to the matrix material. An initial examination leads to the correct assumption that the composite material will have very different properties in the fiber direction than it will in the transverse (across fiber) direction. Whereas an isotropic material has a single value of modulus of elasticity, a composite material has a modulus of elasticity in the fiber direction and a modulus of elasticity in the transverse direction. Likewise, composites have different strength values in the two directions. An isotropic material has a single value of Poisson's ratio, unlike a composite material that has four Poisson's ratios, two of which are independent values. The notation that will be used with respect to composite materials is shown in Figure 6.1.

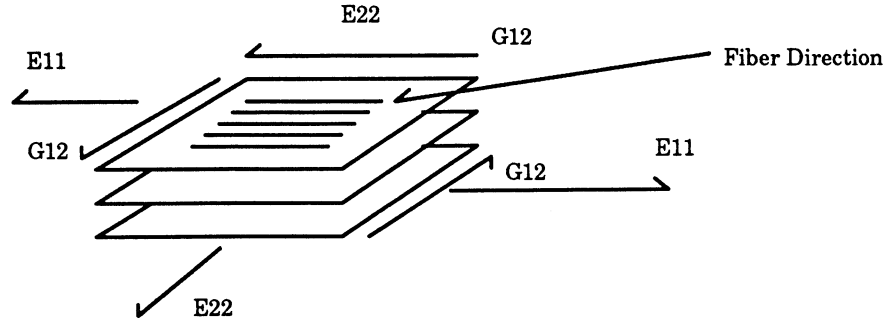


Figure 6.1

The fiber direction will be noted with a 1, while the transverse directions will be noted as the 2 and 3 directions. For this case, the fibers will be equally spaced and therefore the 2 and 3 directions will be essentially the same. Using this notation, E_{11} represents the modulus of elasticity in the fiber direction. Figure 6.2 shows this notation with respect to a three ply material, assuming that all fibers run parallel to those shown. If the fibers were arranged in different directions, the material would have a local coordinate system for each fiber orientation. Poisson's ratio - ν_{12} represents the corresponding percentage of strain that is observed in the 2 direction when a strain occurs in the 1 direction. Likewise ν_{23} represents the corresponding percentage of strain that is observed in the 3 direction when a strain is observed in the 2 direction. The two other Poisson's ratios can be calculated from known material parameters from the following equations:

$$\nu_{21} = \nu_{12} \left(\frac{E_{22}}{E_{11}} \right)$$

$$\nu_{32} = \nu_{23}$$

Eq. 6.2

The tank uses a set of global coordinates in the tank's reference frame along with the local coordinates used for the reference frame of each composite material. The vertical axis of the cylinder will be taken as the x direction. The tangent to the tank in the circumferential direction is noted as the y-direction. Therefore, the internal pressure causes a hoop stress that will be located in the y direction, while the axial load and applied bending moment cause a stress in the x-direction. The global coordinate system is shown for the cylindrical portion of the tank under consideration. (Figure 6.2)

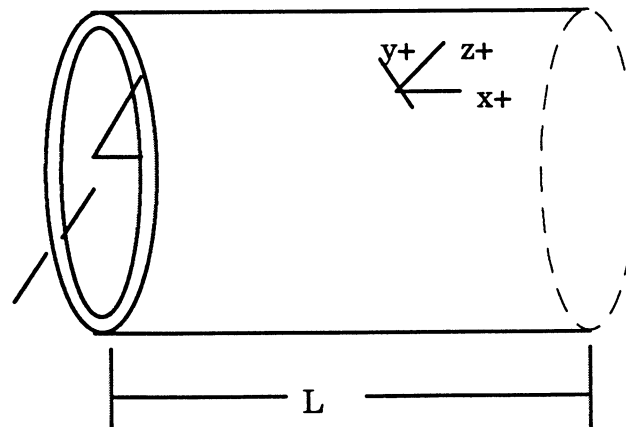


Figure 6.2

The goal associated with this study of lamination theory is to accurately approximate the laminate properties in the x-y coordinate system knowing the number of layers in the tank wall, the orientation of the fibers in each layer, and the material properties of each layer. This involves approximating the behavior of the individual layers of fibers and matrix as a single material with isotropic properties. The first assumption that is made to accomplish this is that the plane sections of material remain plane. This assumes that the layers of the material have an infinitely strong bond that will not separate or yield during the loading of the material. While bond failure in composite materials is not impossible, it will not be considered in this preliminary design effort.

Hooke's law for composite materials is given as:

$$\begin{array}{rcl} \epsilon_{11} & \frac{1}{E_{11}} & -\frac{\nu_{21}}{E_{22}} & 0 & \sigma_{11} \\ \epsilon_{22} & = & -\frac{\nu_{12}}{E_{11}} & \frac{1}{E_{22}} & \sigma_{22} \\ \gamma_{12} & 0 & 0 & \frac{1}{G_{12}} & \tau_{12} \end{array} \quad \text{Eq. 6.3}$$

where $i=1,2,3,\dots,nmat$ and $nmat = \#$ of materials present in the laminate. (The material properties in the matrix are inputs to the buckling program.) The three by three matrix above is denoted as the S-matrix for layer i and its inverse is the stiffness matrix known as the Q_i -matrix. Using the assumption above that plane sections remain plane, it is observed that the strains in each layer must be equal for a given global direction:

$$\begin{aligned} (\epsilon_x)_1 &= (\epsilon_x)_2 = \dots = (\epsilon_x)_{nlayer} \\ (\epsilon_y)_1 &= (\epsilon_y)_2 = \dots = (\epsilon_y)_{nlayer} \\ (\gamma_{xy})_1 &= (\gamma_{xy})_2 = \dots = (\gamma_{xy})_{nlayer} \end{aligned} \quad \text{Eq. 6.4}$$

Therefore, the strains in each layer in equation 6.3 can be converted into strains in the global directions and must be equal for all layers. Using this transformation, the stiffness matrix (Q) of each material is transferred into the stiffness matrix in the global coordinates (\bar{Q}) _{i} for each layer, $i=1,2,3,\dots,nlayer$. The force per unit width is calculated for each global coordinate direction knowing the stress in each direction and the thickness of each layer (both are inputs to program).

$$\begin{aligned} \sum_{i=1}^{nlayer} F_{xi} &= \sigma_{xi} t_i = N_x \quad (N_x \text{ is the force per unit width}) \\ \sum_{i=1}^{nlayer} F_{yi} &= \sigma_{yi} t_i = N_y \quad (N_y \text{ is the force per unit width}) \\ \sum_{i=1}^{nlayer} F_{xi} &= \tau_{xy} t_i = N_{xy} \quad (N_{xy} \text{ is the shear force per unit width}) \end{aligned} \quad \text{Eq. 6.5}$$

Having the Q matrix for each layer of the laminate, the calculation of the total laminate matrices can be made: A, B, and D. The laminate matrices are computed by summing the effect that each layer has on the overall properties of the laminate, assuming that the amount of effect that a particular layer has is proportional to the thickness of that layer. The matrices are calculated from the following equations:

$$\begin{aligned} A_{ij} &= \sum_{k=1}^{nlayer} \overline{Q}_{ij} [h_k - h_{k-1}] & [i,j = 1, 2, 6] \\ B_{ij} &= \frac{1}{2} \sum_{k=1}^{nlayer} \overline{Q}_{ij} [h_k^2 - h_{k-1}^2] & [i,j = 1, 2, 6] \\ D_{ij} &= \frac{1}{3} \sum_{k=1}^{nlayer} \overline{Q}_{ij} [h_k^3 - h_{k-1}^3] & [i,j = 1, 2, 6] \end{aligned} \quad \text{Eq. 6.6}$$

The A matrix represents the extensional stiffness matrix relating the in-plane stress resultants (N's) to the mid-surface strains (ϵ_0 's) (Vinson and Sierakowski¹⁰, 1987) as:

$$\begin{matrix} N_x \\ N_y \\ N_z \end{matrix} = A \begin{matrix} \epsilon_x \\ \epsilon_y \\ \gamma_{xy} \end{matrix} \quad \text{Eq. 6.7}$$

Similarly, the D matrix is the flexural stiffness matrix relating the stress couples (M's) to the curvatures (κ 's). The B matrix relates M's to ϵ_0 's and N's to κ 's and is called the bending-stretching coupling matrix. It should be noted that a laminated structure can have bending-stretching coupling even if all lamina are isotropic, for example in our case, a laminate composed of one lamina of graphite epoxy and another of Boron Aluminum separated by a honeycomb interior. In fact, only when the structure is exactly symmetric about its middle surface are all of the B_{ij} components equal to zero, and this requires symmetry in laminae properties, orientation, and location from the middle surface. Stretching shearing coupling occurs when A_{16} A_{26} are non zero. Twisting stretching coupling occurs when the B_{16} B_{26} terms are non-zero. usually, the 16 and 26 terms are avoided by proper stacking sequences. For the present design, the tank lamina are carefully chosen to insure that the B-matrix, A_{16} , and A_{26} , are equal to zero.

Vinson and Sierakowski¹⁰ (1987), gives the buckling equations for a circular cylindrical shell shown in Figure 6.3 with a mean radius R, wall thickness h, and length L, subjected to a compressive load P, and a beam-type bending moment M.

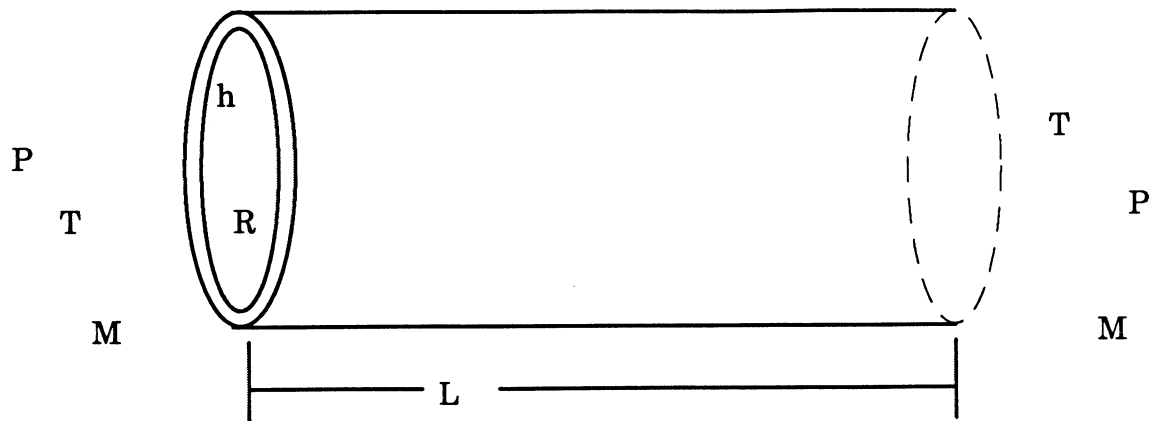


Figure 6.3

Making the assumptions that special anisotropy exists, that is $()_{16} = ()_{26} = 0$ for the A, B, and D matrices, that prebuckled deformations are not taken into account, and that the ends of the cylindrical shell are supported by rings rigid in their plane, but have no resistance to rotation or bending out of their plane, the buckling load for the case that assumes mid-plane symmetry (that is $B_{ij}=0$) and $n > 4$ is given as:

$$\frac{N_{x\sigma}}{\pi D_{11}} = m^2 \left(1 + 2 \frac{D_{12}}{D_{11}} \beta^2 + \frac{D_{22}}{D_{11}} \beta^4 \right) + \frac{\gamma^2 L^4}{\pi^4 m^2 D_{11} R^2} \cdot \frac{A_{11} A_{22} - A_{12}^2}{A_{11} + \left(\frac{A_{11} A_{22} - A_{12}^2}{A_{66}} - 2 A_{12} \right) \beta^2 + A_{22} \beta^4}$$

Eq. 6.8

where:

m = # of buckle half waves in the axial direction

n = # of buckle waves in the circumferential direction

$$\beta = \frac{nL}{\pi Rm} \quad \text{Eq. 6.9}$$

$$\gamma = 1.0 - .901(1 - e^{-\phi}) \quad \text{for axial loads} \quad \text{Eq. 6.10}$$

$$\gamma = 1.0 - .731(1 - e^{-\phi}) \quad \text{for bending moments} \quad \text{Eq. 6.11}$$

$$\phi = \frac{1}{29.8} \left(\frac{R}{\sqrt{\frac{D_{11} D_{22}}{A_{11} A_{22}}}} \right)^5 \quad \text{Eq. 6.12}$$

Here, gamma is an empirical (knock down) factor that insures that the calculated buckling load will be conservative with respect to all experimental data that are available. The critical buckling load is found by varying the integers m and n to determine the minimum value of $N_{x\sigma}$ which will be the predicted buckling load. The number of buckle waves in the circumferential direction must be greater than 4, in order to agree with experimental evidence that a structure that buckles due to circumferential waves will form a four corner, saw-toothed shape that corresponds to $n > 4$.

The tank undergoes simultaneously loading in that the tank experiences axial load, bending moment and internal pressure at the same time. Therefore, the Miner's Rule (Law of Cumulative Damage) will be used to determine the critical axial load - bending moment couple for the tank. To do this, we take the applied axial load per unit circumference divided by the critical axial load per unit circumference and add it to the applied bending moment per unit circumference divided by the critical value of this:

$$\frac{N_{x \text{ compression}}}{N_{x \text{ critical}}} + \frac{N_{x \text{ bending}}}{N_{x \text{ critical, bend}}} < 1 \quad \text{Eq. 6.13}$$

If this summation is less than 1, the design is predicted to be stable. The internal pressure will act to stabilize the tank, but will not be accounted for in this study. It is expected that the stability gained from the internal pressure will make up for imperfections that will lead to instability in the tank that are also unaccounted for in this preliminary effort.

To further insure against tank failure, the internal stresses that the applied loads cause must not exceed the allowable material stresses. This design uses a FORTRAN program which calculates the stresses in each layer of the material in the fiber direction and the transverse direction and divides these values by the allowable stresses. When these values are all less than 1, the tank is predicted to have sufficient strength to undergo both the x-direction stresses caused by the applied loading and the y-direction stresses, a hoop stress caused by the internal pressure of the vessel.

The final computation that the FORTRAN program makes is to determine the total mass of the tank. Knowing the outer radius of the vessel and the thickness of each layer, the total volume of each material in the structure can be calculated. The volume of each layer is multiplied by the density of that layer to give the mass of each layer, which are then added to result in the total tank mass.

The resulting tank configurations are calculated using a FORTRAN program of the above theory. The results can be found in section 6.12

6.6 Heat Transfer

6.6.1 Overview

The TR model examines the heat transfer through the wall of the fuel tank. Based upon the assumption that the fluid contained within the tank is static, the heat transfer is considered to be largely conductive. The model described in this analysis assumes that convective and radiative heat transfer are negligible. Calculations were made only with respect to conductive heat transfer.

The control of heat transfer through the tank wall is important for at least two reasons. Excessive pressures within the tank due to thermal expansion may cause gas leakage or catastrophic failure. Frost collecting on the outside surface of the tank will increase the mass of the aircraft and may cause additional complications during flight. This design compares the total TR of NASA's current project to the total TR of the selected composite materials of this design. If the TR of this design is greater than the TR of NASA's current project, then an additional TR is not required. On the other hand, if the TR of this design is less than that of NASA's current project, additional TR is required.

Additional TR can be achieved by adding one last layer of material to the outside of the tank. The material used to make up the deficit of TR will be insulation. This portion of the design evaluates the properties of TR and mass of different insulation materials. Insulation will be selected based upon the superior characteristics of its TR at cryogenic temperatures and material density.

6.6.2 Thermal Resistance Model

TR is a function of material thickness and TC. In the case of calculating the total TR of a system which contains a series of layers of different materials, a TR is calculated for each material and then summed over the total layers. Each material's TR is calculated by the following equation.

$$R = \frac{\ln \frac{ro}{ri}}{2\pi K} \quad \text{Eq. 6.14}$$

Where: ro = Outside radius of the material with respect to the tank center.
ri = Inside radius of the material with respect to the tank center.
K = Thermal conductivity of each material.

The cross section of the tank shown in Figure 6.4 demonstrates the location of each material with respect to the center of the tank.

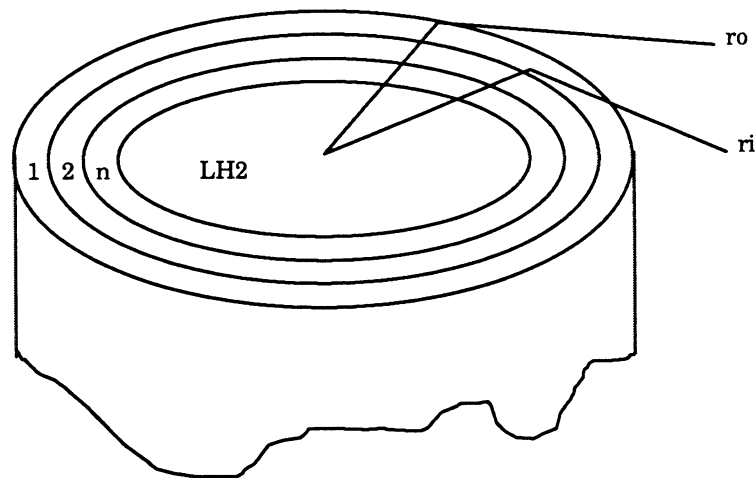


Figure 6.4

The total TR of the tank is calculated by the following equation.

$$R_t = R_1 + R_2 + R_n \quad \text{Eq. 6.15}$$

In this equation, 'n' represents the inner most layer of the tank.

Since TC for all materials are a function of temperature, specific material TC were selected as close to or within cryogenic temperature ranges. Some values of TC had to be extrapolated from charts which did not indicate temperatures as low as liquid hydrogen.

The materials that have been selected for this design are mixtures of materials, and therefore the rule of mixture was used to determine each material's TC. The spatial mixture of aluminum 2024 vacuum sealed honeycomb presented a slightly more complicated study. Vacuum sealed honeycomb yields an extremely small TC and an extremely large TR, but the portion of aluminum exposed to the conductive heat transfer still had to be accounted for. The effective surface area in contact with the tank was calculated over one square foot. Based upon the percentage of aluminum in contact with the tank, the rule of mixture was initiated to determine the aluminum 2024 vacuum sealed honeycomb's TC. The geometry of the hexagonal cross section is shown in Figure 6.5.

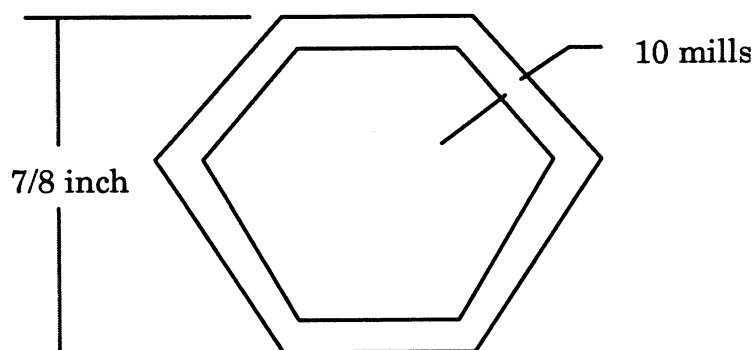


Figure 6.5

The effective area of aluminum 2024 honeycomb in contact with the tank was calculated to be approximately 1.5% of the total area of applied honeycomb. This was based in a one square foot calculation. Listed below are thermal conductivities for the materials that have been selected for this design.

Boron - Aluminum	$(0.5)(27) + (0.5)(177)$	$= 102 \text{ W/m}^*\text{K}$
Al 2024 Honeycomb	$(0.015)(177)$	$= 2.65 \text{ W/m}^*\text{K}$
High Modulus Graphite - Epoxy		$= 1.75 \text{ W/m}^*\text{K}$

Note: These TCs are listed at room temperature, and the rule of mixture has been applied to Boron - Aluminum and the Al-2024 Honeycomb.

6.6.3 Insulation

A proper insulation must be selected based upon superior thermal resistance at cryogenic temperatures and low material density. Many comparisons have been made to select the best insulation. The best selection is Polystyrene (Nominal). Polystyrene is compared to Rohacell in this report since Rohacell is the current selection of NASA's project. Polystyrene (Nominal) characteristics are listed below.

Density (ρ) = 32 kg/m^3
TC (K) = $0.005 \text{ W/m}^*\text{K}$.

Note: These data were found without extrapolation. (Nonmetallic Materials and Composites at Low Temperatures, 195)

Rohacell's characteristics were given from NASA (Comer¹², 1994). Notice that the thermal conductivity is given as a function of temperature. The current application thickness is approximately one inch.

Table 6.2. Thermoconductivity of Rohacell at various temperatures.

<u>T (°F)</u>	<u>Thermal Conductivity (BTU*in/(ft^2*hr*R))</u>	
-256	0.104	0.132
-148	0.132	0.146
-40	0.159	0.194
+68	0.194	0.234
+176	0.243	0.284
+284	0.291	0.333

Since this design requires insulation properties to exist at cryogenic temperatures, and observing that as TC increases - TR decreases, numerical values for Rohacell have been selected as listed below (Comer¹², 1994).

$$K_{\text{Rohacell}} = 0.104 \text{ BTU*in/(ft}^2\text{*hr*R)} = 0.0149 \text{ W/K*m}$$

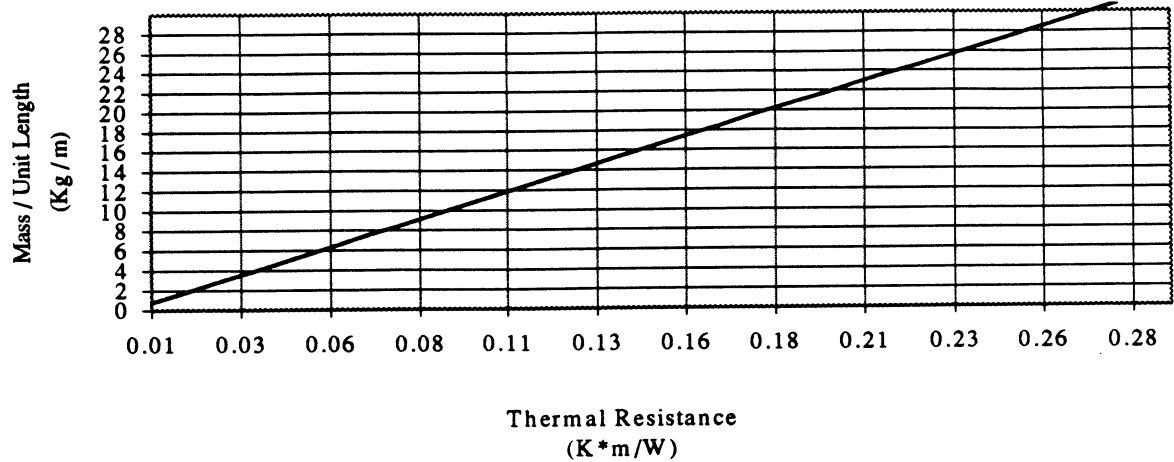
$$\rho_{\text{Rohacell}} = 51.3 \text{ kg/m}^3$$

By observation, Polystyrene (Nominal) has a much greater advantage when comparing TC and material density.

Based upon the assumption that Polystyrene (Nominal) will offer a greater TR as well as a minimum mass, a spreadsheet was constructed to further define the insulation's characteristics. Charts were created which define mass per unit length vs thermal resistance and mass per unit length vs insulation thickness of each selected insulation material. These charts serve as a tool to determine specific thickness. These charts are seen below as Chart Figures 1 through 4. Once the thermal resistance deficit is known, the curve may be used to find the mass per unit length. (See Graph 6.1 or 6.3).

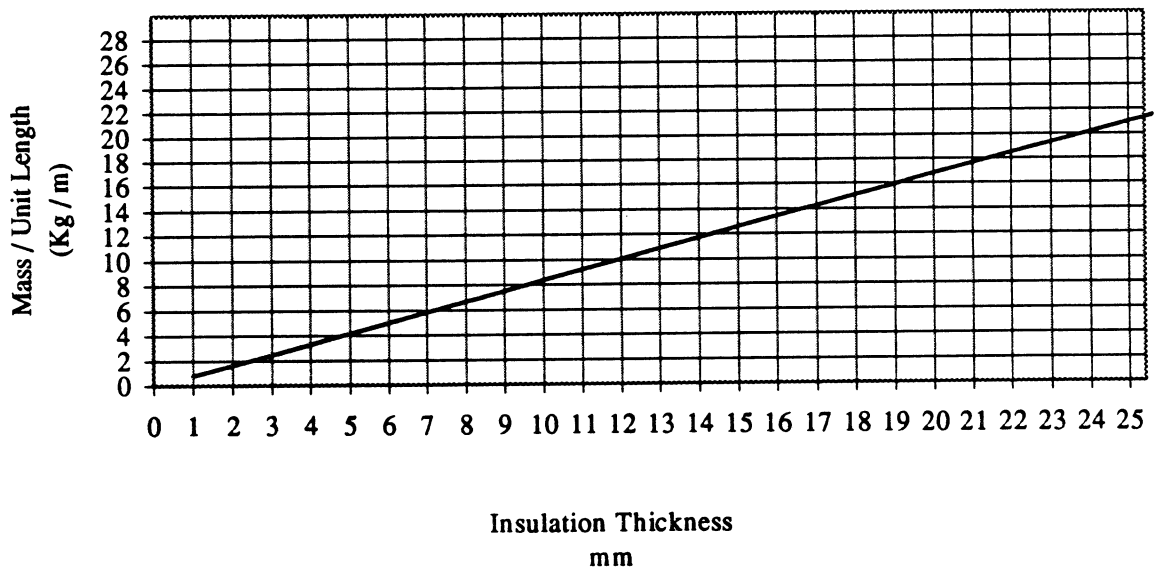
Once the mass per unit length of the selected material is known, this value can be taken to Graph 6.2 or 6.4. Using the same technique as described above, an insulation thickness can be determined. The insulation will be applied to the tank on its exterior layer. The charted thickness will supply the specific thermal resistance needed to be equivalent to NASA's current project..

Graph 6.1. Mass vs Thermal Resistance
Expanded Polystyrene (Nominal)
 $T = 33 \text{ K}$
 $\text{Density} = 32 \text{ Kg} / \text{m}^3$
 $\text{Thermal Conductivity} = .005 \text{ W} / (\text{K} \cdot \text{m})$



Graph 6.2. Mass/Unit Length vs Insulation Thickness

Expanded Polystyrene (Nominal)



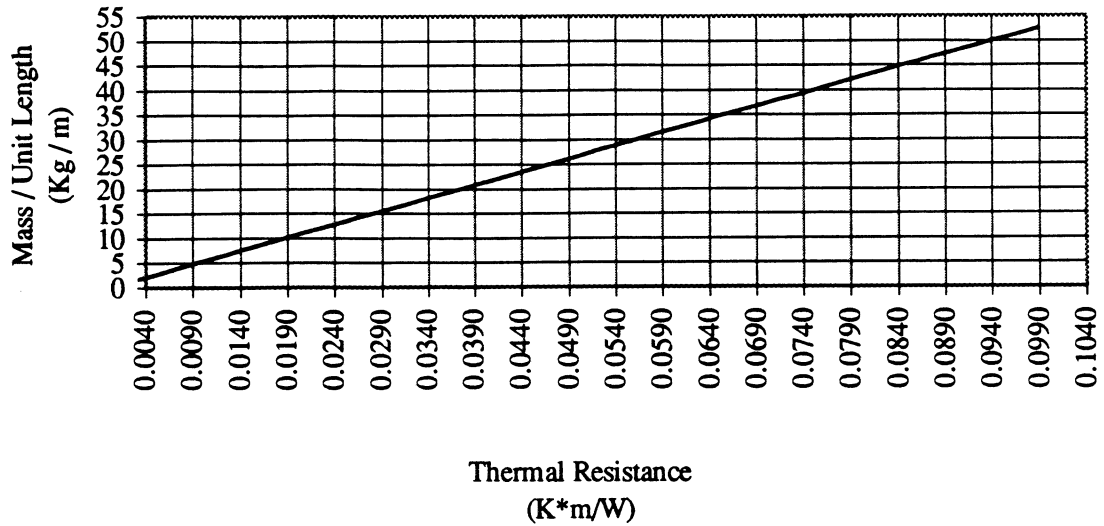
Graph 6.3. Mass/Unit Length vs Thermal Resistance

Rohacell.

$T = 33 \text{ K}$

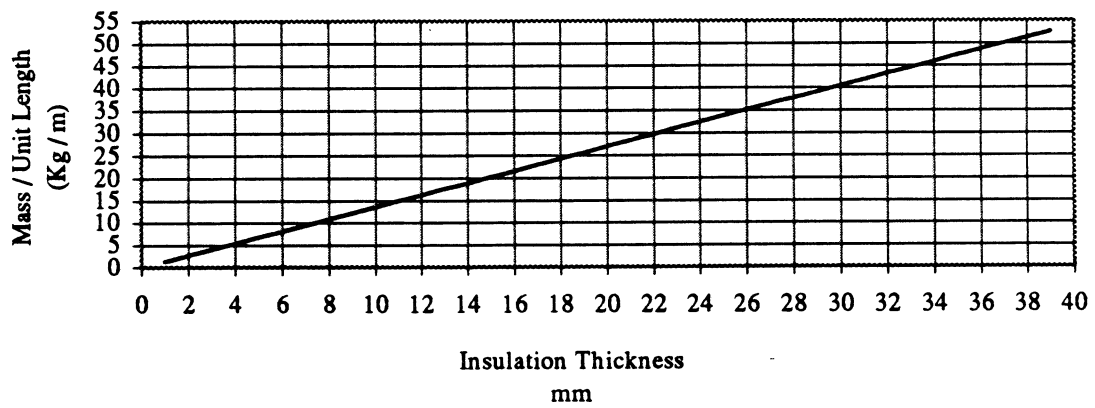
Density = 51.3 Kg/m^3

Thermal Conductivity = $.014999 \text{ W / (K*m)}$



Graph 6.4. Mass vs Thickness

Rohacell.



Note that the equation used to plot all graphs were created from the following equation.

$$R = \frac{\ln \frac{ro}{ri}}{2\pi K} \quad \text{Eq. 6.16}$$

Where a unit length of the cylindrical section was used. Only dimensions of insulation thickness were varied to redefine thermal resistance as a function of thickness.

6.6.4 Defining the Total Insulation Mass

Once the total insulation thickness is known, the volume of the insulation can be determined. Recall that the insulation will be applied to the exterior section of the tank, thus reducing the inside diameter. Since the outer diameter of the tank is fixed at 331 inches, and the volume of the tank is fixed at 46241.7 ft³, the design required a new length to be established. Also recall that this design only relates to the cylindrical section of the tank (i.e. the end caps excluded in this analysis). This new length can be calculated as shown.

$$L = \frac{Volume}{\pi r^2} \quad \text{Eq. 6.17}$$

Since a new value of length (L) has been established, the volume of insulation can be calculated by the following equation.

$$V(inspection) = \pi L(ro^2 - ri^2) \quad \text{Eq. 6.18}$$

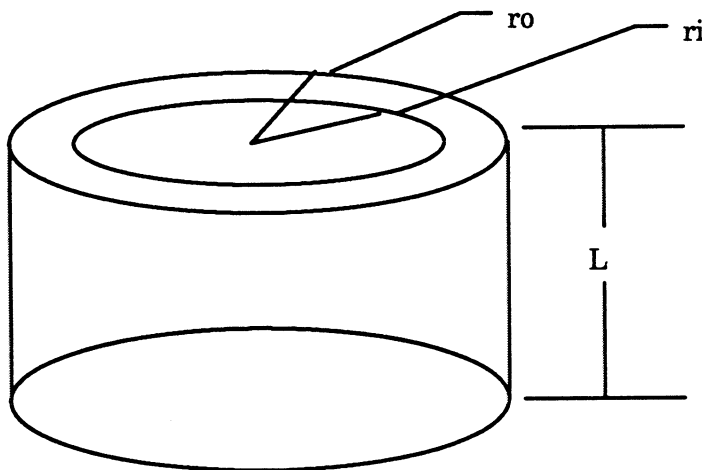


Figure 6.6

Since the volume of the insulation is known, the mass of the insulation can be calculated by the following equation.

$$mass = V(insulation) * \rho(insulation) \quad \text{Eq. 6.19}$$

6.6.5 Insulation Application

Rohacell is pre-formed and adhesively bonded to an applied surface area (Comer¹², 1994). This application will require additional labor and bonding agents. These agents need to be evaluated since they will add mass to the tank. Adhesive agents should not be considered negligible due to the enormous applied surface area.

Polystyrene (Nominal) is a spray applied foam which can bond by itself as it cures. This reduces labor and excludes additional bonding agents, thus minimizing extra mass.

Note: Exposures to high temperatures have not been evaluated in this report.

6.6.6 Thermal Expansion

The definition of composite moduli, thermal conductivities, specific heat and thermal expansion coefficients are properties that must be taken into consideration when analyzing thermoelastic problems for composites. Evaluation of the response of composite materials to temperature changes is important not only for high and low-temperature applications but also for fabrication considerations, i.e. the cure temperature. Thermal expansion behavior is also important when composite materials are used in conduction with other materials. The reason for this is because it is necessary to match the thermal expansion coefficient of one structural component with another for dimensional stability and mechanical compatibility. From an engineering standpoint, the understanding of thermal expansion coefficients of unidirectional composites is significant because of the wide use of fibrous composites in various applications in recent years, such as in the development of a liquid hydrogen fuel tank for use by NASA. Thermal residual stresses cannot be calculated without full information about the thermal expansion behavior and elastic response of unidirectional composites.

The effective thermal expansion coefficients are defined as the average strains resulting from a unit temperature rise for a traction-free material. For the unidirectional composite (one fiber direction) of two isotropic phases, there are two different expansion coefficients (the axial (α_{11}) and the transverse (α_{22}) given by the following equations:

$$\alpha_{11} = (c_f \alpha_f + c_m \alpha_m) + \left(\frac{\alpha_f - \alpha_m}{\frac{1}{k_f} - \frac{1}{k_m}} \right) \cdot \left(\frac{3(1 - 2\nu_{12})}{E_{11}} - \left(\frac{c_f}{k_f} + \frac{c_m}{k_m} \right) \right)$$

$$\text{Eq. 6.14}$$

$$\alpha_{22} = (c_f \alpha_f + c_m \alpha_m) + \left(\frac{\alpha_f - \alpha_m}{\frac{1}{k_f} - \frac{1}{k_m}} \right) \cdot \left(\frac{3}{2k_{23}} - \frac{3v_{12}(1 - 2v_{12})}{E_{11}} - \left(\frac{c_f}{k_f} + \frac{c_m}{k_m} \right) \right)$$

Eq. 6.20

In these equations, the new variables introduced are: the phase volume fraction c , the coefficient of thermal expansion α , and k the bulk modulus.

Theoretical predictions of the effective coefficient of thermal expansion by Rosen(1970) using a concentric model have indicated that the transverse coefficient of thermal expansion of the composite can be higher than that of its constituents at low fiber volume fraction. This effect is especially noticeable with fiber of high modulus and low axial expansion (e.g. boron or carbon) in a low-modulus matrix having a high coefficient of thermal expansion (e.g. epoxy resin).

6.7 Diffusion rate of Liquid Hydrogen

Diffusion is best described by Fick's first law, which gives the equation:

$$J = -D \frac{dC}{dx} \quad \text{Eq. 6.21}$$

where J is given as the diffusion flux(kg/m²-sec), D is the diffusion coefficient (m²/sec), and dC/dx is the concentration gradient (kg/m⁴). The diffusion coefficient is found by the Arrhenius equation::

$$D = D_o \cdot e^{-(Q_d/RT)} \quad \text{Eq. 6.22}$$

Here, D_o is a constant with units of (m²/sec). Q_d is the activation energy for diffusion with units of (J/mole). R is the Gas constant, and T is temperature.

In the above equations it is apparent that time and temperature have a profound influence on diffusion. Therefore, several assumptions were made about the diffusion of liquid hydrogen (LH2) through the composite tank design. Since the LH2 is being stored in the tank at cryogenic temperatures (approximately -423 °F), the diffusion coefficient, being temperature dependent, is so small that it can be approximated to be zero. This makes the diffusion rate zero. Furthermore, the LH2 is not being stored in the tank long enough to consider any serious diffusion problems. For these reasons, the diffusion of LH2 in the design of the tank was neglected.

6.8 Design Analysis

This section will apply the theory discussed in section 6.4 to produce an actual tank configuration. Any analysis methods used for iterating the tank design can be found in the appendix.

6.8.1 Structural Configuration

To determine the lightest tank possible, each configuration discussed earlier was tested to determine the lightest tank possible. For a given configuration, the total wall thickness, each layer thickness, orientation of the fibers in a layer, and the honeycomb thickness were chosen randomly. The weight of the tank was then calculated by the method discussed previously. The tank parameters were varied to ensure buckling stability, strength limitations, and the lightest weight. The optimum designs for each configuration are shown below:

Boron - Aluminum (solid wall)

wall thickness = .78 in.
tank length = 580.8 in.
tank mass = 47,440 lbm.
all fibers in axial direction

Boron Aluminum (honeycomb middle)

wall thickness = .78 in.
thickness of B-AL, outside = .14 in.
thickness of honeycomb = .5
thickness of B-AL, inside = 0.14 in.
tank length = 580.8 in.
tank mass = 22,415 lbm.
all fibers in the axial direction

Boron Aluminum, Graphite, Honeycomb

wall thickness = 1.25 in.
thickness of B-AL, outside = 0.0375 in.
thickness of graphite, outside = 0.1145 in.
thickness of honeycomb = .946 in.
thickness of graphite, inside = 0.1145 in.
thickness of B-AL, inside = 0.0375 in.
tank length = 584 in.
tank mass = 14,845 lbm.
all graphite fibers in the axial direction
all AL-B fibers in the hoop direction

The initial assumption made that the tank would be stiffness limited is accurate only to a degree. A single material tank is strongly stiffness limited, but the addition of the honeycomb allows the thickness of the composite material to decrease as the thickness of the honeycomb increases. Therefore, the actual limitation on our design is a combination of buckling and strength. The thickness of the honeycomb increases to provide a higher buckling resistance, but as this happens, the actual load bearing sections decrease in thickness. Therefore, optimum design occurs when the honeycomb thickness increases and leaves the critical amount of wall thickness to withhold the internal pressure. The circumferential strength can be increased by orientating fibers in this direction along with the axial fibers used to provide stiffness.

The lightest tank configuration found using composite structures is to put the high modulus graphite fibers oriented in the axial direction along with the honeycomb to give superior buckling stiffness. The graphite has low strength in the transverse direction which results in hoop stress limiting the design. The metal matrix composite (B-AL) is oriented in the hoop direction to hold back the internal pressure caused stress. The B-AL composite was chosen due to the high strength in the fiber direction, but also due to the relatively high stiffness in the transverse direction. Therefore, this design makes more efficient use of all material properties than the others, thereby lowering the overall mass of the tank.

6.8.2 Insulation Configuration

To determine the lightest tank design possible, it is important to choose an insulation which has a low density. Without compromise to the TR of the material, a selection of material must be made which considers high TR and a light mass. For this reason, the selection of Polystyrene (Nominal) was preferred. The comparison between Rohacell made Polystyrene (Nominal) the best selection due to higher TR, lighter mass and simpler application techniques.

The Polystyrene (Nominal) insulation is to be applied in a uniform thickness over the entire exterior of the fuel tank. The optimal insulation thickness necessary to meet NASA's required thermal resistance of the tank was determined to be 1.9 mm. This is a significant decrease in comparison to the current level of insulation used by NASA. The insulation is to be applied by a spray-on procedure, allowing precise control of the thickness of the insulation. At this thickness, the total mass of the insulation is 38.4 kg. NASA's current design using a thickness of 1 inch of Rohacell (Comer¹², 1994) results in a total insulation mass of 830 kg. If Rohacell is used in the new design, an insulation thickness of 5.9 mm would be necessary to maintain the proper thermal resistance. This would result in a total insulation mass of 191 kg. These data can be seen in section 6.12. The insulation analysis resulted in a maximum mass savings of 791.6 kg.

6.9 Thermal Expansion

The scope of this report for thermal expansion is limited to calculated thermal expansion coefficients for each of the materials used in the final configuration. A further thermal expansion analysis would be required for the tank in order to insure that integrity of the system will be maintained.

Thermal expansion coefficients:

Aluminum	$\alpha = 13.2 \times 10^{-6} \text{ in/in-}^{\circ}\text{F}$ (Al)
Boron	$\alpha = 4.61 \times 10^{-6} \text{ in/in-}^{\circ}\text{F}$ (B)
Epoxy	$\alpha = 50.0 \times 10^{-6} \text{ in/in-}^{\circ}\text{F}$ (Ep)
Graphite	$\alpha = 9.40 \times 10^{-6} \text{ in/in-}^{\circ}\text{F}$ (Gr)

Thermal expansion coefficients for composites (assume 50-50 ratio):

Metal matrix	$\alpha = 8.91 \times 10^{-6} \text{ in/in-}^{\circ}\text{F}$ (Al-B)
Honeycomb	$\alpha = 13.2 \times 10^{-6} \text{ in/in-}^{\circ}\text{F}$ (Al 2024)

Organic matrix $\alpha = 29.7 \times 10^{-6} \text{ in/in-}^{\circ}\text{F}$ (Gr-Ep)

6.10 Recommendations

It must be noted that this is a preliminary study. Topics for further research must include fracture, stresses due to thermal expansion, interface with vehicle and the addition of the hemispherical ends of the tank.

6.11 References (in order of use)

- (1) "Comparison of Materials." Materials Engineering, December 1989: 79 - 241.
- (2) Composites: Engineered Materials Handbook, Volume 1, New York: ASM International, 1987: 27, 167.
- (3) Hackman, Lloyd, "Sandwich Construction and Design," Analysis and Design of Flight Vehicle Structures, C12.1 - C12.8. Edited by Elmer F. Bruhn, Indianapolis: S.R. Jacobs & Associates, 1973.
- (4) Kasen, M.B., "Mechanical Performance of Graphite and Aramid Reinforced Composites at Cryogenic Temperatures," Advances in Cryogenic Engineering, Volume 28, 165 - 177. Edited by R.P. Reed and A.F. Clark, New York: Plenum Press, 1982.
- (5) Rosen, B.W. *Proc. Roy. Soc. Lond. Ser. A* 319 (1970) 70.
- (6) Graham, Bart. Reference 1, Meeting at MSFC. January, 1994.
- (7) Graham, Bart. Reference 2, Telephone conversation, February, 1994.
- (8) Graham, Bart. Reference 3, Telephone conversation, March, 1994.
- (9) Graham, Bart and Paul Luz. LaRC 001 SSV Configuration, December 10, 1993.
- (10) Vinson, J. R. and Sierakowski, R. L. The Behavior of Structures Composed of Composite Materials. Dordrecht: Martinus Nijhoff Publishers, 1987.
- (11) Mark's Standard Handbook for Mechanical Engineers, Ninth Edition, New York: McGraw - Hill, 1987: Sections 19-36
- (12) Comer, Gene. Telephone conversation, March, 1994
- (13) Clark, A.F., Reed, R.P. and Hartwig, G. Nonmetallic Materials and Composites at Low Temperatures, New York: Plenum Press, 1979.

6.12 Appendix: Material Properties

GRAPHITE-EPOXY COMPOSITE (Kasen, pp. 168)

Graphite fibers (GY-70) in epoxy resin (934)

60% FIBERS, UNIDIRECTIONAL

Orientation	Modulus (10^6 psi)	Poisson's Ratio	Ultimate Strength (ksi)
Tensile, 0	46.8	0.454	105
Tensile, 90	0.97	0.009	3.22
Compressive, 0			62.5
Compressive, 90			22.8

BORON-ALUMINUM COMPOSITE (Composites, pp. 167)

Boron fibers (5.6 mil) in aluminum (2024) matrix

50% FIBERS, UNIDIRECTIONAL

Temp (K)	Modulus (10^6 psi)	Poisson's Ratio	Ultimate Strength (ksi)
Tensile, 0	34	0.23	160
Tensile, 90	20	0.17	16
Compressive, 0	30		176
Compressive, 90	19		23

ALUMINUM HONEYCOMB

Base Material = Al 2024

Density = 5.92 lbm / ft³

6.12 Appendices:

Table 1
Input Data:

Input material selection with respect to the location in which each material will be placed from outside of the tank to the inside of the tank.

Input data:
Material, Thickness, Thermal Conductivity.

Note: Thickness of material must be entered in units of mm, and thermal conductivity must be entered in units of W / K*m.

Layer Reference	Material	Thickness t mm	Outer Radius ro mm	Inner Radius ri mm	Thermal Conductivity K W/K*m	Thermal Resistance R K*m/W
Ext. 1	Boron - Al	0.95	4203.70	4202.75	102.00	3.54E-07
2	Graphite - Epoxy	2.91	4202.75	4199.84	1.75	6.30E-05
3	Honeycomb Al - 2024	24.03	4199.84	4175.81	2.65	3.45E-04
4	Graphite - Epoxy	2.91	4175.81	4172.90	1.75	6.34E-05
5	Boron - Al	0.95	4172.90	4171.95	102.00	3.56E-07

6.12 Appendices:

Table 2
Output Data:
Orentation of Material.
Specific Material.
Thickness of Each Layer.
Thermal Resistance.

Layer Reference	Material	Thickness t mm	Therm. Resistance R K*m/W
Ext. 1	Boron - Al	0.95	3.54E-07
2	Graphite - Epoxy	2.91	6.30E-05
3	Honeycomb Al - 2024	24.03	3.45E-04
4	Graphite - Epoxy	2.91	6.34E-05
5	Boron - Al	0.95	3.56E-07

Table 3
Output Data:
Total Material Thermal Resistance.
NASA Current Thermal Resistance.
(Rohacell)
Thermal Resistance Deficit.

Total Material Thermal Resistance K*m/W
4.72E-04

Thermal Resistance Deficit K*m/W
0.014

NASA Material Thermal Resistance K*m/W
0.0149

6.12 Appendices:

Table 4
Output Data:

**Length of Tank's
Cylindrical Section.**

Tank Length m	Fluid Volume m ³	ri (Liner) m
23.92	1309.42	4.17

Table 5
Input Data:

**Insulation and material selection with respect to the location it will be placed
from outside of the tank to the inside of the tank.**

Input data:
Material, Thickness, Thermal Conductivity.

**Note: Thickness of material must be entered in units of mm, and thermal
conductivity must be entered in units of W / K*m.**

Layer Reference	Material	Thickness t mm	Outer Radius ro mm	Inner Radius ri mm	Thermal Conductivity K W/K*m	Thermal Resistance R K*m/W
Insulation	Polystyrene	1.90	4203.70	4201.80	0.01	1.44E-02
Ext. 1	Boron - Al	0.95	4201.80	4200.85	102.00	3.54E-07
2	Graphite - Epoxy	2.91	4200.85	4197.94	1.75	6.30E-05
3	Honeycomb Al - 2024	24.03	4197.94	4173.91	2.65	3.45E-04
4	Graphite - Epoxy	2.91	4173.91	4171.00	1.75	6.34E-05
5	Boron - Al	0.95	4171.00	4170.05	102.00	3.56E-07

6.12 Appendices:

Table 6
Output Data:

Orentation of Material
Specific Material
Thickness of Each Layer
Thermal Resistance

Layer Reference	Material	Thickness t mm	Thermal Resistance R K*m/W
Insulation	Polystyrene	1.90	1.44E-02
Ext. 1	Boron - Al	0.95	3.54E-07
2	Graphite - Epoxy	2.91	6.30E-05
3	Honeycomb Al - 2024	24.03	3.45E-04
4	Graphite - Epoxy	2.91	6.34E-05
5	Boron - Al	0.95	3.56E-07

Table 7
Output Data:

Total Material Thermal Resistance

NASA Current Thermal Resistance
(Rohacell)

Thermal Resistance Deficit

Total Material Thermal Resistance K*m/W	NASA Material Thermal Resistance K*m/W	Thermal Resistance Deficit K*m/W
1.49E-02	0.0149	0.000

6.12 Appendices:

Table 8
Output Data:

**Volume of Tank's
Applied Insulation**

Tank Length m	Tank Volume m ³	ro ² - ri ² m ²
23.92	1.20E+00	0.0160

Table 9
Output Data:

**Mass of Tank's
Insulation
(Polystyrene)**

Tank Insulation Mass Kg	Tank Insulation Volume m ³	Tank Insulation Density Kg/m ³
3.84E+01	1.20E+00	32

6.12 Appendices:

Table 10
Input Data:

Insulation and material selection with respect to the location it will be placed from outside of the tank to the inside of the tank.

Input data:
Material, Thickness, Thermal Conductivity.

Note: Thickness of material must be entered in units of mm, and thermal conductivity must be entered in units of W / K*m.

Layer Reference	Material	Thickness t mm	Outer Radius ro mm	Inner Radius ri mm	Thermal Conductivity K W/K*m	Thermal Resistance R K*m/W
Insulation	Rohacell	25.40	4203.70	4178.30	0.01	6.43E-02
Ext. 1	Boron - Al	0.95	4178.30	4177.35	102.00	3.56E-07
2	Graphite - Epoxy	2.91	4177.35	4174.44	1.75	6.33E-05
3	Honeycomb Al - 2024	24.03	4174.44	4150.41	2.65	3.47E-04
4	Graphite - Epoxy	2.91	4150.41	4147.50	1.75	6.38E-05
5	Boron - Al	0.95	4147.50	4146.55	102.00	3.58E-07

6.12 Appendices:

Table 11
Output Data:

Orentation of Material
Specific Material
Thickness of Each Layer
Thermal Resistance

Layer Reference	Material	Thickness t mm	Thermal Resistance R $K^{\circ}m/W$
Insulation	Rohacell	25.40	6.43E-02
Ext. 1	Boron - Al	0.95	3.56E-07
2	Graphite - Epoxy	2.91	6.33E-05
3	Honeycomb Al - 2024	24.03	3.47E-04
4	Graphite - Epoxy	2.91	6.38E-05
5	Boron - Al	0.95	3.58E-07

Table 12
Output Data:

Total Material Thermal Resistance

NASA Current Thermal Resistance
(Rohacell)

Thermal Resistance Deficit

NASA Material Thermal Resistance $K^{\circ}m/W$	Total Material Thermal Resistance $K^{\circ}m/W$	Thermal Resistance Deficit $K^{\circ}m/W$
0.0149	6.48E-02	-0.050

6.12 Appendices:

Table 13
Output Data:

**Volume of Tank's
Applied Insulation**

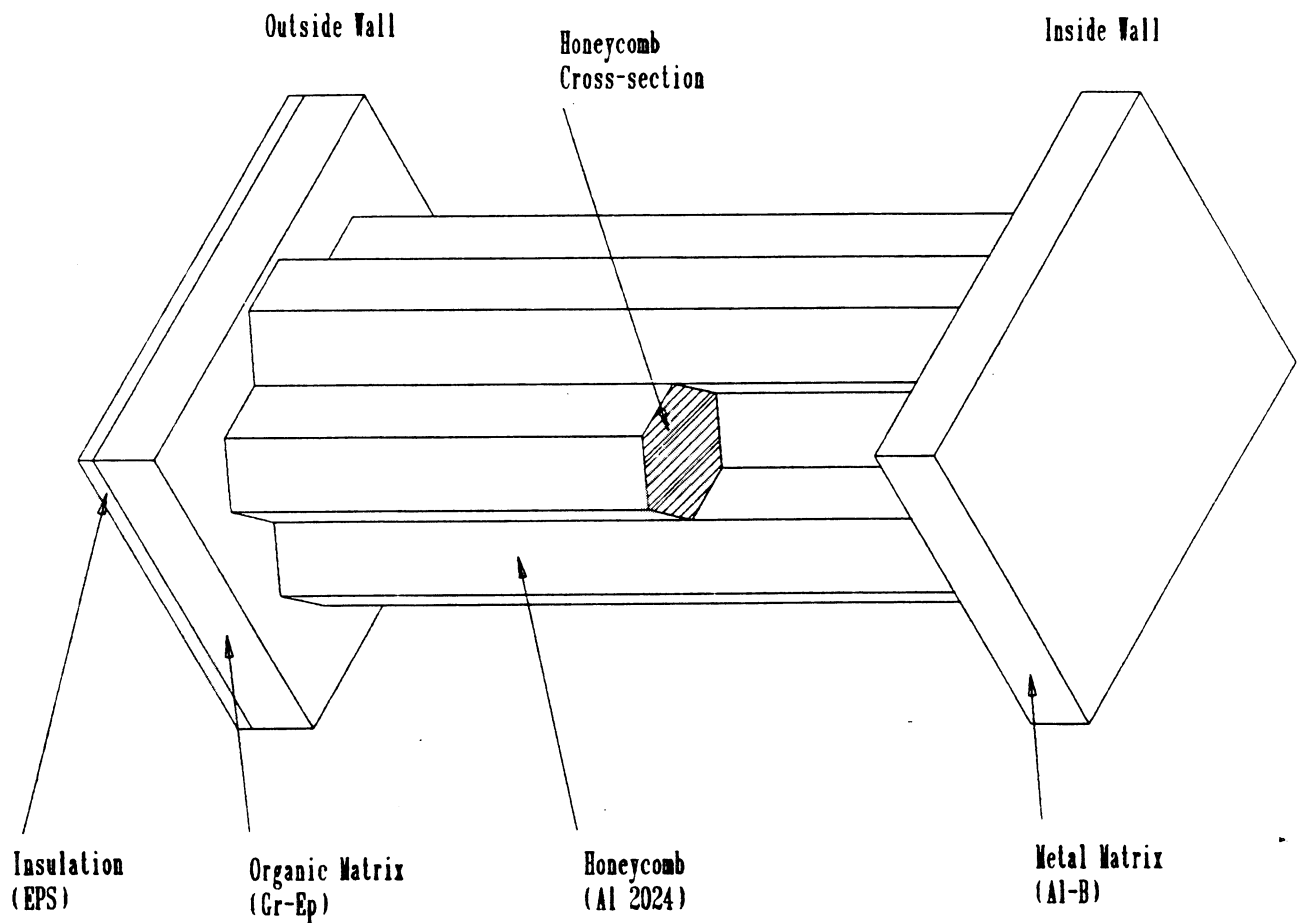
Tank Length m	Tank Volume m ³	ro ² - ri ² m ²
24.20	1.62E+01	0.2129

Table 14
Output Data:

**Mass of Tank's
Insulation
(Rohacell)**

Tank Insulation Mass Kg	Tank Insulation Volume m ³	Tank Insulation Density Kg/m ³
8.30E+02	1.62E+01	51.3

Cut-away Portion of Tank Configuration



7 Feed System Design for a Reduced Pressure Tank

7.1 Summary

7.1.1 Design Objective

To devise a suitable fuel feed system for a tri-propellant single stage shuttle which complies with all start-up and steady-state conditions and reduces the weight of the vehicle.

7.1.2 Abstract

Three designs were considered to satisfy the design objective. These designs were the current design, a Land Based Pressurized Feed System, and a fuel recirculation system. A computer code was developed to analyze the current feed system and assist in the analysis of the two experimental systems. After comparing the three concepts, the Land Based Pressurized Feed System seemed to be the most promising new development. This design coupled with the piping configuration described in the report provides a justifiable fuel feed system which satisfies all the necessary requirements.

7.2 Glossary

LOX	- Liquid oxygen
LBPFS	- Land Based Pressurized Fuel System
LH2	- Liquid hydrogen
RP-1	- Kerosene
SSTO	- Single Stage to Orbit Vehicle

7.3 Background for SSTO Feed System

One of the main programs currently studied at NASA is the single stage rocket design. This concept would abandon the use of solid fuels due to their lack of throttle control and concentrate on liquid propellants. Because of NASA's recent trend toward international collaboration, the feed system used would be adapted from a system used by the Russian space program. This tri-propellant system burns both liquid hydrogen and RP-1, a form of kerosene, with liquid oxygen.

The current feed system considered by NASA requires high pressures in the shuttle fuel tanks to meet the engine's required mass flow rates. The high pressures, along with turbo pumps in the feedlines, rapidly increase the fuel flow, enabling the engine to receive the fuel at the more rigorous start-up conditions.

Because of the high back pressures, the fuel tank walls must be thick enough to withstand the stresses created. If the pressure in the fuel tanks can be reduced, then the fuel tank wall thickness can be decreased, resulting in thinner, lighter tanks. Since the fuel tanks make up a significant fraction of the total weight of the vehicle, reducing the tank weights would satisfy the desired objective of weight reduction.

The shuttle engine receives fuel in two stages. The first stage makes up the initial fuel requirement conditions. These conditions, which are known as start-up, are the more difficult to meet because the engine needs extremely high mass flow rates. The second stage makes up the steady state conditions. These are the conditions in which the shuttle reaches equilibrium, then lifts off. The mass flow rates during

this stage are not as demanding as start-up, and high pressures in the fuel tanks are not needed to push the fuels. Therefore, a reduction in fuel tank pressure could be achieved if the start-up conditions could be met by a means other than pressurizing the tanks.

7.4 The Design Concept

The conceptual design was broken down into three phases. The first phase consisted of the development of a basic internal feed system for all three fuels. This phase includes pipe configuration, diameter and other properties of the pipes. In conjunction with this approach a computer model was developed to determine how this feed system would act. The second phase consisted of the development of a system using low pressure turbo pumps in a recirculating feed system. This system would allow the fuel to recirculate in the feedlines until the proper start-up conditions were attained. The third approach was the development of an external land based pressurized fuel system. This system would supply the shuttle engines with the necessary initial fuel requirements needed for start-up. This system would eliminate the high pressure constraints in the internal tank system.

7.4.1 Feed System Modeling

7.4.1.1 Feed System Design

7.4.1.1.1 Feed System Introduction

The feed system configurations for the Liquid Oxygen (LOX), Liquid Hydrogen (LH2), and the Kerosene (RP-1) fuels are explained in this section of the report. This section consists of the schematic of the three feed systems, the description of each piping section, the assumptions made about the feed system configurations, and the errors which are present in the feed system configurations.

7.4.1.1.2 LOX Feed System Configuration

A diagram labeling each part of the LOX feed system, is shown in Figure 7.1. The entire system is approximately 1100 inches in length. The system starts with two tank outlets, located at the bottom of the LOX tank, feeding 20 inch trunk lines. These trunk lines are routed around the RP-1 tank, LH2 tank, and the cargo bay. At the end of the lines a manifold is present which directs fuel to the inner and outer engines.

The crossover lines attached to the trunk line manifold provide fuel to the center engine and aid in circulating the fuel. The crossover line manifold connects the two crossover lines and directs fuel towards the center engine. Attached to the crossover manifold is a pre valve which monitors fuel entering the center engine feedline. The center engine feedline is connected directly to the engine and contains three gimbals to allow for thermal movement and misalignment. A screen is located at the end of the feedline.

Located just below the trunk lines are out-board manifolds. Each of these manifolds directs fuel to two of the out-board engines. A pre valve is attached to both exits of the out board manifold to monitor fuel flow. Attached to these pre valves are the out board engine feedlines which contain three gimbals to allow for thermal movement and misalignment. Located at the end of each feedline is a screen.

To aid in passive fuel conditioning all of the feedlines are sloped at least 15 degree from horizontal. To maintain proper fuel temperatures and aid in circulation all of the feedlines except those containing gimbals are insulated.

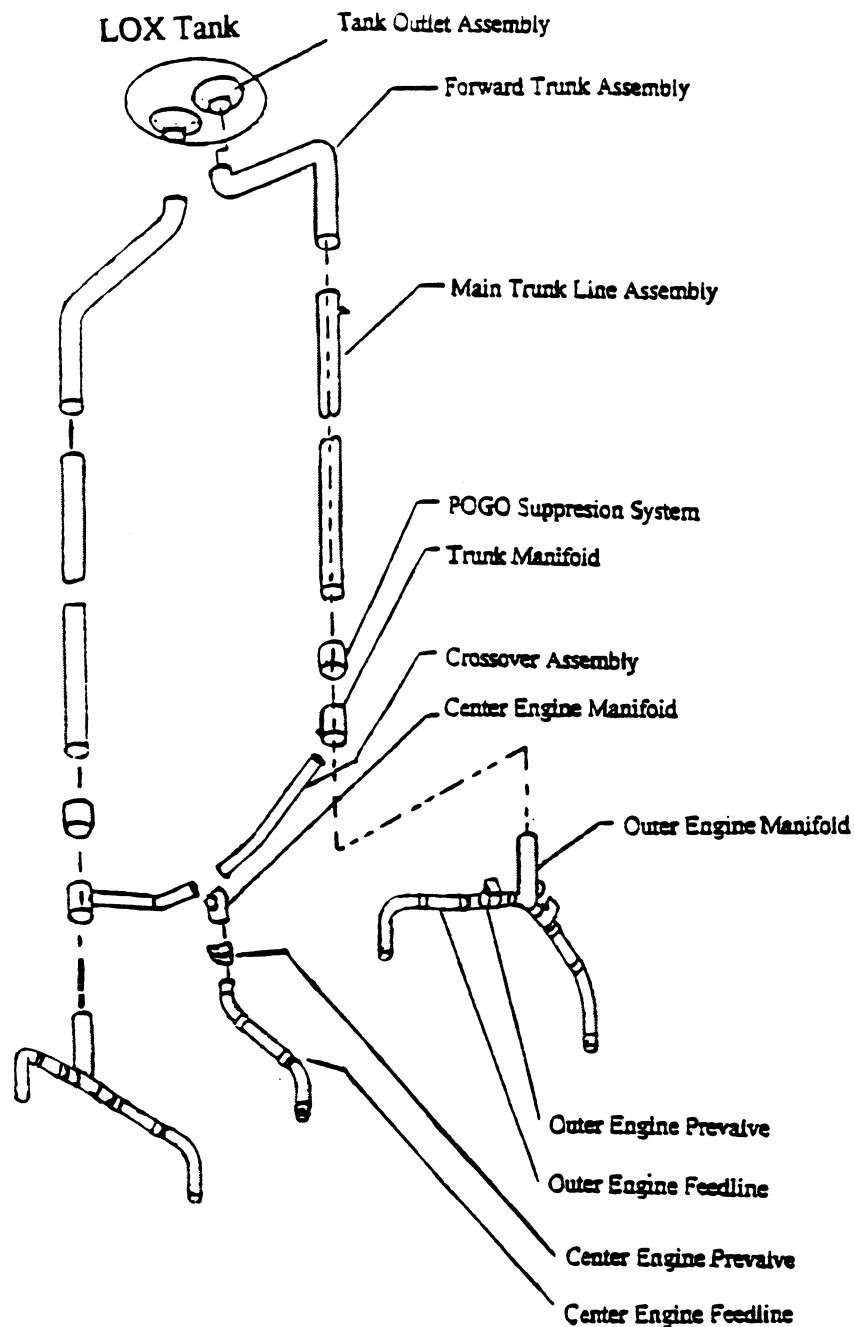


Figure 7.1--LOX Feed System Configuration

7.4.1.1.3 LOX Piping Descriptions

The LOX Tank Outlet Assembly- These two outlets allow fuel to leave the LOX tank and enter the feed system fuel lines. At the bottom of these outlets, screens are placed which help reduce impurities flowing through the feedlines. The Outlets are made of stainless steel and have been computer analyzed to minimize flow restrictions.

Qty: 2

Flow Coefficient: 1.08¹

Diameter: N/A

The Forward LOX Trunk Assembly- These sections direct the fuel around the RP-1 tanks to the outer shell of the vehicle. The forward trunk line assembly contains two elbows, a straight section and three BSTRA gimbals. The straight section and the elbows are insulated, the gimbals are not. The trunk lines are made of stainless steel.

Qty: 2 Flow Coefficient: 0.886^2 Diameter: 20"

The Main LOX Trunk Line Assembly- These sections direct the fuel along the outer shell of the vehicle. These sections are the longest of the feed system, encompassing approximately 900 inches. The main trunk line assembly is composed of four flanged sections flanged together. The entire section is insulated and made of stainless steel.

Qty: 2 Flow Coefficient: 0.68^3 Diameter: 20"

The LOX POGO Suppression System- These sections of the feed system maintain the controlled flow of the fuel. These sections contain baffles to restrict the fuel from swirling in the pipes before it reaches the engines. These baffles also help maintain the constant flow rate of the fuel. These sections are made of stainless steel and are fully insulated.

Qty: 2 Flow Coefficient: 0.0^4 Diameter: 20"

The LOX Trunk Manifold- These sections of the feed system direct the fuel into two separate paths, one leading to the center engine and the other path leading to the outer engines. The entire manifold is insulated and is made of stainless steel.

Qty: 2 Flow Coefficient: 0.27- Through
0.77- Branch⁵ Diameter: 17"- Through
8.5"- Branch

The LOX Crossover Assembly- This section directs fuel to the center engine and aids in recirculating the fuel. This section is made of stainless steel and contains three BSTRA flexible mechanism which account for thermal movement and misalignment. All but the gimbals are insulated.

Qty: 2 Flow Coefficient: 0.419^6 Diameter: 8.5"

The LOX Center Engine Manifold- This section joins the two crossover lines which bring fuel to supply the center engine. The section is made of stainless steel and is insulated all around.

Qty: 1 Flow Coefficient: 0.56 Diameter: 8.5"- Inlet
12"- Outlet

The LOX Center Engine Prevalve- The prevalve allows the flow to the center engine to be cut off in case a leak is detected. The section is made of stainless steel.

Qty: 1 Flow Coefficient: 0.1^7 Diameter: 12"

The LOX Center Engine Feedline- This section delivers fuel directly to the center engine. The feedline has three BSTRA gimbals to accommodate thermal movement and misalignment. This section is

made of stainless steel and all but the gimbals are insulated. A screen is located at the end of the feedline to filter out impurities in the fuel.

Qty: 1 Flow Coefficient: 1.08 Diameter: 12"

The LOX Outer Engine Manifold- This section of pipe directs the fuel into two branches, each feeding one of the outer engines. This section is made of stainless steel and is fully insulated.

Qty: 2 Flow Coefficient: 0.56⁸ Diameter: 17"- Inlet
12"- Outlet

The LOX Outer Engine Prevalve- These prevalves allow flow to be cut off to the outer engines in case a leak in the feedlines is detected. This section is made of stainless steel.

Qty: 4 Flow Coefficient: 0.1 Diameter: 12"

The LOX Outer Engine Feedline- These sections of pipe deliver fuel directly to the outer engines. They are made of stainless steel and contain three BSTRA gimbals to allow for thermal movement and misalignment. All but the gimbals are insulated. A screen is present at the end of the feedline to filter out impurities present in the fuel.

Qty: 4 Flow Coefficient: 1.53⁹ Diameter: 12"

7.4.1.1.4 RP-1 Feed System Configuration

A diagram showing the configuration of each part of the RP-1 feed system configuration is shown in Figure 7.2. The feed system is approximately 850 inches in length. The configuration of the RP-1 system is identical to the LOX system except that the RP-1 system uses two separate tanks each supplying one feedline.

7.4.1.1.5 RP-1 Piping Descriptions

The RP-1 Tank Outlet Assembly- One outlet assembly is located at the bottom of each of the two RP-1 tanks. These two outlets allow fuel to leave the RP-1 tank and enter the feed system fuel lines. At the bottom of these outlets are screens to help reduce impurities flowing through the feedlines. The outlets are made of stainless steel and have been computer analyzed to minimize flow restrictions.

Qty: 2 Flow Coefficient: 1.08 Diameter: N/A

The Forward RP-1 Trunk Assembly- These sections direct the fuel around the LH2 tanks and the cargo bay to the outer shell of the vehicle. The forward trunk line assembly contains two elbows, a straight section and three BSTRA gimbals. The straight section and the elbows are insulated; the gimbals are not. The trunk lines are made of stainless steel.

Qty: 2 Flow Coefficient: 0.886 Diameter: 20"

The Main RP-1 Trunk Line Assembly- These sections direct the fuel along the outer shell of the vehicle. These sections are the longest of the RP-1 feed system, encompassing approximately 650 inches.

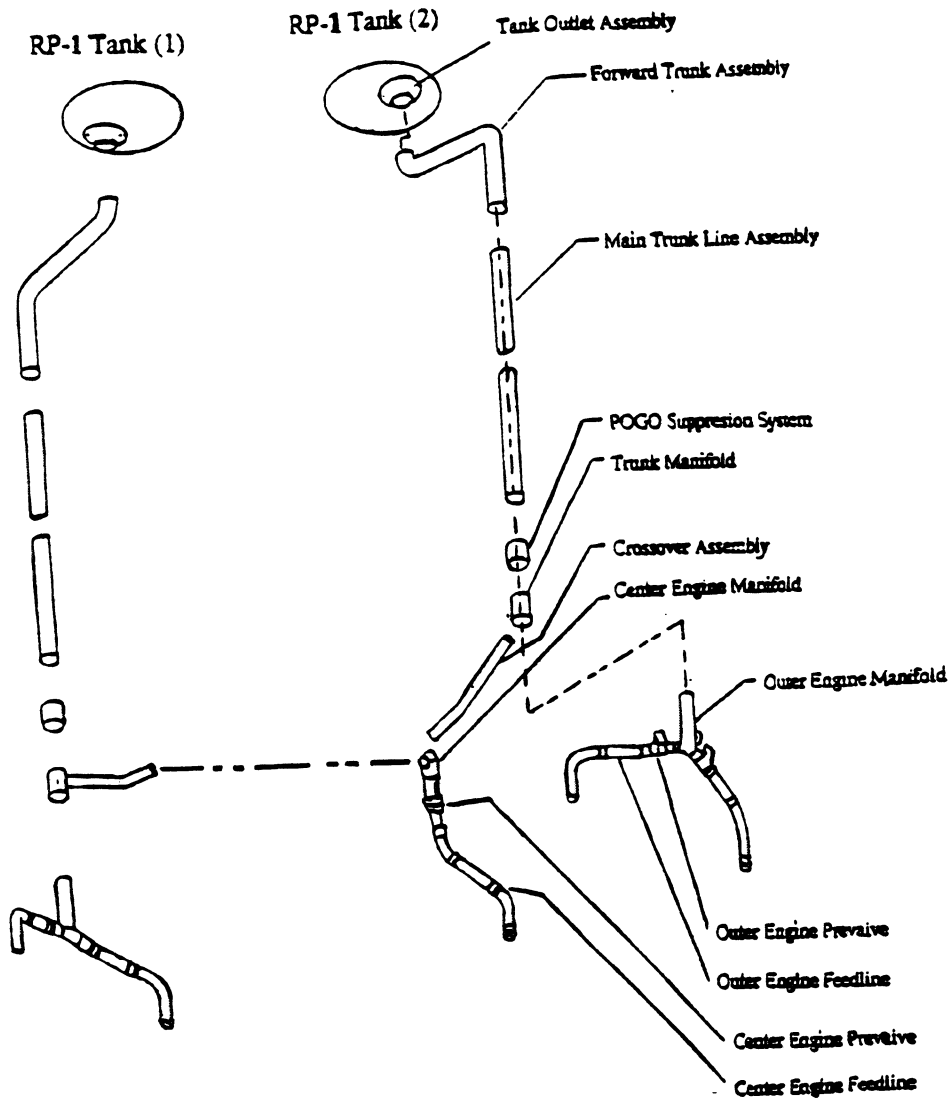


Figure 7.2--RP-1 Feed System Configuration

The main trunk line assembly is composed of four flanged sections flanged together. The entire section is insulated and made of stainless steel.

Qty: 2

Flow Coefficient: 0.68

Diameter: 20"

The RP-1 POGO Suppression System- These sections of the feed system maintain the controlled flow of the fuel. These sections contain baffles to restrict the fuel from swirling in the pipes before it reaches the engines. These baffles also help maintain the constant flow rate of the fuel. These sections are made of stainless steel and are fully insulated.

Qty: 2 Flow Coefficient: 0.0 Diameter: 20"

The RP-1 Trunk Manifold- These sections of the feed system direct the fuel into two separate paths, one leading to the center engine and the other path leading to the outer engines. The entire manifold is insulated and is made of stainless steel.

Qty: 2 Flow Coefficient: 0.27- Through
0.77- Branch Diameter: 17"- Through
8.5"- Branch

The RP-1 Crossover Assembly- This section directs fuel to the center engine. The section is made of stainless steel and contains three BSTRA flexible mechanisms which account for thermal movement and misalignment. All but the gimbals are insulated.

Qty: 2 Flow Coefficient: 0.419 Diameter: 8.5"

The RP-1 Center Engine Manifold- This section joins the two crossover lines which bring fuel to supply the center engine. The section is made of stainless steel and is insulated all around.

Qty: 1 Flow Coefficient: 0.56 Diameter: 8.5"- Inlet
12"- Outlet

The RP-1 Center Engine Prevalve- The prevalve allows the flow to the center engine to be cut off in case a leak is detected. The section is made of stainless steel.

Qty: 1 Flow Coefficient: 0.1 Diameter: 12"

The RP-1 Center Engine Feedline- This section delivers fuel directly to the center engine. The feedline has three BSTRA gimbals to accommodate thermal movement and misalignment. This section is made of stainless steel and all but the gimbals are insulated. A screen is present at the end of the feedline to filter out impurities in the fuel.

Qty: 1 Flow Coefficient: 1.08 Diameter: 12"

The RP-1 Outer Engine Manifold- This section of pipe directs the fuel into two branches, each feeding one of the outer engines. This section is made of stainless steel and is fully insulated.

Qty: 2 Flow Coefficient: 0.56 Diameter: 17"- Inlet
12"- Outlet

The RP-1 Outer Engine Prevalve- These prevalves allow flow to be cut off to the outer engines in case a leak in the feedlines is detected. This section is made of stainless steel.

Qty: 4 Flow Coefficient: 0.1 Diameter: 12"

The RP-1 Outer Engine Feedline- These sections of pipe deliver fuel directly to the outer engines. They are made of stainless steel and contain three BSTRA gimbals to allow for thermal movement and misalignment. A screen is located at the end of the feedline to filter out impurities which may exist in the fuel.

Qty: 2

Flow Coefficient: 1.08

Diameter: N/A

7.4.1.1.6 LH2 Feed System Diagram

A diagram showing each part of the LH2 Feed system is shown in Figure 7.3. The LH2 feed system is approximately 100 inches in length. This feed system has three outlets located at the bottom of the LH2 tank. Two of these outlets are identical in diameter while the third one, located in the center, is smaller. Each of these outlets feeds its own trunk line assembly, with the two outer trunk lines providing fuel to the four out board engines. The center feedline is the sole supplier of LH2 to the center engine.

This feed system does not allow for circulation since there is no circular path associated with these feedlines. All of the pipes in the LH2 feed system are insulated except for the flexible gimbals.

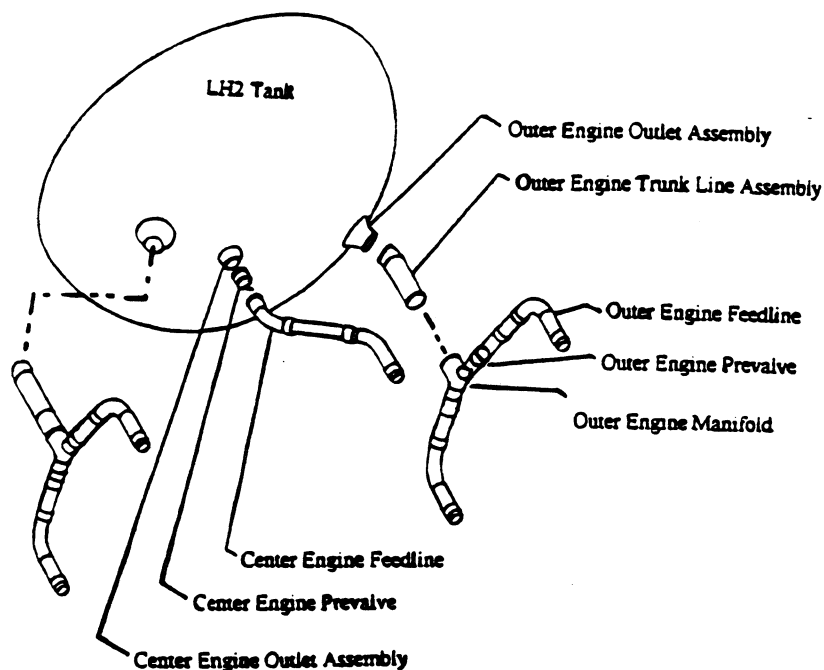


Figure 7.3--LH2 Feed System Configuration

7.4.1.1.7 LH2 Piping Descriptions

The LH2 Outer Engine Outlet Assembly- These two section allow fuel to the leave the LH2 tank and enter the fuel lines. These two sections deliver fuel to the feed lines servicing the outer engines. Located within each of these outlet assemblies is a screen to filter out impurities which exist in the fuel. These sections are made of stainless steel and have been computer analyzed to minimize flow restrictions.

Qty: 2 Flow Coefficient: 1.08 Diameter: N/A

The LH2 Outer Engine Trunk Line Assembly- These sections contain one elbow and direct the fuel from the center of the structure in an outward direction to serve the out-board engines. The entire section is insulated and made of stainless steel.

Qty: 2 Flow Coefficient: 0.4¹⁰ Diameter: 17"

The LH2 Outer Engine Manifold- This section of piping in the feed system channels the fuel off into two branches each delivering fuel to one of the outer engines. This section is made of stainless steel and is fully insulated.

Qty: 2 Flow Coefficient: 0.56 Diameter: 17"- Inlet
12"- Outlet

The LH2 Outer Engine Pre Valve- These sections allow the fuel going to the engines to be cut off in case a leak is detected in the feed system. The section is made of stainless steel and is fully insulated.

Qty: 4 Flow Coefficient: 0.1 Diameter: 12"

The LH2 Outer Engine Feedline- This section of piping delivers fuel directly to the out board engines. It contains three BSTRA flexible gimbals to allow for thermal movement and misalignment. Located at the end of the feedline is screen which is used to eliminate impurities in the fuel. This section contains one elbow, is insulated, and is made of stainless steel.

Qty: 4 Flow Coefficient: 1.1¹¹ Diameter: 12"

The LH2 Center Engine Outlet Assembly- This section allows fuel to leave the LH2 tank and be delivered to the center engine. This section is made of stainless steel and has been computer analyzed to reduce the flow restrictions. Located within this assembly is a screen used to eliminate impurities in the fuel.

Qty: 1 Flow Coefficient: 1.08¹² Diameter: 12"

The LH2 Center Engine Prevalve- This section allows the fuel to be cut off to the center engine when a leak is detected in the feed system. The pre valve is fully insulated and is made of stainless steel.

Qty: 1 Flow Coefficient: 0.1 Diameter: 12"

The LH2 Center Engine Feed Line- This section delivers fuel directly to the center engine. The section contains two elbows and three BSTRA flexible gimbals. The gimbals allow for thermal movement and misalignment. The section is made of stainless steel and all but the gimbals are insulated.

Qty: 1 Flow Coefficient: 1.26¹³ Diameter: 12"

7.4.1.1.8 Feed System Assumptions

The LOX and LH2 feed systems configurations described in the above sections of this report were based on the National Launch System (NLS) configurations. The piping configurations, diameters, and flow coefficients were all taken from the NLS data. The RP-1 configuration was modeled after the LOX configuration since many of the design parameters were the same.

Because the NLS configuration was designed for a six engine set up in which the booster engines disconnected, certain assumptions had to be made which would allow for the SSTO five engine set up. The assumptions and the feed systems to which those assumptions pertain are described below.

The LOX Feed System Configuration- The center engine plumbing was changed to accommodate a single center engine. The center engine manifold and center engine feedline were changed to convert the twin center engine NLS configuration into the single center engine SSTO configuration. The diameter of the crossover pipes were also reduced to compensate for the reduced fuel flow to the center engine. The disconnect valves used in the NLS system were scrapped since the SSTO vehicle is designed to stay with its engines. All of the other pipe characteristics, including diameters and flow rates, were kept the same.

The RP-1 Feed System Configuration- The RP-1 configuration was modeled directly after the modified LOX system described above. A few minor changes were made to the system since the RP-1 feed system uses two separate tanks located closer to the outer shell of the vehicle. This altered configuration led to the shortening of the forward and main trunk lines. Other than the changes to these two piping sections the rest of the characteristics of the configuration were kept the same.

The LH2 Feed System Configuration- To accommodate for a single center engine one of the center outlets and feedlines was dropped from the LH2 configuration. All of the pipe dimensions and flow coefficients were kept the same as those described in the NLS configuration.

7.4.1.1.9 Error Analysis

The feed systems described in this section of the report provide preliminary plans for fuel feed systems which could be used in the SSTO vehicle. Since the system described here is based on the NLS configuration there are some errors which are present. These errors include:

- possible variations in pipe diameters
- possible variations in flow coefficients
- possible variations in pipe routing
- possible variations in pipe materials

The largest error will probably be seen in the flow coefficients since they depend upon the pipe dimensions, routing and construction. Although the flow coefficients may change along with the other variables the changes should be small enough such that the validity of the calculations made in reference to the three feed systems is maintained.

7.4.1.2 Computer Feed System Model

7.4.1.2.1 Computer Program Introduction

A computer model was written to determine the time necessary to accelerate the fuel to the necessary velocity within the required time period. The model is based on the conservation of momentum principle and calculates the velocity of the fuel based on the inlet and outlet pressures, the geometric properties of the feed system, and the fuel properties. The simplifying assumptions limit the accuracy and

applicability of the model, but when the correct parameters are input into the program, a realistic simulation is achievable.

7.4.1.2.2 Model Development

The computer model is based on the conservation of momentum equation

$$\oint_S -p \hat{n} ds = \frac{\partial}{\partial t} \oint_V \rho \vec{u} dv + \oint_S \rho \vec{u} (\vec{u} \cdot \hat{n}) ds \quad (7.1)$$

which can be written in time discrete form as

$$P_i A_i - P_o A_o = \frac{\rho V [u(t + \Delta t) - u(t)]}{\Delta t} - \rho u_i(t)^2 A_i + \rho u_o(t)^2 A_o \quad (7.2)$$

where p_i and p_o represent the inlet and outlet pressures, A_i and A_o represent the inlet and outlet areas, u_i and u_o represent the inlet and outlet velocities, $u(t)$ represents the velocity of the fuel at time t , $u(t+\Delta t)$ represents the velocity of the fuel at time $t+\Delta t$, and n represents the normal vector.¹⁴

Several assumptions are necessary to simplify the equation into a form which can be used to model the fuel flow. It was assumed that the flow through the pipes was one-dimensional. This means that the fuel velocity is identical at all points within a cross-section. Since the fuel is in liquid form, it was assumed that the fuel is incompressible. Therefore, the fuel velocity is identical at all points within a constant diameter pipe. It is also assumed that the fuel properties are constant throughout the system.

Assuming that the velocities at all points within similar diameter pipes are equal allows the last two terms of the equation to cancel if we assume similar diameter pipes. The pressure terms in the equation need to be modified to account for the pressure losses through the system and for the affect of gravity. The pressure losses are determined from

$$\Delta P = \frac{1}{2} \rho u(t)^2 \Sigma K \quad (7.3)$$

where K is the loss coefficient¹⁵. The final equation is

$$P_i A - P_o A - \frac{1}{2} \rho u(t + \Delta t)^2 \Sigma K A + \rho g h A = \frac{\rho A h [(u(t + \Delta t) - u(t))]}{\Delta t} \quad (7.4)$$

The computer program solves this equation numerically for each time step. The final equation was solved for $u(t+\Delta t)$.

$$u(t + \Delta t) = \left[\frac{2hg - Ku(t + \Delta t)}{2h} + \frac{P_i - P_o}{\rho h} \right] \Delta t + u(t) \quad (7.5)$$

The equation was solved numerically by guessing the value for $u(t+\Delta t)$ and substituting that into the right-hand side of the equation. The value for $u(t+\Delta t)$ obtained from the equation was used to obtain a new guess for $u(t+\Delta t)$. The iteration continued until the value for $u(t+\Delta t)$ was constant. This process was repeated for each time step. The control volume used for the calculations includes all fuel inside the feed system from the tank's outlet to the engine's inlet. The computer code was written using Turbo Pascal 6.0 and is shown in Appendix I.

7.4.1.2.3 Computational Results

Using the values for the geometric properties of the feed system and the fluid properties of the fuel, the computer code calculates the velocity history for the transient period of the fuel flow. Using the feed system described in Section 7.4.1.1, velocity histories for each of the fuels (LOX, LH2, RP-1) were calculated. The properties are shown in Table 7.1. The velocity curves are shown in Figure 7.4. The curves show the fuel velocity increasing up to the steady-state solution. The steady-state solution is the same as the solution calculated using Bernoulli's equation. From the curves, the time required to reach the steady-state velocity can be determined and, from that, the duration of the transient period.

	Pi (psi)	Po (psi)	Density (lb/ft ³) ¹⁶	L (in.)	K
LOX	43	38	71.03	1100	4.8
LH2	6	5	4.42	100	3.08
RP-1	25	18	50.28	850	4.8

Table 7.1--Properties Used in Computer Code

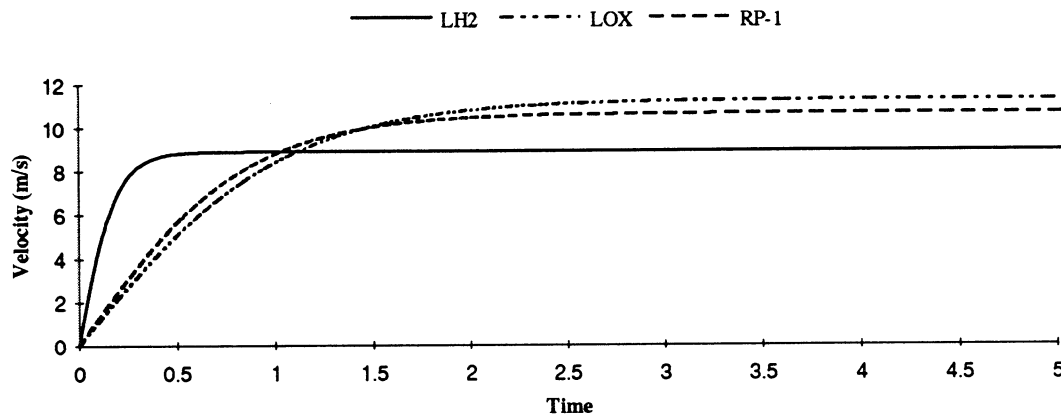


Figure 7.4--Fuel Velocity vs. Time

The duration of the transient period, defined as the time required for the velocity to reach 99% of the steady-state velocity, is 0.51 seconds, 2.73 seconds, and 2.26 seconds for LH2, LOX, and RP-1 respectively.

7.4.1.2.4 Errors

Errors in the calculations are introduced through the assumptions used to simplify the model. The actual feed system does not use pipes of identical diameter. The model assumes that constant diameter pipes are used. This assumption allowed for one of the terms in the conservation of momentum equation to be eliminated. The eliminated terms do affect the calculation and their absence introduces an error. An additional error is introduced by the change in diameter because the exit velocity is affected.

The model does not account for the multiple pipes which are present as the main pipe is split into a pipe for each engine. The flow through the individual pipes will vary depending on the configuration and the pressure losses associated with each section. The model assumes that the flow remains in one pipe, therefore the model does not accurately reflect the affects of multiple pipes.

Although there are errors present in the computer program, the program provides a preliminary estimate of the fuel flow characteristics. The program can be corrected to account for these errors producing more exact results.

7.4.1.2.5 Future Efforts

The next improvements in the computer model should be to model the presence of multiple pipes at the exit of the system. This can be accomplished by determining the pressure at the location of the split and calculating the flows through all of the pipes based on the intermediate pressure. The intermediate pressure should be adjusted iteratively until the continuity equation is satisfied between the main pipe and the smaller secondary pipes. If this adjustment is made correctly, it will be possible to analyze the effects of staggering the starting of the engines on the overall performance of the feed system. A more realistic simulation of a simultaneous start can also be achieved by properly handling multiple pipes.

The code can be used to analyze the other feed systems considered, the LBPFS and the recirculation system, by altering the code to account for the hardware configuration used in each system. The code's calculations could be used to determine the requirements of each system. Accurate comparisons between the systems could then be made on specific performance issues. The analysis presented here is an example of the capabilities of this code; further modifications are necessary for the code to be applicable to the feed system designs considered.

7.4.2 Fluid Recirculation Feed System

Another concept for eliminating the need for back pressure in the tanks involves the circulation of the fluids before ignition. The main purpose of this would be removing the need for the fluids to reach the engine as quickly as possible. The fluids could be recirculated before ignition until the appropriate flow rates are achieved, then the engines could be ignited. Eliminating the need for rapid startup could allow lighter pumps in the feed system and remove the need for back pressure in the storage tanks, resulting in thinner and lighter tanks.

7.4.2.1 Description

In each of the current space shuttle main engines, there are two pumps in the feed line for each fluid leading into the combustion nozzle. A low pressure pump is located near the entrance of the engine, and a high pressure pump is located near the nozzle. The purpose of these two pumps, along with the back pressures in the storage tanks, is to push the fluids rapidly from the tanks to the combustion chambers so that thrust can be attained as quickly as possible. As expected, the pressure differences across these pumps are enormous due to the inertial effects of the fluids.

The theory of the recirculation system is to place a valve downstream of the pumps and circulate the fluids back up to the storage tanks before ignition. The pumps would be given as much time as required to achieve the appropriate flow rates, so transient times would not be as critical. Also, with the need for rapid startup removed, the engine would require only one pump for each fluid which could handle the same flow rates but achieve less pressure gains and a slower response time.

After analysis of the three fluids and their feed systems, it was determined that only the LOX feed system would be altered. The liquid hydrogen is such a light substance that the inertial effects of its flow into the engines are not substantial. Also, because of the cylindrical shape of the LH2 storage tank, its design is limited by buckling instead of stress failure. As a result, some back pressure is required in the tank to prevent failure, so the design of the tank would remain the same. The RP tank's relative size would not produce a significant weight loss.

7.4.2.2 Preliminary Assumptions

The pump used in the recirculation system would need to satisfy initial requirements. The mass and volume flow rates must remain constant at all stages of the feed system. The pump must also supply the liquid oxygen with enough pressure to overcome the pressure head and flow back up to the storage tank.

General calculations were made to determine the specifications of the pump necessary to operate the conceptual feed system. The diameter of the recirculating feed line was assumed to be the same size as the line entering the pump. The recirculating line was also assumed to be straight with no bends or elbows. The velocity of the fluid was set at zero where reentering the storage tank. The fluid was also considered to have the same density at all areas of the feed system, so that both the volumetric and mass flow rates are constant throughout the lines.

7.4.2.3 Feed Line Specifications

In the preliminary design of the single stage shuttle, NASA made some information on shuttle operation available. A diagram with the shape and dimensions of the shuttle was supplied, and is shown in Figure 7.5. This information included estimates of distances between tanks and from tanks to engines.

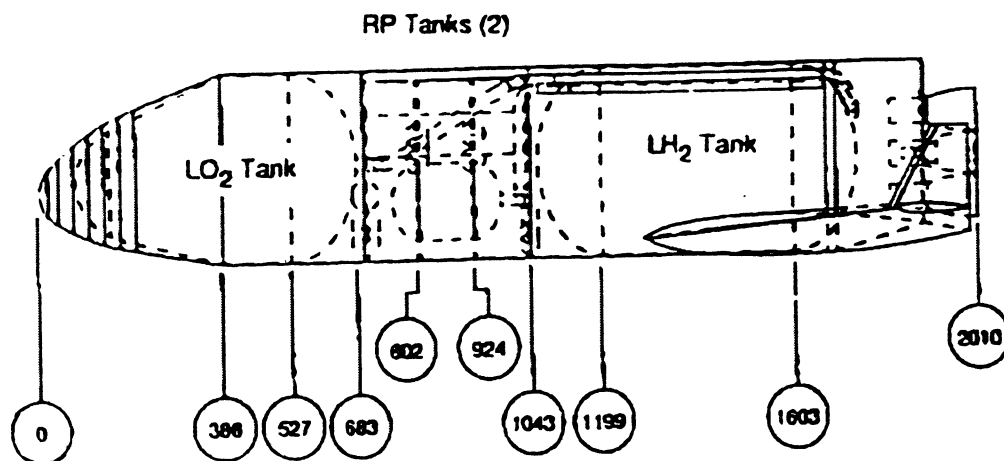


Figure 7.5--SSTO Configuration

For this project NASA also supplied feed system characteristics. The feedline velocity was set at about 20 feet per second, and the feedline diameter was set at 26 inches. From these numbers and knowing

the density of liquid oxygen (at -297° F), the volumetric and mass flow rates for the feed system were determined.

$$\begin{aligned}\text{density of LOX} &= 2.208 \text{ slug/ft}^3 \\ \text{volume flow rate} &= 73.74 \text{ ft}^3/\text{s} \\ \text{mass flow rate} &= 162.8 \text{ slug/s}\end{aligned}$$

7.4.2.4 Calculation of Pump Requirements

The general pump specifications were determined using basic principles of fluid mechanics. Position 1 was placed just upstream of the desired pump, and position 2 was at the recirculation line's entrance back into the tank. Bernoulli's equation was used to roughly estimate the pressure head the pump would need to supply to push the fluid back up to the tank.

$$\frac{p_1}{\gamma} + z_1 + \frac{V_1^2}{2g} = \frac{p_2}{\gamma} + z_2 + \frac{V_2^2}{2g} + h_L \quad (7.6)$$

V_1 was set as the feedline velocity of 20 ft/s, while V_2 was set at zero. The height of the line, $z_2 - z_1$, was estimated from the shuttle dimensions as 100 ft. The head loss in the feed line was determined through the calculation of the Reynolds number and friction factor of the pipe.

$$R = \frac{DV}{\nu} \quad (7.7)$$

$$f = \frac{h_L}{(L/D)V^2/2g} \quad (7.8)$$

The pipe was assumed to be rather smooth, so the friction factor f was found from a Moody diagram to be only 0.008. The head loss h_L was then found to be 2.29 feet. Therefore, the pressure supplied by the pump ($p_1 - p_2$) was calculated to be about 48 psi.

7.4.2.5 Disadvantages of the Recirculation System

One of the major disadvantages of the recirculation system is the additional plumbing configurations required. For each of the five engines, an additional liquid oxygen line must be attached that leads back to the storage tank. This necessity creates problems in adding more weight to the vehicle, taking up space in the vehicle, and complicating the insulation of the feedlines. The weight savings in the storage tank design from the removal of the back pressure must be compared to the weight gained from the additional plumbing. The additional weight available for payload in the shuttle must be compared to the space lost to the new feedlines. Finally, more insulation must be added to the system to prevent the LOX from vaporizing and causing more problems in the feed system.

7.4.2.6 Conclusions

Several tasks would be ahead in order to determine if the recirculation system would be possible to use. First a proper pump must be chosen which would satisfy all the requirements listed above. A study would be performed on the reactions that would occur inside the tank when the return fuel pipe reenters.

This includes calculating the pressure changes inside and an ideal velocity that the incoming fuel should have. From a structural point of view, research has to be done on how the additional piping would fit into the current system. Another important task would be to find out if the pump used would be suitable for the spacecraft once it leaves the ground and begins ascending.

7.4.3 Land Based Pressurized Fuel System

The LBPFS reduces the required pressure in the fuel tank by providing the engine with the necessary start-up conditions. The LBPFS is not a component of the shuttle itself, but instead a supplement to reduce the high pressures in the fuel tank.

7.4.3.1 Description

Although the actual LBPFS has not been designed, the essential components have been defined. The shuttle will not need excess amounts of the three fuel types for the interval from startup to steady state conditions. Each of these fuels (LOX, LH₂, and RP-1) will be contained in a separate pressurized container inside the LBPFS. The LBPFS will also contain necessary turbo pumps in order to transport the fuel to the shuttle fuel lines through a pipe. The LBPFS will be run by a computer which monitors and controls the flow rates of each of the fuels during the initial, transition, and steady state conditions.

7.4.3.2 Safety Concerns

The largest safety concerns are in the area of leakage. Since the LBPFS contains highly flammable fuels, leakage must be prevented to avoid the risks of explosion. The focus area involving leakage concerns is around the joint where the LBPFS connects to the shuttle fuel lines. After examining several connectors, the connector selected was the one currently used to connect the external fuel tank to the space shuttle tank.

Once the gate valve is closed on the LBPFS, the excess fuel in the hoses will be sucked out by vacuum pressure for safety reasons. If the fuel remained in the hoses, the shuttle engines could heat the fuel to the point of ignition. Therefore it is necessary to evacuate the fuel from the hoses to prevent a back flow explosion. Although other safety concerns may arise with a more detailed design, the primary safety concerns with the LBPFS have been addressed.

7.4.3.3 LBPFS Operation

The purpose of the LBPFS is to provide the fuel to the engines from the period of the start-up conditions until steady state is reached, and then the shuttle can provide its own fuel. First the LBPFS pipes should be connected to the shuttle using the joints described in the above section. Once the shuttle is cleared for lift-off, the LBPFS begins its operation. The LBPFS provides the engine with the initial (start-up) engine requirements, and maintains necessary fuel flow rates during the transition to steady state conditions. Once steady state conditions are reached, valves simultaneously close on the LBPFS and open on the shuttle fuel tanks. The pipes on the LBPFS are immediately evacuated for safety reasons, and disconnected from the shuttle. The shuttle system has reached steady state and is providing its own fuels, and lift-off can quickly be achieved.

7.4.3.4 LBPFS Weight Reduction

The reduction in the required flow rate potential and inertial effects represents the basis of the LBPFS weight reduction. The flow rates in the system lines is a function of the fuel properties and the tank

pressure. Therefore a direct relationship exists between the flow rates and tank pressure for the shuttle fuel system.

Although the on-board system consists of three different tanks, this study only examines the LOX tank. The LH2 tank was not examined because it is limited by buckling, and a pressure reduction would not prove beneficial. The RP-1 tank was not examined because of its small tank size, and any weight reduction in this area would be negligible. The LOX tank was the selected because it presents the largest inertial problems due to the long distance from the tank to the engine.

7.4.3.5 LBPFS Weight Reduction

The outside geometry of the LOX tank is fixed therefore any reduction in tank weight will be a function of the tank wall thickness. The LOX outside geometry consists of a short cylindrical shell, two ellipsoid caps, and a conical section. The following equations were found relating the tank pressure to the tank wall thickness:

$$\text{Cylindrical shell: } P = \frac{SEt}{R - .4t} \quad (7.9)$$

$$\text{Ellipsoid : } P = \frac{2SEt}{D - 1.8t} \quad (7.10)$$

$$\text{Cone: } P = \frac{2SEt \cos \alpha}{D - .8t \cos \alpha} \quad (7.11)$$

P = pressure

S = stress = 50ksi

E = joint efficiency = 1

t = wall thickness

R = outer radius = 201"

D = outer diameter = 402" bottom/ 219" top

α = cone angle = 23 degrees

The limiting section for the LOX tank is the conical section. The reason the conical section is the limiting one is that the stress is always greatest in this section. Equation 7.8 was then used to create the following graph relating tank pressure to tank wall thickness.

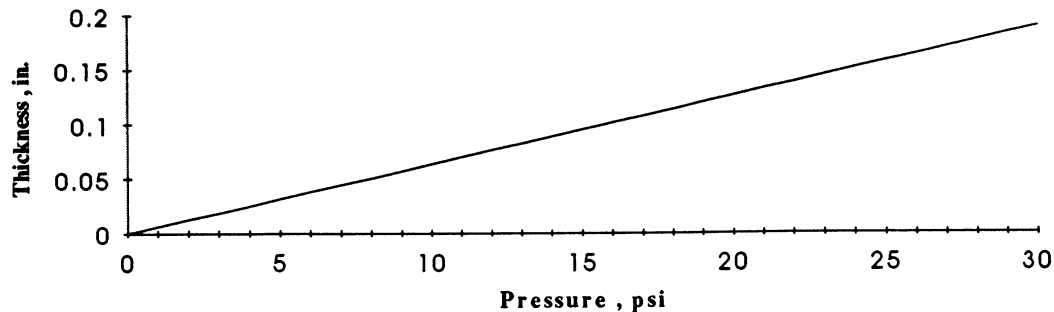


Figure 7.6

Figure 7.6 can be used to show that by reducing the back pressure required in the tanks, the wall thickness of the tank can be reduced. This reduction in tank wall size produces weight savings for the vehicle. The percentage reduction in tank wall thickness will be the same percentage reduction in tank weight. Figure 7.6 gives a means of relating the required tank pressure to the wall thickness. Two pressures can be used to determine the percentage weight reduction for the pressure drop. The equation relating tank pressure to thickness is as follows:

$$P = .0063[\text{lb/in}] t [\text{in}] \quad (7.12)$$

Other weight savings exist due to the lower required potential of the feed system. These are in area of the piping system and the saved fuel. Since most of the fuel consumed during early stages of takeoff is provided by the LBPFS, the tanks will not have to carry as much fuel. Also, the pipes will not have to be as thick because they will not have to handle the high flow rates necessary at start-up. These weight reductions although not as sizable as that of the tank, do provide additional means of reducing the weight of the vehicle.

7.4.3.6 Deficiencies and Future Efforts

The deficiencies in this study are primarily due to certain assumptions. The most significant assumption is that the LOX tank is yield limited and not buckling limited. If the tank is not yield limited, then a reduction in tank pressure has a negative affect on the tank. The tank though is thought to be yield limited because it is on the top and does not support the weight of the other tanks and fuel as does the LH2 tank which is buckling limited. Equations exist which can prove if the LOX tank is indeed yield limited. These assumptions are thought to be valid, but should be addressed in any further studies. The pipe system could be analyzed in a similar fashion as the tank. The amount of fuel saved could be determined by integrating the fuel flow curves over the time the LBPFS is active.

7.5 Recommendations

The LBPFS in conjunction with the feed system configuration described in Section 7.4.1.1 is the most promising system considered. The LBPFS is a feasible method for reducing the pressure in the tank and thereby reducing the weight of the tank. The feed system described in Section 7.4.1.1 offers the basis for a feasible piping configuration to be combined with the LBPFS. Further analysis should be directed into adapting the computer model to handle the LBPFS and refining the LBPFS to quantify the improvements which would be achieved.

The recirculation plan was eliminated because of the considerable problems caused by the addition of the recirculation piping. The weight savings obtained from the tank would be negated by the additional weight from the pumps and piping. Additionally, the recirculation piping would be restricted by spatial constraints.

7.6 References

- (1) USAF/NASA, "National Launch System", Presented at NASA Marshall on 2/12/92, p.3.1.23.
- (2) Ibid, p.3.1.24.
- (3) Ibid, p.3.1.25.
- (4) Ibid, p.3.1.26.
- (5) Ibid, p.3.1.28.
- (6) Ibid, p.3.1.29.
- (7) Ibid, p.3.1.35.
- (8) Ibid, p.3.1.31.
- (9) Ibid, p.3.1.33.
- (10) Ibid, p.3.1.44.
- (11) Ibid, p.3.1.48.
- (12) Ibid, p.3.1.49.
- (13) Ibid, p.3.1.51.
- (14) Patankar, Suhas V., Numerical Heat Transfer and Fluid Flow, Hemisphere Publishing Company, 1980.
- (15) White, Frank M., Fluid Mechanics, second edition, McGraw-Hill, Inc., 1986, p. 333.
- (16) Sutton, George P., and Ross, Donald M., Rocket Propulsion Elements, fifth edition, Wiley, 1986, p. 234-237.